

Inaugural dissertation
for
obtaining the doctoral degree
of the
Combined Faculty of Mathematics, Engineering and Natural
Sciences
of the
Ruprecht - Karls - University
Heidelberg

presented by

Frederik Bergler, M.Sc.

born in Mühlacker

oral examination: 20.04.2023

Impact of FATP4 upregulation and related parameters on trans-endothelial fatty acid transport

Referees: Mr. Prof. Dr. rer. nat. Walter Nickel

Mr. apl. Prof. Dr. rer. nat. Joachim Füllekrug

Declaration

Declaration / eidesstattliche Versicherung

gemäß § 8 der Promotionsordnung der Gesamtfakultät für Mathematik, Ingenieur- und Naturwissenschaften der Universität Heidelberg

Bei der eingereichten Dissertation mit dem Titel:

“Impact of FATP4 upregulation and related parameters on trans-endothelial fatty acid transport”

handelt es sich um meine eigenständig erbrachte Leistung.

Ich habe nur die angegebenen Quellen und Hilfsmittel benutzt und mich keiner unzulässigen Hilfe Dritter bedient. Insbesondere habe ich wörtlich oder sinngemäß aus anderen Werken übernommene Inhalte als solche kenntlich gemacht.

Die Arbeit oder Teile davon habe ich bislang nicht an einer Hochschule des In- oder Auslands als Bestandteil einer Prüfungs- oder Qualifikationsleistung vorgelegt.

Die Richtigkeit der vorstehenden Erklärungen bestätige ich.

Die Bedeutung der eidesstattlichen Versicherung und die strafrechtlichen Folgen einer unrichtigen oder unvollständigen eidesstattlichen Versicherung sind mir bekannt. Ich versichere an Eides statt, dass ich nach bestem Wissen die reine Wahrheit erkläre und nichts verschwiegen habe.

place and date

Summary

Fatty acids (FAs) are essential metabolites for membrane synthesis, energy generation and signalling. Most cells in higher organisms receive FAs circulating in the bloodstream only after their transport across endothelial cells. Many questions regarding this process have remained unresolved. Here, FA-CoA synthesis and metabolism, extracellular concentration of FAs and basolateral FA trapping were analysed in a time resolved manner for their effect on the efficiency of trans-endothelial FA transport. The model system were human umbilical vein endothelial cells (HUVECs) grown on transwell filters incubated with radiolabelled oleate.

Uptake of radiolabelled oleic acid into endothelial cells was initially high but attenuated rapidly. During prolonged incubation, non-esterified FA (NEFA) levels remained relatively constant whereas labelled lipids increased over time. The assessed rate of transport was higher than the rate of metabolism. Results showed that the apical FA concentration drives FA uptake and upregulation of the putative fatty acid transport protein FATP4 has only a minor effect. Due to low FA metabolic capacity, endothelial cells retained a large pool of non-esterified FAs that is rapidly diminished for FA transport.

It was remarkably that lipolysis of triacylglycerol (TG) contributed to the efflux of FAs. The lipolysis of TG for FA transport was reduced by inhibition of the adipose triglyceride lipase (ATGL). Increasing the extracellular apical FA concentration or the storage capacity in the basolateral compartment increased the transport of FAs. Increase in esterification rate due to FATP4 upregulation did not show any significant effect on trans-endothelial FA transport, but reduction in total ACS activity due to AcsI3 knockdown increased the efflux of FAs from endothelial cells in a time dependent manner. The lipid fraction of the basolateral compartment contained only fatty acids, as analyzed by thin-layer chromatography (TLC). This suggests that efflux of lipids consists only of NEFA, but not lipoproteins or complex lipids.

Keywords: Endothelium, FATP4, fatty acids, transport, metabolism

Zusammenfassung

Fettsäuren (FS) sind essentielle Metaboliten für die Membransynthese, Energieerzeugung und Signalübertragung. Die meisten Zellen in höheren Organismen erhalten erst nach ihrem Transport durch Endothelzellen, die im Blutkreislauf enthaltenen zirkulierenden FS. Viele Fragen zu diesem Prozess sind noch ungeklärt. In dieser Studie wurden FA-CoA-Synthese und Metabolismus, extrazelluläre Konzentration von FS und basolaterales FS-Trapping auf ihre Wirkung und Effizienz hinsichtlich des transendothelialen FS-Transports zeitaufgelöst analysiert. Das Modellsystem waren humane Nabelschnurvenen-Endothelzellen, die auf Transwell-Filtern gezüchtet und mit radioaktiv markiertem Oleat inkubiert wurden. Die Aufnahme von radioaktiv markierter Ölsäure in Endothelzellen war anfangs hoch, nahm aber schnell ab. Während längerer Inkubation blieben die Spiegel an nicht-veresterten FS relativ konstant, während markierte Lipide mit der Zeit zunahmen. Die ermittelte Transportgeschwindigkeit war höher als die endotheliale Stoffwechselgeschwindigkeit. Die Ergebnisse zeigten, dass die apikale FS-Konzentration die FS-Aufnahme antreibt und die Hochregulierung des mutmaßlichen Fettsäuretransportproteins FATP4 nur einen geringen Effekt hat. Aufgrund der niedrigen FS-Stoffwechselkapazität behielten Endothelzellen einen großen Pool an nicht veresterten FS, der für den FS-Transport schnell abgebaut wurde. Bemerkenswert war, dass die Lipolyse von Triacylglycerol (TG) zum Efflux von FS beitrug. Die Lipolyse von TG für den FS-Transport wurde durch Hemmung der adipösen Triglyceridlipase (ATGL) reduziert. Eine Erhöhung der extrazellulären apikalen FA-Konzentration oder der Speicherkapazität im basolateralen Kompartiment erhöhte den Transport von FAs. Die Erhöhung der Veresterungsrate aufgrund der Hochregulierung von FATP4 zeigte keine signifikante Wirkung auf den transendothelialen FA-Transport, aber die Verringerung der gesamten ACS-Aktivität erhöhte den Efflux von FS aus Endothelzellen in einer zeitabhängigen Weise. Die Lipidfraktion des basolateralen Kompartiments enthielt nur Fettsäuren, wie durch Dünnschichtchromatographie analysiert wurde. Dies deutet darauf hin, dass der Lipidausfluss nur aus nicht-veresterten FS, aber nicht aus Lipoproteinen oder komplexen Lipiden besteht.

Schlüsselwörter: Endothel, FATP4, Fettsäuren, Transport, Stoffwechsel

Table of contents

| | |
|--|-------------|
| Declaration / eidesstattliche Versicherung | i |
| Summary | iii |
| Zusammenfassung | v |
| Table of contents | vi |
| List of figures | viii |
| List of tables | ix |
| List of abbreviations | x |
| 1. Introduction | 1 |
| 1.1 The Endothelium | 1 |
| 1.2 Physiology of fat uptake | 2 |
| 1.3 Theories of Trans-endothelial fatty acid transport | 3 |
| 1.3.1 Theory 1 – protein-mediated transport (active) | 3 |
| 1.3.2 Theory 2 – diffusion driven transport (passive) | 4 |
| 1.3.3 Focus of this study | 5 |
| 1.4 Thesis aims | 6 |
| 2. Material and methods | 7 |
| 2.1 General information | 7 |
| 2.2 Isolation and cultivation of primary endothelial cells (HUVECs) | 7 |
| 2.3 Retroviral transduction | 10 |
| 2.3.1 Generation of amphotropic retroviral particles | 10 |
| 2.3.2 Application of retroviral particles for transduction | 10 |
| 2.4 Molecular biology and plasmid cloning | 11 |
| 2.4.1 Oligonucleotide annealing | 11 |
| 2.4.2 Restriction digestion | 12 |
| 2.4.3 DNA analysis by agarose gel electrophoresis | 12 |
| 2.4.4 DNA ligation | 12 |
| 2.4.5 Transformation in Escherichia Coli (E. coli) | 12 |
| 2.4.6 Plasmid preparation | 13 |
| 2.4.7 Polymerase chain reaction (PCR) | 14 |
| 2.4.8 Real-Time Quantitative Reverse Transcription PCR (Real-Time qRT-PCR) | 14 |
| 2.5 Biochemical methods for protein analysis | 16 |
| 2.5.1 Gel-electrophoresis and Western Blot | 16 |
| 2.5.2 Immunofluorescence | 17 |
| 2.5.3 Lists of antibodies | 18 |
| 2.6 Biochemical methods for lipid analysis | 20 |
| 2.6.1 Solubilization of [¹⁴ C]OA and preparation of labelling mix | 20 |
| 2.6.2 Uptake of [¹⁴ C]OA in adherent grown HUVECs | 22 |
| 2.6.3 Transport of [¹⁴ C]OA across HUVECs grown on transwell filter | 23 |
| 2.6.4 Lipid Extraction | 26 |
| 2.6.5 Thin-layer chromatography | 26 |
| 2.6.6 Acyl-CoA synthetase activity assay | 28 |
| 2.6.7 Uptake of fluorescent labeled fatty acids (Bodipy-C12) | 28 |
| 2.7 Biophysical and biochemical methods to assess barrier function of confluent grown HUVECs | 29 |
| 2.7.1 Trans-endothelial electrical resistance | 29 |
| 2.7.2 Transport of 70kDa Fluorescein isothiocyanate-Dextran (FITC-dextran) | 29 |
| 3. Statistics and Software | 30 |

| | |
|--|-----------|
| 4. Results | 30 |
| 4.1 Aim 1: Characterization of primary endothelial cells (HUVECs), evaluation of growth parameters and assessment of barrier function | 30 |
| 4.1.1 Morphological and biochemical identification of HUVECs | 30 |
| 4.1.2 Spatial dimensions of endothelial cells (HUVECs) and their growth parameters on trans-well filter | 32 |
| 4.1.3 The confluent monolayer of HUVECs maintains barrier functions while grown on transwell filter | 36 |
| 4.2 Aim 2: Evaluation of the effect of increased FATP4 activity on FA uptake in primary endothelial cells (adherent HUVECs) | 39 |
| 4.2.1 Expression of FATPs and other acyl-coA synthetases in HUVECs | 39 |
| 4.2.2 Upregulation of FATP4 and Acsl3 increases total ACS activity in HUVECs using radiolabelled oleate | 42 |
| 4.2.3 Upregulation of FATP4 activity has a marginal effect on FA uptake compared to the effect of different extracellular OA levels | 45 |
| 4.2.4 Already a slight increase in extracellular OA level outperforms the effect of increased FATP4 activity on FA uptake | 47 |
| 4.2.5 FA uptake increases with availability of free FAs | 49 |
| 4.2.6 Uptake rate of oleate is initially fast and correlates with the rate of esterification during prolonged incubation | 51 |
| 4.2.7 Upregulation of FATP4 activity increases Bodipy-C12 uptake into endothelial cells | 55 |
| 4.3 Aim 3: Assessment of parameters affecting trans-endothelial FA transport | 56 |
| 4.3.1 Besides intracellular non-esterified FAs, also lipolysis contributes to the efflux of fatty acids | 56 |
| 4.3.2 Extracellular OA concentration affects the transport of non-esterified OA 60 | |
| 4.3.3 Endothelial cells provide increased FA transport when intracellular FA metabolism is diminished | 62 |
| 4.3.4 Efflux of FAs from endothelial cells correlates with increasing concentrations of FA-free albumin in the basolateral compartment | 64 |
| 4.3.5 FAs are transported as they are, i.e. non-esterified FA | 66 |
| 5. Discussion | 67 |
| 5.1 Aim 1: Characterization of primary endothelial cells (HUVECs), evaluation of growth parameters and assessment of barrier function | 67 |
| 5.2 Aim 2: Evaluation of the effect of increased FATP4 activity on FA uptake in primary endothelial cells (adherent HUVECs) | 69 |
| 5.3 Aim 3: Assessment of parameters affecting trans-endothelial FA transport | 72 |
| 5.4 Limitations of the study | 76 |
| 6. General conclusion | 77 |
| 7. Appendix | 78 |
| 7.1 Qualitative analysis of upregulation of FATP4 in HUVECs by immunofluorescence and Western Blot | 78 |
| 7.2 Assessment of endogenous FATP4 in HUVECs by IF | 81 |
| 7.3 U6 promoter was more efficient for shRNA transmitted Acsl3 knockdown in HUVECs than H1 promoter | 81 |
| Acknowledgements | 83 |
| 8. References | 84 |

List of figures

| | |
|--|----|
| Figure 1: sequence of methodological steps from isolation to assay. | 9 |
| Figure 2: Schematic figure illustrating the experimental approach to measure [¹⁴ C]OA uptake in adherent grown endothelial cells (HUVECs). | 22 |
| Figure 3: Schematic overview of a pulse/ chase experiment applying HUVECs grown on transwell filter inserts. | 23 |
| Figure 4: Spatial dimensions of one transwell filter. | 25 |
| Figure 6: Image of HUVECs just after detaching from a cell culture plate. | 34 |
| Figure 7: IF of endothelial marker (VE-Cadherin) expressed in isolated HUVECs. | 34 |
| Figure 8: Schematic overview on mean height calculation of endothelial cells. | 35 |
| Figure 9: HUVECs provide electrical impedance caused by VE-Cadherin related adherence junctions that can be disrupted by EDTA treatment. | 37 |
| Figure 10: HUVECs diminish the transport of FITC-dextran across the filter membrane. | 38 |
| Figure 11: Relative comparison of expression levels between different target proteins of the Acsl and FATP families. | 40 |
| Figure 12: Absolute quantification of Acsl and FATP members with endogenous expression in HUVECs. | 41 |
| Figure 13: Acyl-CoA synthetase activity of FATP4, FATP5 or FATP6 upregulation in HUVECs. ... | 43 |
| Figure 14: Acyl-CoA synthetase activity of either Acsl3 or Acsl4 upregulation or Acsl3 knockdown in HUVECs. | 44 |
| Figure 15: Uptake of FAs correlates with extracellular FA concentration while the putative FA transport protein FATP4 has a minor effect. | 46 |
| Figure 16: Increasing the extracellular OA concentration increases FA uptake to a larger extent than increased FATP4 activity. | 48 |
| Figure 17: Increasing the FA to albumin binding ratio increases FA uptake. | 50 |
| Figure 18: Separation of lipid classes after incubation with 200µM (6:1) radiolabeled oleate. . | 53 |
| Figure 19: oleate metabolism of adherent endothelial cells after incubation with 200µM [¹⁴ C]OA for 1, 5 and 30min. | 54 |
| Figure 20: Upregulation of FATP4 increases Bodipy-C12 uptake into endothelial cells. | 55 |
| Figure 21: Lipolysis of TG contributes to the efflux of non-esterified FAs. | 58 |
| Figure 22: Atglistatin treatment reduced lipolysis of TG during FA transport. | 59 |
| Figure 23: Increasing the extracellular OA concentration increases efflux of intracellular non-esterified OA. 20µM apical OA concentration was sufficient to facilitate FA transport. | 61 |
| Figure 24: Oleate transport is increased with reduced intracellular ACS activity. | 63 |
| Figure 25: Oleate transport correlates with different extracellular FA-free albumin concentrations in the basolateral compartment. | 65 |
| Figure 26: Figure: FAs are transported as they are, i.e. non-esterified. | 66 |
| Figure 27: Contribution of this study to the concept of trans-endothelial fatty acid transport. . | 77 |

List of tables

| | |
|--|----|
| Table 1: plasmids applied in this study. | 11 |
| Table 2: program parameters applied for standard PCR. | 14 |
| Table 3: list of primary antibodies applied in this study. | 18 |
| Table 4: list of secondary antibodies applied in this study. | 19 |
| Table 5: radiolabelled and non-labelled oleic acids applied in this study. | 21 |
| Table 6: Transwell filter inserts applied in this study. | 25 |
| Table 7: Rf standards of different lipid species. | 27 |
| Table 8: Spatial dimensions and resulting growth parameters of HUVECs on transwell filter. . | 35 |

List of abbreviations

| | |
|-----------------|---|
| °C | Degree Celsius |
| α | Anti-, against |
| ACS | Acyl-CoA Synthetase |
| ACSL | Long-chain Acyl-CoA Synthetase |
| ACSVL | Very long-chain Acyl-CoA Synthetase |
| APS | Ammonium persulfate |
| ATP | Adenosine triphosphate |
| ATGL | Adipose triglyceride lipase |
| a.u. | Arbitrary unit |
| BCA | Bicinchoninic acid |
| BSA | Bovine Serum Albumin |
| cDNA | Complementary deoxyribonucleic acid |
| CD36 | Cluster of differentiation 36 |
| CoA | Coenzyme A |
| CO ₂ | Carbon dioxide |
| C _t | Threshold cycle |
| DG | Diacylglyceride |
| DMSO | Dimethyl sulfoxide |
| dNTP | Deoxynucleotide triphosphate |
| DTT | 1,4-Dithiothreitol |
| EBM-2 | Endothelial basal medium-2 |
| E. coli | Escherichia coli |
| EC | Endothelial cell |
| EDTA | Ethylenediaminetetraacetic acid |
| e.g. | Exempli gratia |
| EGM-2 | Endothelial growth medium-2 |
| ER | Endoplasmic reticulum |
| FA / FS | Fatty acid / Fettsäuren |
| FABP | Fatty acid binding protein |
| FAHFA | Branched fatty acid esters of hydroxy FAs |
| FATP | Fatty acid transport protein |

List of abbreviations

| | |
|----------------------|--|
| F C/B S | Fetal Calf/Bovine Serum |
| FITC | Fluorescein isothiocyanate |
| FLAG | Peptide sequence DYKDDDK, protein tag |
| GA-1000 | Gentamicin sulphate-Amphotericin |
| GPIHBP1 | Glycosylphosphatidylinositol anchored high density lipoprotein binding protein 1 |
| h | Hour(s) |
| hEGF | Human epidermal growth factor |
| hFGF-B | Human fibroblast growth factor (basic) |
| IF | Immunofluorescence |
| kDa | Kilo Dalton |
| LB | Lysogeny broth |
| LCFA | Long-chain fatty acids |
| LD | Lipid droplet |
| LPL | Lipoprotein lipase |
| LTR | Long terminal repeat |
| mg | Milligram |
| min | Minutes |
| ml | Millilitre |
| MMLV | Moloney murine leukaemia virus |
| mp | Millipore |
| n.s. | Not significant |
| OA | Oleic acid (non-esterified) |
| [¹⁴ C]OA | Radiolabelled oleic acid |
| PAGE | Polyacrylamide gel-electrophoresis |
| PBS | Phosphate Buffered Saline |
| PC | Phosphatidylcholine |
| PE | Phosphatidylethanolamine |
| PFA | Paraformaldehyde |
| PI | Phosphatidylinositol |
| Pmol | Picomole |
| PPAR | Peroxisome-proliferator-activated receptor |

List of abbreviations

| | |
|----------|--|
| PS | Phosphatidylserine |
| RNAi | RNA Interference |
| RT | Room temperature |
| R3-IGF-1 | R ³ Insulin-like growth factor |
| rpm | Rounds per minute |
| SD | Standard deviation |
| SDS | Sodium dodecyl sulphate |
| S / sec. | Seconds |
| SG | Saponin Gelatine |
| SGB | Saponin Gelatine BSA |
| shRNA | Small-hairpin RNA |
| SM | Sphingomyelin |
| TAE | Tris/Acetate-EDTA |
| TBS | Tris Buffered Saline |
| TEER | Trans-endothelial/epithelial electrical resistance |
| TEMED | Tetramethylethylenediamine |
| TG | Triacyl glyceride |
| TLC | Thin Layer Chromatography |
| TRIS-HCL | Tris(hydroxymethyl) aminomethane hydrochloride |
| TWEEN-20 | Polysorbate 20 |
| VEGF | Vascular endothelial growth factor |
| VLCFA | Very long-chain fatty acids |
| VSV-G | Vesicular stomatitis virus G |
| WB | Western Blot |
| µg | Microgram |
| µl | Microlitre |
| µm | Micrometre |
| µM | Micromolar |

1. Introduction

1.1 The Endothelium

The endothelial monolayer lines all blood and lymphatic vessels inside the human body. Taking a closer look, the distance between the basal side of the endothelium and the underlying tissue is ranging between ~ 50 to ~ 100 μm but can be less than ~ 15 μm [1, 2]. With its specific location as an interface between blood stream and systemic tissue, the endothelium provides unique features to maintain important functions of the human body. On one hand, the endothelium builds up a protective barrier to prevent direct access of potentially harmful substances from the blood towards the cellular components of organs [3]. On the other hand, the endothelium offers active transport for substances that are crucial for homeostasis of the organs [4]. The highly heterogeneous endothelium varies in its phenotypic morphology depending on the location in the human body [5]. For instance, the endothelium in the brain capillaries is very dense and expresses proteins involved in tight junctions, such as claudins and occludins, that share features with epithelial cells, known to prevent paracellular transport of most molecules [6] [7]. In contrast, the discontinuous and fenestrated sinusoidal endothelium in the liver tissue provides gaps ranging in size up to ~ 100 nm allowing transport of complex molecules [8, 9]. The microvascular endothelium lining blood vessels in metabolic active organs, such as heart and skeletal muscles, is continuous and non-fenestrated, but requires high rates of substance exchange. This type of endothelium is finely tuned for nutrients and oxygen transport [10]. In the microvascular endothelium, paracellular transport is restricted due to adherence junctions [11].

Generally, there are two distinct ways for trans-endothelial transport. Firstly, small molecules and ions can pass the microvascular endothelium on a paracellular way through space between cell-to-cell connections [12, 13]. Secondly, molecules that are not able to utilize paracellular transport are retained until actively transported by transcellular transport mechanisms [12, 14]. While distinct transport mechanism for glucose and oxygen have already been described, the trans-endothelial fatty acid transport remains an unsolved mystery.

1. Introduction

1.2 Physiology of fat uptake

Dietary fats vary dependent on food patterns of individuals. In general, dietary fats consist of 90% triacylglycerols and 10% phospholipids, cholesterol, and cholesterol esters [15]. Triacylglycerols in dietary fats consist mostly of long-chain fatty acids (C16-C18) esterified to glycerol [16]. After food intake the roughly distributed dietary fats in the chymus are emulsified and hydrolysed in the alkaline milieu of the duodenum [17]. Herein, triacylglycerols are hydrolysed by lipases and colipases to build up free fatty acids, glycerol and 2-monoacylglycerol [17]. Cholesterol esters are hydrolysed by cholesterol esterase and phospholipids are hydrolysed by phospholipases, respectively [18, 19]. In the hydrophilic environment the products of the hydrolysis build up micelles and near the enterocytes the micelles release their cargo [20]. Short- and middle-chain fatty acids as well as glycerol are absorbed passively by diffusion into enterocytes followed by diffusion into the blood stream [20, 21]. Cholesterol, Monoacylglycerol and long-chain fatty acids (LCFA) are absorbed by carrier-mediated receptors [22]. In the intracellular lumen, LCFAs are activated and re-esterified to Monoacylglycerol at the endoplasmic reticulum to form triacylglycerols that bind to proteins to build up chylomicrons [23]. Chylomicrons are lipoprotein particle and consist of triacylglycerols (85%), phospholipids (9%), cholesterol, fat soluble vitamins (4%) and proteins (2%) [24-26]. Eventually, Chylomicrons are transported by vesicle mediated exocytosis into lymphatic vessels to reach the blood circulation [27]. When high amounts of fatty acids are required, for example during fasting or prolonged exercise activity the concentration of total free fatty acids in the blood plasma (~500 $\mu\text{mol/l}$, normal) can increase up to two to three-fold [28, 29]. At the basolateral side of the endothelium the increase of plasma concentrations of free fatty acids is followed by the sensing of the parenchyma cells towards the endothelium to increase the trans-endothelial fatty acid transport via the release of messengers. For instance, 3-hydroxyisobutyrate or VEGFB were shown to increase the trans-endothelial fatty acid transport [30, 31]. At the apical side of the endothelium Glycosylphosphatidylinositol anchored high density lipoprotein binding protein 1 (GPIHBP1) anchors the circulating lipoprotein lipase (LPL) from the blood stream and enables the LPL to hydrolyse triglycerides into two free fatty acids and Monoacylglycerol [32]. At this point, free fatty acids are near the endothelial cells, however the mechanism how the fatty acids pass the endothelium is hardly investigated and therefore not fully understood.

1.3 Theories of Trans-endothelial fatty acid transport

There is a variety of theories and speculation about how FAs cross the endothelial barrier to reach the underlying tissue. In addition, the driving force and further parameters of the trans-endothelial fatty acid transport are hardly investigated. Here, two different prominent theories about trans-endothelial fatty acid transport are described:

1.3.1 Theory 1 – protein-mediated transport (active)

Numerous studies support the theory of the trans-endothelial FA transport being linked to the presence and expression of putative transport proteins. Some of these studies argue that free FAs are transported by translocases, via putative transport proteins while other studies support a vesicle-mediated transport [33, 34] [35] [36]. FA transport underlies regulation and is potentially transcellular with regard to a number of proteins that can increase fatty acid uptake and that might play a role in trans-endothelial fatty acid transport [37]. It has been shown that specific deletion of CD36 reduces FA uptake into endothelial cells as well as cells of the parenchyma [38]. CD36 can bind free FAs with its hydrophobic extracellular side chains and transfers them to the plasma membrane where FAs are translocated across the membrane [38, 39]. CD36 as well as FABP4 (fatty acid binding protein 4) are expressional regulated by the nuclear receptor peroxisome proliferator activated receptor gamma (PPAR γ) [40]. Knockout of the transcriptional regulator PPAR reduces FA uptake into basolateral located tissue. FABP4 is known to bind and transport free FAs through the intracellular compartment of endothelial cells [41, 42]. Therefore, intracellular FABPs are very important to solubilized fatty acids in the hydrophilic cellular lumen. In addition, knockout of FABPs lead to reduction in cellular fatty acid uptake and reduced cell proliferation [43, 44]. Another commonly known fatty acid transporter is human serum albumin. In the human body albumin binds and solubilizes plasma FAs in the blood stream. Hence, there is the possibility that fatty acids are transported through endothelial cells while bound to albumin, suggesting an albumin-mediated FA transport [45, 46]. The glycoprotein (gp60) was introduced to be able to bind albumin from the blood stream at the cell surface of endothelial cells and initiate uptake of the albumin complex [46]. A prominent protein complex in facilitating vesicle-mediated transcellular transport is caveolae, which enables endocytosis and trans-migration of vesicles from the apical to the basolateral side of the endothelium [47]. Caveolin-1 is the dominant caveolin isoform required for

1. Introduction

the formation of intracellular vesicles build up from caveolae [48, 49]. Recent results suggest that the trans-endothelial transport and uptake of albumin is executed through caveolae related vesicle formation [50]. Other prominent putative fatty acid transporters are the Fatty Acid Transport Proteins (FATPs). When the first member of the family (FATP1) was cloned from an adipocyte cell line and heterologous expressed by Schaffer and Lodish, this protein family was named fatty acid transport protein due to its ability to increase the uptake of long-chain fatty acids (LCFAs) [51]. The FATP family consists of six members (FATP 1-6) and is expressed in different tissues throughout the human body [52]. However, all of them are membrane associated proteins, increase the uptake of FAs, and most importantly obtain acyl-CoA synthetase activity prioritizing different target LCFAs [53-57]. In summary, many putative FA transporter were identified and investigated for their functionality. However, a classification of their individual contribution to trans-endothelial FA transport has not yet been performed in a convincing manner.

1.3.2 Theory 2 – diffusion driven transport (passive)

Another theory is that FAs cross the endothelial barrier by diffusion. Due to their hydrophobic nature and hydrophilic head group when in anionic form, unbound FAs naturally bind to the outer cell membrane and enter the outer leaflet of the phospholipid bilayer [58]. Inside the phospholipid bilayer two major effects are happening. Firstly, FAs travel by lateral diffusion with a speed of $\sim 1 \mu\text{m/s}$ through the cell membrane and secondly, FAs can enter the inner leaflet of the cell membrane by transverse diffusion (flip flop) [59, 60]. It must be noted that transverse diffusion requires protonation of the FA head-group [61]. Very likely, this process is facilitated by changes of pH in the microenvironment of the membrane [61, 62]. FAs reside in the inner leaflet, until intracellular mechanisms, such as FA binding proteins (FABPs) carry the FAs to their distinct targets [63]. In addition, this theory opens the possibility that FAs can bypass the endothelial barrier by traveling inside the outer leaflet of the cell membrane from the apical to the basolateral side without moving across the intracellular environment [33]. Furthermore, intracellular FA metabolism can decrease the intracellular FA concentration and enhance the passive diffusion of FAs from the extracellular- towards the intracellular space. With acylation of the carboxyl group being the initial step of FA metabolism, this mechanism was called “vectorial acylation” or

1. Introduction

“metabolic trapping” [64-66]. FATP4 was proposed for being the responsible protein for cellular FA uptake [1] by facilitating vectorial acylation [64, 67]. In addition, FA transport across the endothelium was linked to the up- and downregulation of FATP4 [31, 68]. In 2006, Milger et. al. demonstrated that the putative fatty acid transporter FATP4 is located at the endoplasmic reticulum (ER) rather than in the plasma membrane [69]. Furthermore, this study showed that the primary function of FATP4 is the activation of FAs by thio-esterification which is similar to other acyl-CoA synthetases, such as ACSL3 [69]. These observations have been a breakthrough in this research field, as they combine both theories: protein based and diffusion dependent uptake of FAs. Moreover, Milger et. al. stressed the importance of spatial organization of molecular processes in order to understand their functionality [69]. How crucial spatial organization is for the molecular mechanisms involved in FA transport has been shown by numerous recent studies. Ibrahim et. al. showed that adenosine triphosphate (ATP) required for FATP4 activity is derived from mitochondria while at the same time endothelial cells generate most (>75%) of their ATP by anaerobic glycolysis in the cytosol [70-72]. These observations suggests that FATP4 is situated in the ER that forms node-points with mitochondria and by its proximity can utilize the mitochondrial derived ATP. As described by Füllekrug et. al., the relatively small (~7 nm to ~33 nm) distances between different cellular compartments, such as ER and plasma membrane junctions may enable efficient intracellular transport of FAs [65].

1.3.3 Focus of this study

As described in 1.3.1 and 1.3.2, FATP4 has been implicated as a relevant protein for FA transport and metabolism. In addition, expressional upregulation of FATP4 activity was introduced as major driving force of FA uptake and transport [68, 70]. In this study FATP4 upregulation in primary endothelial cells (HUVECs) was tested for the efficiency to drive FA uptake and transport and the impact was compared to related parameters, such as extracellular FA concentrations.

1.4 Thesis aims

Despite intensive studies on FA transport, the exact mechanisms remain largely unknown. Multiple research questions – some of which addressed in this thesis – may contribute to a better understanding. Therefore, the aims of this study are as follows:

Aim 1: Characterization of primary endothelial cells, evaluation of growth parameters and assessment of barrier function

In this study primary endothelial cells were isolated from the human umbilical cord vein and characterized by morphological assessment and identification of HUVEC specific biomarkers. Then, spatial growth parameters of HUVECs grown on transwell filters was evaluated and the endothelial barrier function was assessed.

Aim 2: Evaluation of the effect of increased FATP4 activity on FA uptake in HUVECs

The expression of Acyl-CoA synthetases and their contribution to the total ACS activity was analysed. Upregulation of FATP4 in primary endothelial cells was generated by retroviral induced stable expression of FATP4. Upregulation of FATP4 activity was validated by assessment of the total acyl-CoA synthetase activity in the cellular supernatant. In the next step, upregulation of FATP4 was compared to different extracellular FA concentrations regarding FA uptake in primary endothelial cells. Then, the total incorporated lipids were analysed and the rate of metabolism in HUVECs with FATP4 upregulation was evaluated.

Aim 3: Assessment of parameters affecting trans-endothelial FA transport

In this study, HUVECs were grown on transwell filter and incubated with radiolabelled OA to investigate trans-endothelial FA transport in a time-resolved manner. In addition, the rate of endothelial FA metabolism was compared to the rate of FA transport in relation to extracellular- and intracellular FA concentrations. Furthermore, the chemical identity of transported FAs was analysed. Lastly, different parameters, such as intracellular ACS activity, extracellular FA concentrations and different basolateral FA-free albumin concentrations were evaluated for their efficiency to drive trans-endothelial FA transport.

2. Material and methods

2.1 General information

This study was carried out between february.2019 until december.2022 in the molecular biology research group AG Füllekrug in the department inner medicine 4. affiliated to the university hospital Heidelberg.

2.2 Isolation and cultivation of primary endothelial cells (HUVECs)

Human umbilical cord vein endothelial cells were applied as primary cells to model microvascular endothelium. HUVECs were provided by isolation from umbilical cords and ethically approved (file number: S-374/2019) by the ethical commission university hospital Heidelberg.

For coating of cell culture dishes, cell culture plates were incubated for at least 15 min with 150 µg/ml Collagen R (2mg/ml in 0.1% acetic acid, SERVA Electrophoresis GmbH, Heidelberg, Germany) diluted in 1XPBS at 37 °C and 5% CO₂. After incubation the Collagen R solution was discarded, and coated cell culture plates were gently washed with 1X PBS prior to cell seeding. Umbilical cords were collected immediately after childbirth and stored at 4 °C for a maximum of 24 hours. For isolation of HUVECs two surgical cannula (Berger-meditec, Neu-Isenburg, Germany) were inserted in both ends of the umbilical vein. The inner lumen of the vein was washed twice with 1X PBS and endothelial cells were detached by 3,13 g/l dispase (REF 17105-041, LOT 1854818, Gibco, Thermo Fisher Scientific, Waltham, Massachusetts, USA) treatment for 30 min at 37 °C. After incubation, the dispase solution containing HUVECs was spilled into a 50 ml Falcon Tube and centrifuged for 5 min at 200 x g. The supernatant was discarded and HUVECs were re-suspended in pre-warmed EGM-2 (Lonza, Basel, Switzerland). The cell suspension was transferred into a pre-coated cell culture dish (Greiner AG, Kremsmünster, Österreich).

HUVECs were cultured in endothelial growth medium (EGM-2) (Lonza, Basel, Switzerland) at 37 °C and 5% CO₂ atmosphere. EGM-2 consists of endothelial basal medium (EBM-2) supplemented with EGM-2 supplements (Lonza, Basel, Switzerland), including Hydrocortisone, hFGF-B, VEGF, R3-IGF-1, ascorbic acid, hEGF, GA-1000, heparin and 5% FBS v/v. For cell propagation, HUVECs were detached by washing once

2. Material and methods

with 1XPBS and incubated with 0,05% Trypsin/EDTA (Gibco, Thermo Fisher Scientific, Waltham, Massachusetts, USA).

As described in figure 1, HUVECs were applied for experiments at a maximum of 6 passages / < 1 month of cultivation after isolation.

2. Material and methods

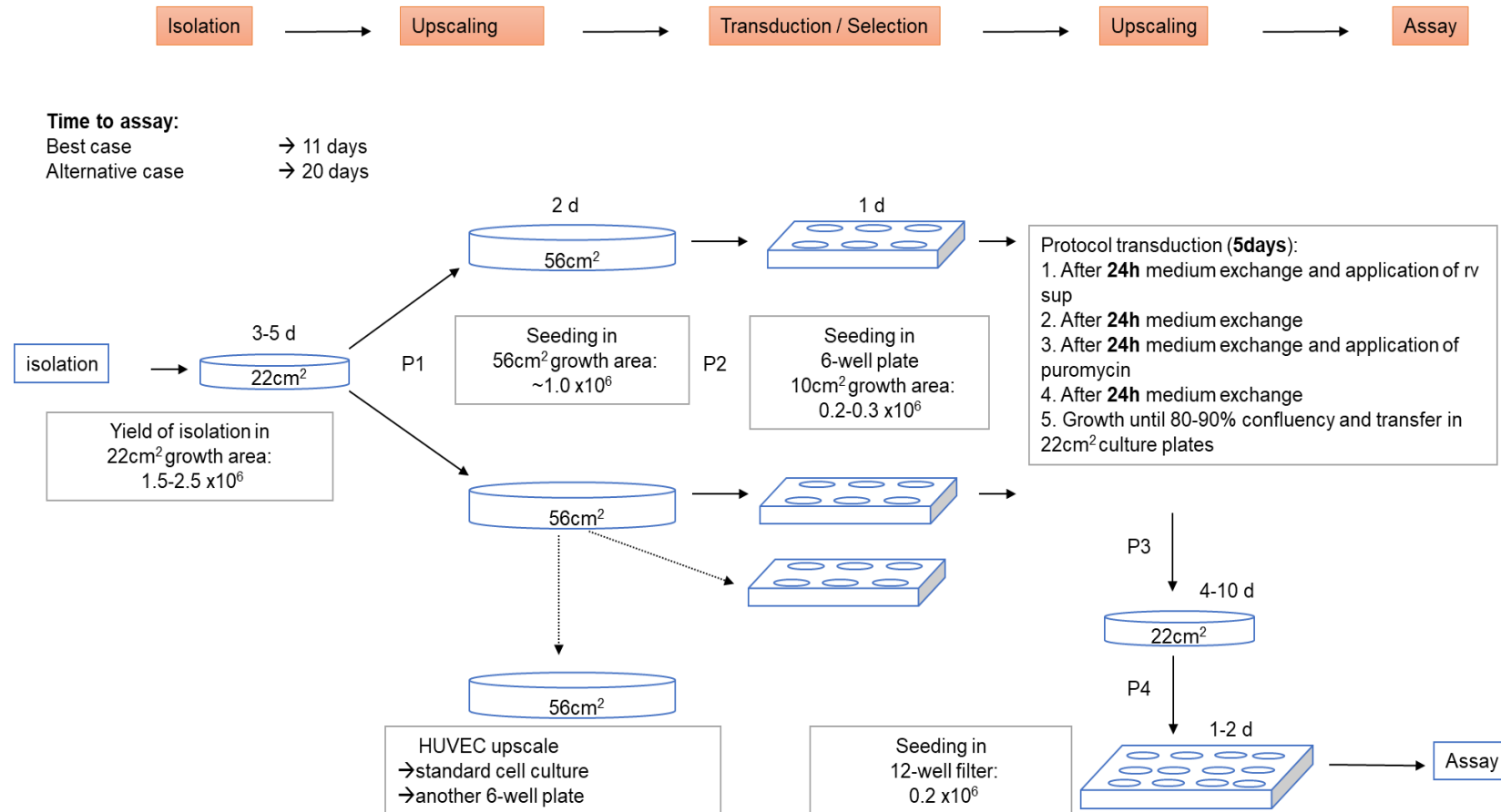


Figure 1: sequence of methodological steps from isolation to assay.

After isolation, HUVECs were expanded for 3 to 5 + 2 days, then seeded for transduction. After transduction, HUVECs were selected and expanded over 4 to 10 days. Then, HUVECs were seeded for the experimental approach between 11 to 20 days after isolation

2.3 Retroviral transduction

Primary cells (including HUVECs) are commonly known for being difficult-to-transfect, therefore retroviral transduction was applied for stable expression of target cDNAs or small-hairpin RNAs [73].

2.3.1 Generation of amphotropic retroviral particles

The packaging system for production of amphotropic retroviral particles was developed by the Nolan Lab, Stanford University (Retroviral Systems, stanford.edu, updated 15.01.2023). The application of the retroviral particles to induce stable overexpression of target cDNA was conducted according to Schuck et al. 2004 [74].

The retroviral genome was truncated no longer providing the matrix- and capsid proteins (gag) and retroviral polymerase and integrase (pol) gene required for functional reproduction of the retrovirus. For the generation of retroviral particles, the gag- as well as pol-genes are provided by HEK-293 (phoenix gp) cells stably expressing gag and pol proteins. For switching the retroviral tropisms to amphotropic, additionally the vesicular stomatitis virus G protein (VSV-G) was heterologous expressed in phoenix gp cells. For generating retroviral particles that lead to integration and expression of a specific target cDNA/shRNA in the host, the packaging signal of murine leukemia virus (MMLV) and the protein of interest flanked by virus specific long terminal repeats (LTRs) was co-expressed with the VSV-G protein in phoenix gp cells.

Phoenix gp cells were seeded in 60 cm² cell culture dishes. When phoenix gp cells reached 70-80% confluency, the cells were transfected with target plasmids using Ca₃(PO₄)₂ precipitation. After 48h, retroviral particles were collected from the supernatant, frozen and stored at -80 °C until they were applied for transduction.

2.3.2 Application of retroviral particles for transduction

Prior to transduction, 3x10⁵ HUVECs were seeded in one well of a collagen-R coated 6-well plate (Corning, New York, USA). After 24 hours, medium was replaced by transduction solution (1 ml specific retroviral supernatant, 4 µg/ml polybrene (Sigma-Aldrich, St-Louis, Missouri, USA)) and incubated overnight at 32 °C and 5% CO₂ atmosphere. Then, 1 ml EGM-2 was added to each well and the 6-well plate was transferred to 37 °C and 5% CO₂ atmosphere for another overnight incubation. After a total of 48h incubation, the transduction solution was replaced by 2 ml EGM-2

2. Material and methods

containing required antibiotics for selection. Here, 2 µg/ml puromycin (Clontech, Takara Bio USA, Mountain View, California, USA) was applied for 48 hours. After transduction HUVECs were cultivated until 70-90% confluency and transferred to Collagen-R coated cell culture dish.

2.4 Molecular biology and plasmid cloning

The plasmid JF1329 (FATP5) was acquired by subcloning the cDNA of FATP5 from the progenitor plasmid (JF569, origin: P. Watkins, laboratory DNA database). The cDNA for FATP6 was acquired by isolation of total mRNA from isolated HUVECs P1, reverse transcription and PCR of total cDNA using FATP6-specific primers (sense: ctgattaattaaatgcttctgtcatggctaac, antisense: gatctgtacacaagttttattcccctaac). The plasmid JF1337 was generated by cloning the cDNA coding for a shRNA specifically targeting Acsl3 into JF1330. JF1330 was generated by cloning the U6 promoter from progenitor plasmid (JF1045) into the plasmid prvH1.puro (JF338), replacing the H1 promoter with the U6 promoter. The plasmids JF1082, JF825, JF804 were already available in the laboratory DNA database, as shown in the following table 1.

Table 1: plasmids applied in this study.

| Name of plasmid | application | Internal reference |
|----------------------------|---------------------------------------|---------------------------|
| hsFATP4-3xFLAG.pRIJ | retroviral expression of FATP4-FLAG | JF1082 (M. Langer) |
| GFP-ACSL3.pRIJ | retroviral expression of GFP-Acsl3-HA | JF825 (M. Poppelreuther) |
| GFP-ACSL4.pRIJ | retroviral expression of GFP-Acsl4-HA | JF804 (I. Zhang) |
| hFATP5-FLAG.pRIJ | retroviral expression of FATP5-FLAG | JF1329 |
| hFATP6-FLAG.pRIJ | retroviral expression of FATP6-FLAG | JF1334 |
| ACSL3-RNAi.pRVU6 | retroviral knockdown of Acsl3 | JF1337 |

2.4.1 Oligonucleotide annealing

Purchased single strand oligonucleotides were dissolved in appropriate volume of H₂O achieving a final concentration of 100 µM. The sense- and antisense strands were mixed achieving a final concentration of 50 µM and heated up to 95 °C. Then, the temperature was decreased stepwise by 1 °C every 30 seconds until 25 °C was reached.

2. Material and methods

2.4.2 Restriction digestion

The restriction digestion was set up in an Eppendorf tube applying 1-2 µg of target plasmid DNA, 5-10 U/µg target DNA of specific enzyme pairs, 1X reaction buffer (10X) and required volume of H₂O reaching a final volume of 30 µl. The restriction digestion was run for at least 1 hour at 37 °C. When sequential restriction digestion was required, two separate reactions were run sequentially and between reactions the digestion buffer was exchanged using gravitational force filtering with a column retaining DNA when high salt concentrations were applied. By lowering salt concentrations (elution in H₂O or TRIS-HCl 5 mM, pH 8.5) the DNA was eluted from the column.

2.4.3 DNA analysis by agarose gel electrophoresis

Agarose gel-electrophoresis was applied to analyse plasmid DNA or DNA fragments according to size differences. The agarose gel was prepared by dissolving 0.5 - 2% agarose (Invitrogen, Carlsbad, CA, USA) in TAE buffer (40 mM Tris, 20 mM acetic acid, 1 mM EDTA). For visualization of DNA under UV light, pEqGREEN (PEQLAB Biotechnologie GmbH, Erlangen, Germany) was homogeneously added to the agarose mixture before polymerization in the running chamber. The gel was run with 120 V for ~45 min. The target bands were cut, and the corresponding DNA was purified by application of the GenElute gel extraction kit (Sigma, Saint Louis, USA).

2.4.4 DNA ligation

Ligation of linear DNA strands was performed by mixing insert and vector in a ratio of 3:1 or 7:1, adding 1X ligase buffer (10X), 10-20 U/ reaction of T4 DNA ligase and H₂O up to a final volume of 5 µl. The ligation reaction was incubated for 10 min at room temperature, directly followed by transformation as described in the following paragraph (3.3.4.).

2.4.5 Transformation in Escherichia Coli (E. coli)

E. coli (DH5α, Invitrogen, Carlsbad, CA, USA) were kept in lysogeny broth medium (LB medium) containing 5 g/l yeast extract (Becton Dickinson, Heidelberg, Deutschland), 10 g/l tryptone (Becton Dickinson, Heidelberg, Deutschland), 10 g/l sodium chloride (Sigma, Saint Louis, MO, USA) and H₂O. In liquid medium *E. coli* were cultured on a heat shaker at 230 rpm and 37 °C. When *E. coli* were kept on solid medium, additionally a galactose-polymer/ polysaccharide Select-Agar (Invitrogen, Carlsbad, CA, USA) was added to the LB medium and the LB-Agar medium was transferred in petri dish, then *E. coli* were kept

2. Material and methods

in an incubator at 37°C. Transformation of plasmid DNA into competent *E. coli* (DH5 α) was performed applying heat-shock. 20-50 μ l of heat-shock competent *E. coli* were added to 50-100 ng of plasmid DNA and incubated 15 min on ice (0 °C). Heat-shock was performed by incubating the transformation approach on a thermo-block for 90 s at 42 °C, followed by incubation on ice for 1 min. The samples were transferred on a pre-warmed (37 °C) LB-Agar plate containing 100 μ g/ml ampicillin (Sigma, Saint Louis, MO, USA) or 50 μ g/ml kanamycin (Sigma, Saint Louis, MO, USA) for colony selection and incubated for 16-24h (overnight) at 37 °C. When plasmids expressing kanamycin resistance were applied, then *E. coli* were incubated in pre-warmed media (37°C) for 45 mins without shaking before transferring them on LB-plates. After >16 hours, single colonies were selected, transferred in LB medium including the appropriate antibiotic (100 μ g/ml ampicillin or 50 μ g/ml kanamycin) and incubated at 37 °C for 16 hours at 230 rpm.

2.4.6 Plasmid preparation

Plasmid DNA was isolated from bacteria using the plasmid DNA purification mini kit from Macherey-Nagel (Macherey-Nagel, Düren, Germany). Two times 1 ml of bacterial suspension was centrifuged at 11,000 x g for 1 min at 4°C. The supernatant was discarded, and the bacterial pellet was resuspended in pre-cooled (4°C) resuspension buffer A1 including RNase. Plasmid DNA was released by SDS/alkaline lysis from host *E. coli* by addition of lysis buffer A2. The lysis suspension was mixed carefully by inverting the tube 5 times. In the next step, the neutralization buffer A3 was added, and the tube was inverted two more times to neutralize the pH of the lysis suspension. After centrifugation at 11,000 x g for 10 min the supernatant including the isolated plasmid DNA was transferred onto a column containing a semi-permeable silica membrane and centrifuged for 11,000 x g for 1 min. The plasmid DNA was washed twice by application of washing buffer A4 and centrifugation at 11,000 x g for 1min. Subsequently, the column was dried by another centrifugation step. The bound plasmid DNA was released by application of elution buffer (5 mM Tris/HCl, pH 8.5) and another centrifugation step. The isolated plasmid DNA was detected by absorption at 260 nm analyzed by the NanoDrop photometer (ThermoFisher, Waltham, MA, USA) and the concentration was calculated by Beer-Lambert law.

2. Material and methods

When increased amounts of plasmid DNA were required for calcium-phosphate precipitation (transfection of phoenix gp cells), volume upscaling for the process of plasmid DNA propagation in e. coli and the plasmid preparation was performed. Hereby, plasmid DNA was prepped from 200ml of bacterial suspension using the Plasmid midi Kit (Qiagen, Venlo, Netherlands). The principle of plasmid preparation was the same as the one from the mini kit, however after midi prep the plasmid DNA was additionally purified by precipitation with isopropanol resulting in higher purity of isolated DNA.

2.4.7 Polymerase chain reaction (PCR)

For amplification of specific DNA sequences, polymerase chain reaction was applied. The reaction was set up in a PCR tube using 100-200 ng of template DNA, 1-5 μ M specific primers (10 μ M), 1X buffer (10X), dNTPs and filled up to a total volume of either 20 or 50 μ l. For elongation Taq Polymerase was applied. The PCR was run according to the following table:

Table 2: program parameters applied for standard PCR.

| Step | Time | Temperature [°C] |
|--|---------------|------------------|
| 1. initiation | 5 min | 95 |
| 2. denaturation | 30 s | 95 |
| 3. annealing | 30 s | 50-70 |
| 4. elongation | 30 s to 2 min | 72 |
| 35 cycles repeating steps 2 – 4 | | |
| 5. termination | 10 min | 72 |

After PCR termination samples are cooled down to 4 °C and kept until they were further processed.

2.4.8 Real-Time Quantitative Reverse Transcription PCR (Real-Time qRT-PCR)

For isolation of mRNA, 1X10⁶ cells were detached from the cell culture plate, washed and pelleted. The cell pellet was directly applied for mRNA isolation without storage at -80°C. The isolation of mRNA was performed using the high pure RNA isolation kit (Roche, Basel, Switzerland). cDNA was generated by reverse transcription using random hexamer primer and 1 μ g of total isolated RNA as described in the manual of the transcriptor first strand cDNA synthesis kit (Roche, Basel, Switzerland).

2. Material and methods

For relative quantification of target genes, the real time PCR was performed as follows. Here, 100 ng of target cDNA was mixed with 500 nM specific primer pairs and applied to 1x Power SYBR® Green PCR Master Mix (Applied Biosystems, CA, USA) in an MicroAmp® Optical 96-Well Reaction Plate (Applied Biosystems, CA, USA). Then, the PCR was run as described in table.2, but using 40 cycles, using Light Cycler 480 Instrument (Roche, Mannheim, Germany).

Absolute quantification was conducted using calibration curves of corresponding plasmids to normalize for differences in primer efficiency. For absolute quantification, a dilution series of plasmids containing the cDNA for specific targets were prepared as follows: 10⁹, 10⁸, 10⁷, 10⁶, 10⁵ (= numbers of copies per μ l). Each dilution step containing calculated copy number of plasmid was mixed with 1x Power SYBR® Green PCR Master Mix (Applied Biosystems, CA, USA) and added to the PCR run with target primer pairs. Quantitative real-time PCR was run using Light Cycler 480 Instrument (Roche, Mannheim, Germany). Gathered Ct values were extracted from Light Cycler 480 instrument software and absolute quantification was performed using Microsoft Excel (Microsoft, Redmond, WA, USA).

2.5 Biochemical methods for protein analysis

2.5.1 Gel-electrophoresis and Western Blot

Proteins were separated according to their respective molecular mass by gel electrophoresis using SDS-polyacrylamide gels (SDS-PAGE). Identity of individual proteins was analysed by Western Blot and immunolabeling.

8% polyacrylamide gels were cast diluting 3.18 ml acrylamide/bis-acrylamide (30:1, BioRad) in separating buffer (1.5 M Tris pH 8.8, 0.4% SDS in H₂O) and 4.86 ml H₂O. The separating gels were polymerized in the BioRad (BioRad, Hercules, CA, USA) system using 200 µl 10% APS (Sigma, Saint Louis, MO, USA) and 10 µl TEMED (Roth, Karlsruhe, Germany). The stacking gel was cast using 1.15 ml acrylamide/bis-acrylamide (30:1, BioRad) diluted in 5.98 ml stacking gel buffer (0.15 M Tris pH 6.8, 0.3% SDS in H₂O). Two million HUVECs were lysed in 100 µl SDS-PAGE sample buffer (0.5 M Tris pH 6.8, 2% w/v SDS, 10% v/v glycerol, 100 mM β-mercaptoethanol, 100 mM bromophenol blue, Orange G). In order to compare retroviral expression of different FATPs in their respective HUVEC cell lines different volume dilutions originating from cell lysis was loaded into the gels. In brief, FATP5 and FATP6 cell lines 20 µl was loaded (100%). For FATP4 20 µl (100%), 1:2 dilution 20 µl (50%) and 1:4 dilution 20 µl (25%) was loaded onto the gel. The gel-electrophoresis was run in the BioRad system using running buffer (25 mM Tris base, 0.19M glycine, 0.1% SDS in H₂O) and electric current of 90V for 15 min while samples passed the stacking gel, then the gel was run with 180V until finished. The semi-dry Western Blot was performed using a combination of Whatman filter paper, nitrocellulose membrane, gel and another layer of Whatman paper soaked in blotting buffer (25 mM Tris base, 0.19M glycine, 0.1% SDS, 20% v/v methanol, H₂O). The Western Blot was run using 100 milliampere / membrane for 1 hour. After Western Blot, total protein on the nitrocellulose membrane was stained using Ponceau staining to evaluate the success and homogeneity of the Western Blot transfer. The nitrocellulose membrane was washed three times using TBS-Tween (10 mM Tris base, 0.15 M sodium chloride, pH 7.4, 0.05% Tween-20, in H₂O). Then, the nitrocellulose membrane was incubated in blocking solution (TBS-Tween, 3 to 5% milk powder) for 1 hour. The blocked nitrocellulose membrane was incubated with primary antibodies diluted in blocking buffer for 2 hours at RT or overnight at 4°C on a shaker. Then, the membrane was washed three times using TBS-Tween and incubated with the secondary antibody for 1

2. Material and methods

hour at RT on a shaker. For each lane the signal of target protein was normalized to the β -actin signal. When the secondary antibody was targeting both primary antibodies, the membrane was cut in halves each containing either the mouse target protein antibody or the mouse β -actin antibody. Applied antibodies are shown in lists of antibodies (3.4.3.). For capturing signals of different exposure times, Odyssey infrared imager (Li-Cor, Lincoln, Nebraska USA) was used. In order to semi-quantitatively evaluate the amount of detected target protein the Western Blot image was densitometrical analysed using Image Studio Lite (LI-COR Biosciences, Lincoln, NE, USA) software.

2.5.2 Immunofluorescence

For immunofluorescence, HUVECs at P1 or P6 were seeded on trans-well filter inserts (0,4mm; PC; 12-well) and grown until confluency (~72h). The filter membrane was cut and HUVECs were fixed with 4% paraformaldehyde for 20 minutes at room temperature. Then, the cells were washed twice with 1X PBS and once with SG solution (0.1% saponin, 0.5% gelatine in PBS). Permeabilization of membranes and blocking was performed in parallel applying SGB solution (0.1% saponin, 0.5% gelatine, 5 mg/ml fatty acid free BSA in PBS). When Triton-X was used as detergent to permeabilize membranes, then a solution containing 0.05% Triton-X in 1X PBS was prepared and applied to the fixed cells instead of SG solution. After permeabilization and blocking the cells were incubated with the primary antibody diluted in SGB solution for 60 minutes at room temperature. Next, the filter membranes were washed three times in 1X PBS and incubation with secondary antibody was performed in SGB solution for one hour. After incubation with secondary antibody, the filters were washed twice with 1X PBS and twice with SG solution. As a final step the filter membranes covered with immunolabelled HUVECs were placed onto mowiol (Calbiochem, San Diego, CA, USA). The images using 10 μ m scalebar were acquired using Olympus Bx41 microscope equipped with a UC90 camera (Olympus Soft Imaging System, Shinjuku, Japan), 60X objective PlanApo NA 1.40 Oil or 10X objective. Images including 200 μ m scalebar were acquired using Olympus iX50 microscope equipped with a CCD-camera (Olympus Soft Imaging System, Shinjuku, Japan), 10x plan objective.

2. Material and methods

2.5.3 Lists of antibodies

Table 3: list of primary antibodies applied in this study.

denotations: α is anti/against, IF is immunofluorescence, WB is Western Blot

| Species/ antigen | supplier | Application / dilution | Internal reference |
|---|--|-------------------------------|---------------------------|
| rabbit α-vWF | abcam (ab154193) | IF: 1/250 - 1/500 | J115 |
| mouse α-VE-Cadherin | Santa Cruz (sc-9989) | IF: 1/200 | J105 |
| rabbit α-FATP4 | abcam (ab200353) | WB: 1/1000 IF: 1/250 | J052L |
| rabbit α-FATP4 C4 C3/5 | affinity purified, laboratory database | WB: 1/20000, IF: 1/2000 | J052e |
| rabbit α-Acsl3 | abcam (ab151959) | WB: 1/2000 | J059g |
| mouse α-FLAG-tag | SIGMA (BioM2, F-1804) | WB: 1/2000 | J046e |
| mouse α-β-actin | SIGMA (clone AC-15, A5441) | WB: 1/40000 | J061 |

2. Material and methods

Table 4: list of secondary antibodies applied in this study.

denotations: IRDye is infrared dye; ex. is excitation; em. is emission; ab. is absorption; WB is Western Blot; IF is immunofluorescence; α is anti/against; nm is nanometre

| Species/ name of antibody | Supplier / internal reference | Application | Detection wavelength |
|--|---|--------------------|-----------------------------|
| goat α-rabbit IRDye 680RD | LICOR (926-68071), J090 | WB: 1/10000 | 694 nm |
| goat α-rabbit IRDye 800CW | LICOR (926-32211), J091 | WB: 1/10000 | 794nm |
| goat α-mouse IRDye 680RD | LICOR (926-68070), J092 | WB: 1/10000 | 694 nm |
| goat α-mouse IRDye 800CW | LICOR (926-32210), J093 | WB: 1/10000 | 794nm |
| donkey α-mouse Cy3 | Dianova (715-165-151), Jackson Immunoresearch, J101 | IF: 1/1000 | Ex.: 550 nm Em.: 570 nm |
| donkey α-rabbit Cy3 | Dianova (715-165-152), Jackson Immunoresearch, J113 | IF: 1/1000 | ex: 550 nm em: 570 nm |
| donkey α-rabbit Alexa 488 | Dianova (711-545-152), Jackson Immunoresearch, J104 | IF: 1/250 | ab: 493 nm em: 519 nm |
| donkey α-mouse Alexa 488 | Dianova (715-545-150), Jackson Immunoresearch, J081 | IF: 1/250 | ab: 493 nm em: 519 nm |

2.6 Biochemical methods for lipid analysis

2.6.1 Solubilization of [¹⁴C]OA and preparation of labelling mix

Stocks of radiolabelled and non-labelled oleic acids (details in table 5) were stored at -20°C and equilibrated to room temperature prior to usage. Radiolabelled oleic acid and non-labelled oleic acid were chemically identical except for one ¹⁴C atom instead of a ¹²C atom located at the carboxyl group of the radiolabelled molecule. To keep radioactivity per experiment at a minimum, radiolabelled and non-labelled oleic acid were mixed in a defined ratio by pipetting required volumes in a 2ml safe-lock Eppendorf tube. Then, solvents were evaporated under nitrogen flow. After evaporation of solvents, sodium hydroxide solution equimolar to 1.2 times of the total amount of oleic acid was added and mixed for 3 min at 37°C with 700 rpm on a warmed shaker. Then fatty acid free bovine serum albumin (FA-free BSA) dissolved in PBS was added. To ensure complete solubilization, the oleate-albumin mixture was thoroughly mixed for 15 min at 37°C with 700 rpm on a warmed shaker. After solubilization, the solution was transferred in a 50 ml Falcon containing EBM-2 (no FBS/FCS or other supplements). The resulting labelling mix was kept at 37°C for a maximum of 2 hours and vortexed just before applying to the target cells. When uptake or transport of oleate was evaluated by liquid scintillation counter a defined value between 0.1 to 0.4 Ci/mol of specific activity was applied in the labelling mix. When incorporation of lipids was determined by thin-layer chromatography and phosphorimaging, the specific activity of the labelling mix was adjusted at a defined value between 0.4 to 1 Ci/mol. The final concentration of oleate as well as the binding ratio to FA-free BSA is specific to the corresponding experiments and therefore given in the brief experimental description of the result figures.

2. Material and methods

Table 5: radiolabelled and non-labelled oleic acids applied in this study.

| Identity of oleic acid stock | Supplier | Specific activity (Ci / mmol) | Date of usage |
|-------------------------------------|---|--------------------------------------|----------------------|
| [¹⁴C]OA (hot) | Moravek Inc. (MC-406) | 0.054 | 2019 to 01/2022 |
| [¹⁴C]OA (hot) | Perkin Elmer (NEC-317) | 0.059 | 01/2022 to 09/2022 |
| [¹⁴C]OA (hot) | American radiolabelled chemicals Inc. (ARC 0279-50) | 0.055 | 09/2022 to 12/2022 |
| OA (cold) | SIGMA (O1383) | no-labeling | 2019 to 2022 |

2. Material and methods

2.6.2 Uptake of [¹⁴C]OA in adherent grown HUVECs

Three days prior to the experiment, 2.0×10^5 cells/well of corresponding HUVEC cell lines were seeded in collagen R (Serva, Heidelberg, Germany) coated 12-well plates (Corning, New York, USA) in technical triplicates. During the following two days the medium was exchanged on daily basis to allow HUVECs to differentiate and form typical cobblestone morphology. On day three, 1 hour prior to the experiment the growth medium (EBM-2, CC-3156, Lonza, Basel, Switzerland) was exchanged with growth medium lacking FCS/FBS and other supplements. Then cells were washed twice with 1x PBS and incubated in labelling mix (e.g. 200 μ M [¹⁴C] oleic acid (0,1 Ci/mol), 50 μ M fatty-acid free BSA, in EBM-2) for defined time duration (e.g., 3 hours). Afterwards cells were washed twice with 1xPBS and lysed (1% SDS, 0,5M NaOH in H₂O). Radioactivity in cell lysate was determined with a scintillation counter (Wallac 1414, Perkin Elmer, Waltham, MA/USA) and normalized to total cellular protein content using Pierce™ BCA Protein Assay Kit (cat.no:23227, ThermoFisher Scientific, Waltham, Massachusetts, USA). The schematic overview of the experimental approach is shown in figure 2.

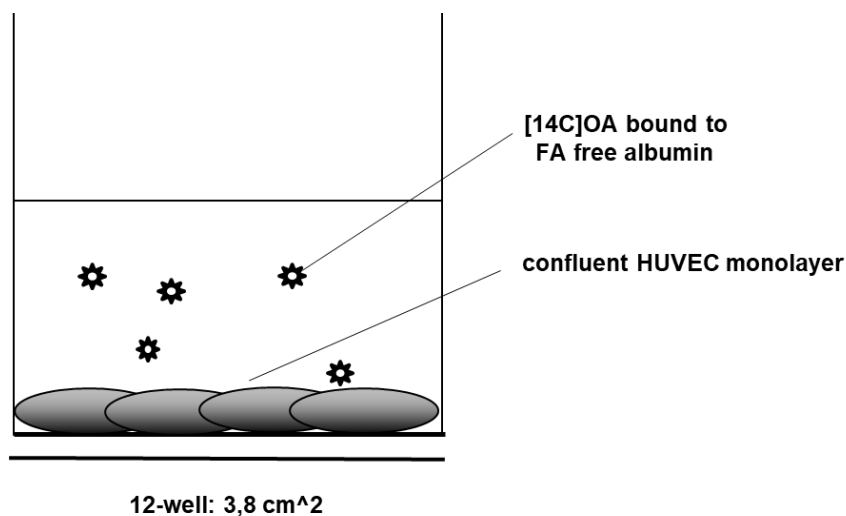


Figure 2: Schematic figure illustrating the experimental approach to measure [¹⁴C]OA uptake in adherent grown endothelial cells (HUVECs).

2. Material and methods

2.6.3 Transport of [^{14}C]OA across HUVECs grown on transwell filter

Three days prior to the transport experiment, transwell filter inserts (details in table 6) were coated with 200 μl of a dilution of 150 $\mu\text{g}/\text{ml}$ collagen R (SERVA, 0.2% in acetic acid, 2mg/ml) in 1X PBS and incubated for at least 15 min at 37°C in the cell culture incubator (NAPCO Series 5400 CO₂ Incubator, Labotect GmbH, Göttingen). After washing the filter inserts once with 1X PBS, 2x10⁵ HUVECs / transwell were seeded in the apical compartment of the transwell filter in a final volume of 0.5 ml EGM-2. Then, 1.5 ml EGM-2 was added to the basolateral compartment. The cells were cultured for 72h with daily medium exchange until the transport experiment was performed.

One hour prior to the transport experiment the medium in the transwell system (details about transwell filters are given in table 6 and figure 4) was exchanged with EBM-2 (EGM-2 w/o supplements, w/o FBS or FCS). In the next step, the EBM-2 in the apical and basolateral compartment was discarded and the pre-prepared labelling mix (according to 3.5.1) was applied to the apical compartment. The EBM-2 media in the basolateral compartment was exchanged with EBM-2 including either non-defatted albumin (A4503, Sigma, Saint Louis, MO, USA) or FA-free albumin (A7030, Sigma, Saint Louis, MO, USA) depending on the aim of the experiment. As shown in figure 3, when pulse / chase experiments were performed, the transwell filters were transferred in a 6-well plate (Corning, New York, USA) for the duration of the pulse/ labelling of HUVECs and re-assembled in the 12- well plate for the duration of the chase.

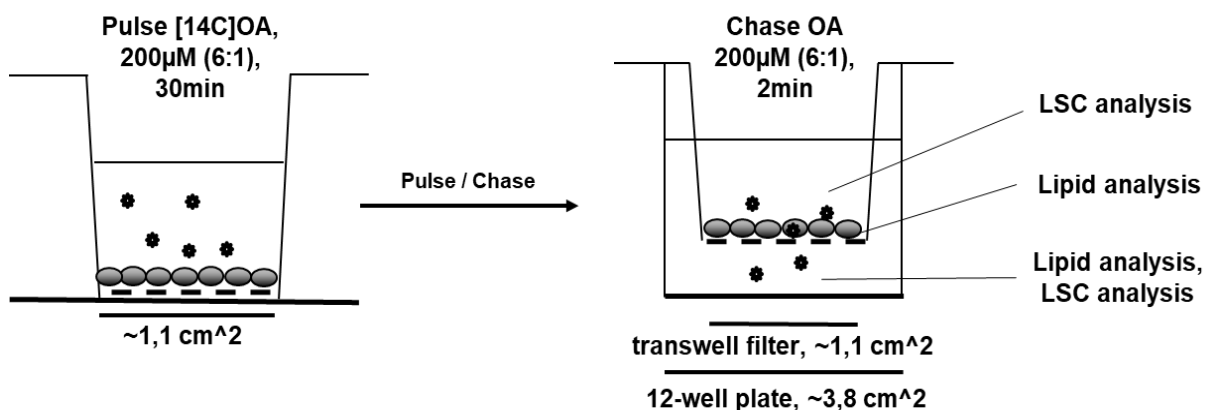


Figure 3: Schematic overview of a pulse/ chase experiment applying HUVECs grown on trans-well filter inserts.

2. Material and methods

The target cells were grown on transwell filters and labelled with [14C]OA bound to albumin while the transwell filter was put onto the well bottom of a 6-well plate (Corning, New York, USA) simulating OA uptake in adherent grown cells. Then, the transwell filter was washed twice, transferred in a 12-well plate and release of [14]OA from the endothelial cells was investigated by liquid scintillation counting (LSC) and lipid analysis after incubation with non-labelled OA bound to albumin. The experimental approach enables assessment of release of [14C]OA after incorporation in HUVECs. The concentrations of oleate, the binding ratio to FA-free BSA and the composition of the basolateral media varied between the different experiments and is therefore given in the respective figure legends in the results.

2. Material and methods

Table 6: Transwell filter inserts applied in this study.

| Well plate format | Cat.No. / Supplier | material | Pore Size /diameter (mm) | Pore density Pores/cm ² | Growth area (cm ²) |
|-------------------|---|---|--------------------------|------------------------------------|--------------------------------|
| 12-well plate | 3401 / Costar Corning, New York, USA | Polycarbonate (PC, translucent, not clear) | 0.4 mm | 10 ⁸ | 1.12 |
| 12-well plate | 931 04 02 / Cellqart, Sabeau, Northeim, Germany | Polyethylenterephthalat (PET, translucent, not clear) | 0.4 mm | 10 ⁸ | 1.1 |

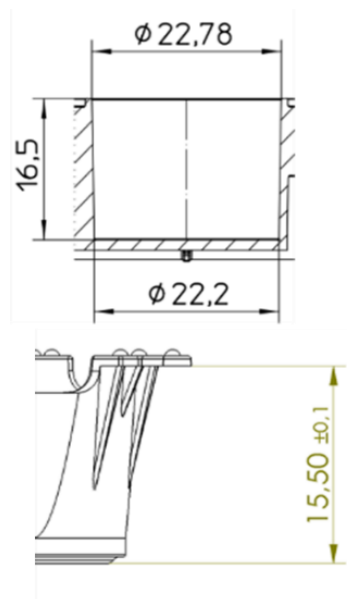


Figure 4: Spatial dimensions of one transwell filter.

Filter type: Sabeau, PET (translucent), item no.: 931 04 02 (<https://cellqart.com/resources/drawings-and-specifications>, date: 08.11.2022), numbers are given in millimetres.

2. Material and methods

2.6.4 Lipid Extraction

For extraction of lipids cells were lysed in methanol/ chloroform (2:1) for 5 min at 37°C and 300 rpm on a plate shaker. Cell lysates were transferred in chloroform/ H₂O (3:1) and mixed thoroughly by vortexing. Then, samples were centrifuged for 1 min at 13000xg. After phase separation occurred, the lipid phase (lower phase) was transferred in a fresh safe-lock Eppendorf tube. For quantification of total labelled lipids, an aliquot from the isolated lipids was removed and CPM were measured using liquid scintillation counter. The remaining isolated lipids were dried by evaporating the solvents in a vacuum centrifuge (Concentrator 5301, Eppendorf, Hamburg, Germany). Dried lipids were stored at -20°C until they were further processed.

2.6.5 Thin-layer chromatography

Different lipid species were analysed applying thin layer chromatography. For preparation of the solid state, silica gel aluminium plates (Merck 1.05582.0001) were prepared/cleaned in a pre-run with methanol as liquid phase/ solvent. Then, the TLC plate was dried for two hours at 105°C in a heating oven. Lipids from cell lysates were extracted as described previously (3.5.2 Lipid Extraction). Dried lipids were resuspended in methanol/ chloroform (2:1) and spotted on the concentration zone of the TLC plates. Then, the plate was put in the pre-equilibrated running chamber and run with chloroform: ethanol: water: triethylamine in the ratio 35:40:9:35 as running solvent. After ~45-55 min, when the running solvent reached the desired running length of 100 mm, the plate was taken out of the running chamber and dried for two hours at 105°C in a heating oven. Next, the TLC plate was put onto a phosphorimaging plate and developed with the BAS-1500 system (Fuji, Tokyo, Japan). The densitometric image analysis was performed using the AIDA analyzer (Raytest, Straubenhardt, Germany). The identification of lipid species was based on determination and comparison of their specific retention factor (R_f). The R_f values of respective lipid species are shown in table 7. The standardized retention factors of individual lipid species were taken from literature and documentation of laboratory experience [69, 75].

2. Material and methods

Table 7: Rf standards of different lipid species.

Running length according to their appearance in the chromatogram using O-Mix as running solvent and silica gel aluminium plates (Merck 1.05582.0001) as solid state.

| Lipid species | Retention factor (R_f) | Lipid class |
|--------------------------------------|---|-----------------------------|
| Sphingomyelin (SM) | 0.02 - 0.06 | Sphingolipid / phospholipid |
| Phosphatidylcholine (PC) | 0.04 – 0.09 | Phospholipids |
| Phosphatidylinositol (PI) | 0.18 – 0.22 | |
| Phosphatidic acid (PA) | 0.18 – 0.22 | |
| Phosphatidylethanolamine (PE) | 0.23 – 0.29 | |
| Non-esterified OA (NEFA) / OA | 0.52 – 0.59 | NEFA / OA |
| Diacylglycerol (DG) | 0.82 – 0.83 | Neutral lipids |
| Triacylglycerol (TG) | 0.84 – 0.85 | |

2. Material and methods

2.6.6 Acyl-CoA synthetase activity assay

Acyl-CoA synthetase activity was determined according to Füllekrug and Poppelreuther described in “Measurement of long-chain fatty acyl-CoA synthetase activity” [76].

Two million HUVECs were lysed in KTX-buffer (130 mM KCl, 25 mM Tris-HCl, pH 7.4, 1% TritonX-100) at 4°C for 30 min. Samples were centrifuged and supernatant was collected whereof 10 µl respective sample was incubated in reaction mix (100 mM Tris-HCl pH 7.4, 5 mM MgCl₂, 200 µM DTT, 10 mM ATP, 200 µM CoA, 0.1% Tx-100 and 20 µM [14C]oleate bound to 5 µM fatty acid free BSA (10 Ci/mol)). After 10 min incubation at 30°C the reaction was terminated applying Dole’s solution (conc. ratio of Isopropanol: Heptane: H₂SO₄ 40:10:1). The extraction of unreacted radiolabelled oleate was performed by repeating washing with heptane and applying phase separation by centrifugation followed by discarding the oily phase. In the last step, the aqueous phase containing radiolabelled oleoyl-CoA was collected and the radioactivity was determined by scintillation counting.

2.6.7 Uptake of fluorescent labeled fatty acids (Bodipy-C12)

The applied Bodipy-FA was Bodipy-C12 (4,4-difluoro-5,7-diphenyl-4-bora-3a,4a-diaza-s-indacene-3-dodecanoic acid, D3823, life technologies, California, USA). For the experimental approach, 1x10⁵ HUVECs / well were seeded into one well of a 24 well plate (Corning, New York, USA) in a final volume of 0,5 ml EGM-2 medium (Lonza, Basel, Switzerland). HUVECs were cultivated for 72 hours with daily media exchange (EGM-2). One hour prior to the experiment, the cells were serum-starved by exchanging the medium with EBM-2 (Lonza, Basel, Switzerland). After 1h incubation the EBM-2 was replaced with 200 µl Bodipy-FA working solution (2 µM Bodipy-FA, 1 µM fatty acid-free albumin in EBM-2) and incubated for defined time intervals. As control, HUVECs were incubated without Bodipy-FA solution or HUVECs were fixed using 4% PFA prior to the addition of Bodipy-FA. After Bodipy-FA incubation the HUVECs were washed twice with 0,5ml 1X PBS then 0,5ml 0,4% Trypan-Blue diluted in 1X PBS was added to quench the extracellular signal. Then, intracellular fluorescence was measured immediately (bottom-read) with a microplate reader (excitation 488 nm, emission 515 nm, cut-off 495 nm, SpectraMax M5, Molecular Probes).

2.7 Biophysical and biochemical methods to assess barrier function of confluent grown HUVECs

2.7.1 Trans-endothelial electrical resistance

2x10⁵ HUVECs / insert were seeded into one pre-coated transwell filter insert (Corning, New York, USA or Sabeau, Northeim, Germany) in a final volume of 0,5 ml EGM-2 medium (Lonza, Basel, Switzerland). The transwell filters were placed into the cellZscope (nanoAnalytics, Münster, Germany). Then, measurements of trans-endothelial electrical resistance (TEER) were performed according to automated software of the cellZscope. The culture medium was exchanged as indicated in the respective results figure. Raw data values were normalized using correction to blank filter.

2.7.2 Transport of 70kDa Fluorescein isothiocyanate-Dextran (FITC-dextran)

2x10⁵ HUVECs / insert were seeded into one pre-coated transwell filter insert (Corning, New York, USA or Sabeau, Northeim, Germany) in a final volume of 0,5 ml EGM-2 medium (Lonza, Basel, Switzerland). The transwell filter inserts were transferred in a 12-well plate and after addition of 1.5ml EGM-2 to the basolateral compartment, the filters were cultivated for 72h with daily media exchange. After 72h, the media in the basolateral and apical compartments were discarded and 0.5ml FITC-dextran (FD70S-100MG, Sigma-Aldrich, Steinheim, Germany) solution (0.1 mg/ml in EBM-2) was applied in the apical compartment, immediately followed by addition of 1.5ml EBM-2 to the basolateral compartment. Every 10 minutes, the plate was gently mixed and 10µl sample was taken from the basolateral compartment and replaced by 10µl EBM-2. The samples were transferred in a clear 96-well plate (Costar, Washington, USA) containing 90µl EBM-2 and fluorescence was measured (bottom-read) with a microplate reader (excitation 492 nm, emission 515 nm, cut-off 520 nm, SpectraMax M5, Molecular Probes).

3. Statistics and Software

Results were analysed applying Microsoft Excel (Microsoft, Redmond, WA, USA). If there is no other indication, the results are presented in mean \pm SD and statistical significance is calculated using student's t-test. Software applied for evaluation of individual methods is given in chapter 3. Materials and methods.

4. Results

Trans-endothelial fatty acid transport consists of three important steps: uptake of FAs, intracellular trafficking, and release to the basolateral side. In this study, HUVECs were assessed for their barrier function while grown on transwell filter. Upregulation of FATP4 activity in endothelial cells was tested for the efficiency to drive FA uptake. At last, HUVECs were cultured on trans-well filter inserts and the path of radiolabelled oleate from the apical to the basolateral side of endothelial cells was traced using pulse/ chase experiments. In addition, the impact of varying extracellular FA concentrations, alterations of intracellular metabolism and shifts in extracellular demand for FAs was tested to affect FA uptake and transport.

4.1 Aim 1: Characterization of primary endothelial cells (HUVECs), evaluation of growth parameters and assessment of barrier function

In this study HUVECs were acquired by isolation from umbilical cords. As the isolation procedure includes a risk of potential contamination with other cell types from surrounding tissue, the cells were qualitatively analysed for HUVEC specific biomarkers. Next, size dimensions were elaborated to classify the intracellular FA trafficking regarding spatial dimensions. In addition, barrier functions of HUVECs grown on transwell filters was assessed.

4.1.1 Morphological and biochemical identification of HUVECs

HUVECs were isolated from umbilical cords by dispase treatment, seeded on collagen-coated cell culture dish and characterized by phase-contrast microscopy regarding HUVEC specific cobblestone morphology. In addition, expression of vascular endothelial cadherin (CD-144) and Von-Willebrand-Factor (vWF) was confirmed by immunofluorescence.

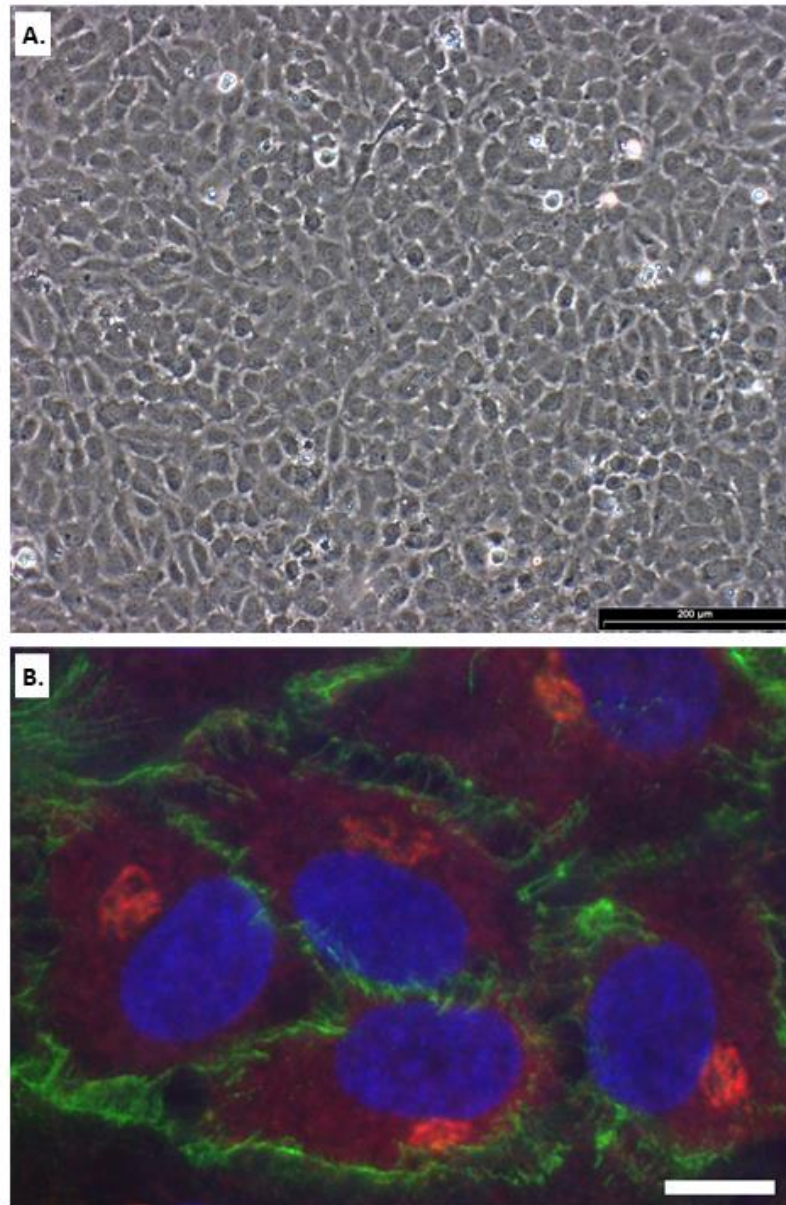


Figure 5: Characterization of endothelial cells.

A. Confluent HUVEC monolayer with cobblestone morphology in collagen coated ~60mm cell culture dish at P0 (~7d after isolation). scalebar is 200μm. **B.** Immunofluorescence of endothelial biomarker. von-Willebrand-Factor (red) was detected in Golgi-like cluster in perinuclear space. VE-Cadherin (green) was detected at cell borders and cell-cell connections. Nuclei were stained using HOECHST dye (blue). scalebar is 10μm (B.) and 200μm (A.).

4. Results, Aim 1

4.1.2 Spatial dimensions of endothelial cells (HUVECs) and their growth parameters on trans-well filter

Trans-endothelial FA transport requires FAs to overcome the intracellular lumen of endothelial cells, therefore the distance from the apical to the basolateral side is an important parameter to consider. In vivo, endothelial cells undergo different states of sizes, as vasodilation and vasoconstriction lead to extension and contraction of blood vessels and their basic modules, which are the endothelial cells. The heterogeneity and momentum of endothelial cells makes acquisition of precise information difficult. However, the general length of cells ranges between 10-100 μM , endothelial cells cover an area of roughly 600 – 1200 μm^2 with a length to width ratio of 7.45 to 2.60. The height of endothelial cells is given at around 0.1 to 1 μm depending on the origin of the human body.

In this study, HUVECs were seeded and cultured on trans-well filters until cells displayed a confluent monolayer. For evaluation of size dimensions in this context, adjacent cell borders were labelled and imageJ was applied for measuring area and circumference of HUVECs. In addition, the volume of spherical HUVECs was measured just after detaching from cell culture plates. Assuming that the volume of HUVECs just after detaching is the same as while attached to the plate, the height of HUVECs was calculated by dividing the volume by the area.

As shown in figure 6, there are protuberances observable at the cell borders making the cells appear inconsistent round. These excrescences were remnants of retraction fibres resulting from detachment from other cells in the united cell structure prior to EDTA/Trypsin treatment. As there were still cell-cell connections remaining directly after detaching, the HUVECs were floating in the medium as clumps. For evaluation of the diameter of single cells, a line was drawn through individual cells and the number of pixels was measured. Then, the number of pixels in the size bar was measured and compared to the true length. As a result, the number of pixels in the line (example is marked red in image) through the diameter, were translated into measurement unit (μm). The acquired mean radius of 7 individual cells was $4.4 \pm 0.4 \mu\text{m}$ and the consequential volume assuming a sphere was $360.6 \pm 90,6 \mu\text{m}^3$.

In the next step the area covered by HUVECs on trans-well filter inserts were investigated. Here, HUVECs were grown on trans-well filter inserts and cell borders were

4. Results, Aim 1

labeled by immunofluorescence of VE-Cadherin. As shown in figure 7, the VE-Cadherin staining was observed to be located between the cell-cell contacts and providing clear separation between individual cells, the staining was used for measuring the size dimensions in HUVECs grown on trans-well filters. For evaluation ImageJ was applied to measure the length of the image scalebar in pixel and the amount of pixel was taken in consideration for the true length in the image. Then HUVECs were manually encircled, and the included pixel numbers were transferred in μm resulting in an average area covered by one HUVEC of $409 \pm 102 \mu\text{m}^2$. In addition, the total size of the image ($180.5 \mu\text{m} \times 144.6 \mu\text{m}$) was divided by the total number of cells in the image (63) resulting in $411,4 \mu\text{m}^2$ per single cell. The high similarity ($\sim 99.5\%$ identity) of both values showed that the filter area within the image section was completely covered by cells.

In the next step, the height of HUVECs grown on trans-well filter was calculated assuming that the volume is constant and HUVECs obtain a squared shape. As shown in figure 8, assuming the volume of HUVECs just after detaching is equal to their volume while attached, the calculated height by dividing the volume with the area is $\sim 0.88 \mu\text{m}$.

As shown in table 8 and in methods figure 4, the height of the trans-well insert is $15.5 \pm 0.1 \text{ mm}$ leaving $\sim 1 \text{ mm}$ space between the bottom of the well plate and the underside of the filter. Assuming that the average size of a cell is ~ 10 to $100 \mu\text{m}$, the remaining space underneath the filter towards the co-cultured cell leaves more than ~ 990 to $900 \mu\text{m}$ of space filled with aqueous solution. As aqueous solution without carrier builds up an artificial obstacle for hydrophobic fatty acids, albumin was applied for simulation of physiological conditions, when experiments were performed. Another important parameter is the total area of transport, which is given by the total growth area available on the filter, which is $\sim 1.1 \text{ cm}^2$. Taking in account that the diameter of one pore is $0.4 \mu\text{m}$ and assuming that the pores are equally round, the open area of one pore is $\sim 0.126 \mu\text{m}^2$ and the total open area available for transport within the plastic filter is $\sim 11.4\%$ of the total filter area. Furthermore, if the pores are equally distributed, the open area located underneath one HUVEC with a total area of $\sim 409.3 \mu\text{m}^2$ is $46.7 \mu\text{m}^2$ for each cell. Regarding the spatial dimension of the trans-well filter, especially the membrane thickness ($11.5 \pm 0.2 \mu\text{m}$) and open space ($11,4\%$ of total area), the plastic filter represents an unphysiological obstacle for FA to overcome.

4. Results, Aim 1

Taken together, for FAs to travel from the apical compartment to the basolateral compartment, they need to cross 0.88 μm endothelial cell lumen and 11.5 μm filter membrane that is restricted to an open area of 11.4%.

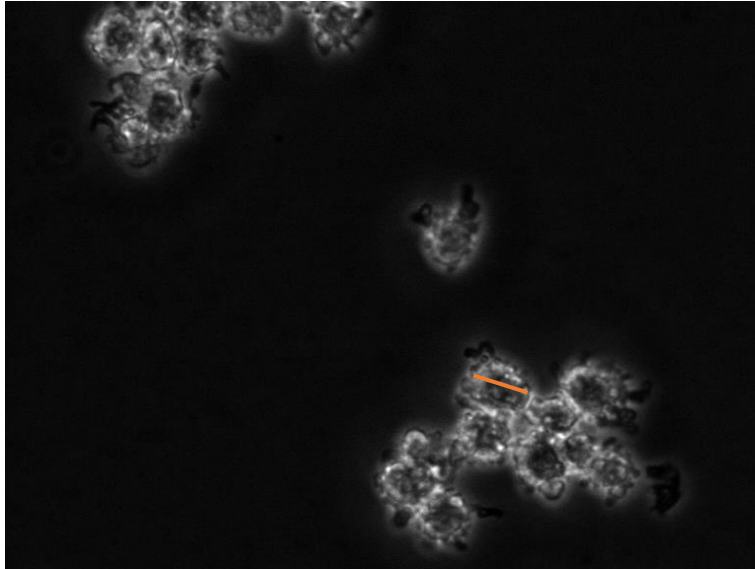


Figure 6: Image of HUVECs just after detaching from a cell culture plate.

HUVECs at P1 were seeded on collagen-coated cell culture plates and were grown until confluency, then HUVECs were detached applying 0.05% EDTA/Trypsin solution. HUVECs were observed and images were taken directly after detaching. Red bar shows example for measuring the diameter from one HUVEC cell. The mean radius was $4.4 \pm 0.37 \mu\text{m}$.

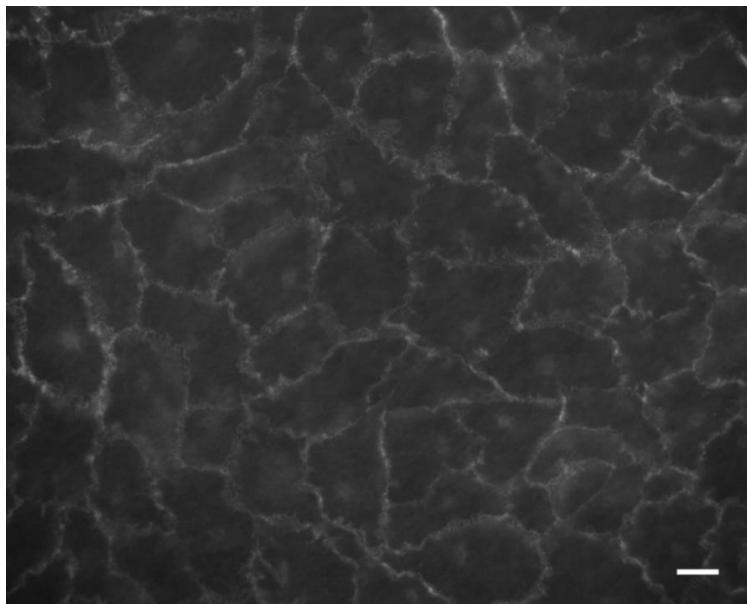


Figure 7: IF of endothelial marker (VE-Cadherin) expressed in isolated HUVECs.

HUVECs at P1 were seeded on trans-well filter inserts (0,4 mm; PET translucent; 12-well, SABEAU) and grown until confluency, HUVECs were fixed using 4% paraformaldehyde followed by disruption of cell membrane using 0,5% Triton-X, immunofluorescence staining of VE-Cadherin (green) was performed. scalebar is 10 μM .

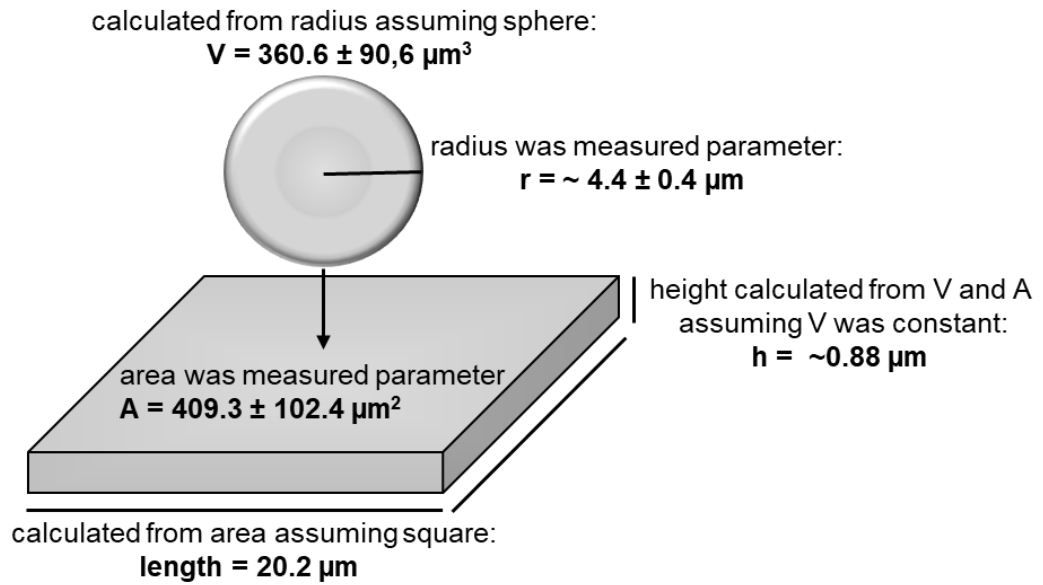


Figure 8: Schematic overview on mean height calculation of endothelial cells.
 Volume and Area of HUVECs was obtained from evaluations of figure 6 and figure 7.

Table 8: Spatial dimensions and resulting growth parameters of HUVECs on transwell filter.

| Parameter | Size dimension |
|-------------------------------------|-----------------------|
| Growth area of filter insert | 1,12 cm ² |
| Diameter of pores | 0,4 μm |
| Area of one pore | 0,126 μm ² |
| Pore/open area of the filter | 11,4 % |
| Pore/open area covered by one HUVEC | 46,7 μm ² |
| Area covered by HUVEC | 409,3 μm ² |

4. Results, Aim 1

4.1.3 The confluent monolayer of HUVECs maintains barrier functions while grown on transwell filter

In order to assess the barrier function of confluent grown HUVECs, the integrity of the cellular monolayer was quantitatively analysed by trans-endothelial electrical resistance (TEER) and evaluation of transport rates using FITC-dextran. In addition, the disruption of barrier functions was induced by EDTA treatment and following changes in transport rates of FITC-dextran and changes in VE-Cadherin specific signal was assessed.

As shown in figure 9, the electrical resistance across the filter membrane increases while HUVECs settle down from suspension and adhere to the filter membrane. After around 24h medium was exchanged, which resulted in a drop in TEER compared to blank filter (12 to ~8). This might be a result of temperature change, culture media change (complex mixture of different molecules that influence conductivity), disposal of dead cells in media or short-term decrease in cellular permeability due to cell stress during media exchange. After ~40h the TEER values equilibrated between 13-14 and media was exchanged again at ~50h with either EGM-2 or EGM-2 + 10mM EDTA. During the initial 30 min after media exchange with EDTA the TEER values dropped ~50%, after ~2 hours the TEER values dropped below the difference to the blank filter (empty filter control). The untreated control dropped slightly and equilibrated at a value around 12. After TEER measurement the trans-well filter was used for immunofluorescence of VE-Cadherin to visualize the effect of EDTA treatment on VE-Cadherin. Endothelial cells build up a confluent monolayer with ubiquitously expressed VE-Cadherin signal which was disrupted by applying EDTA to remove bivalent cation ions. As shown in figure 9 B.1, the VE-Cadherin specific signal in untreated cells is located near cell-cell contacts and located all around the cell borders. After application of EDTA (fig. 9 B.2), the signal at the cell periphery is lost and unspecific, blurred signal accumulates randomly throughout the cells.

As shown in figure 10, the cellular barrier successfully retains FITC-dextran (~70kDa). Applying EDTA to disrupt VE-Cadherin increases the transport rate of FITC-dextran across the cellular barrier.

Taken together, HUVECs seeded on trans-well filter membranes build up a measurable cell barrier assessed by an increase in electrical resistance (TEER). The cellular barrier is

4. Results, Aim 1

based on VE-Cadherin specific adherence junctions and can be disrupted by chelating bivalent cation ions required for the functionality of cell-cell contacts.

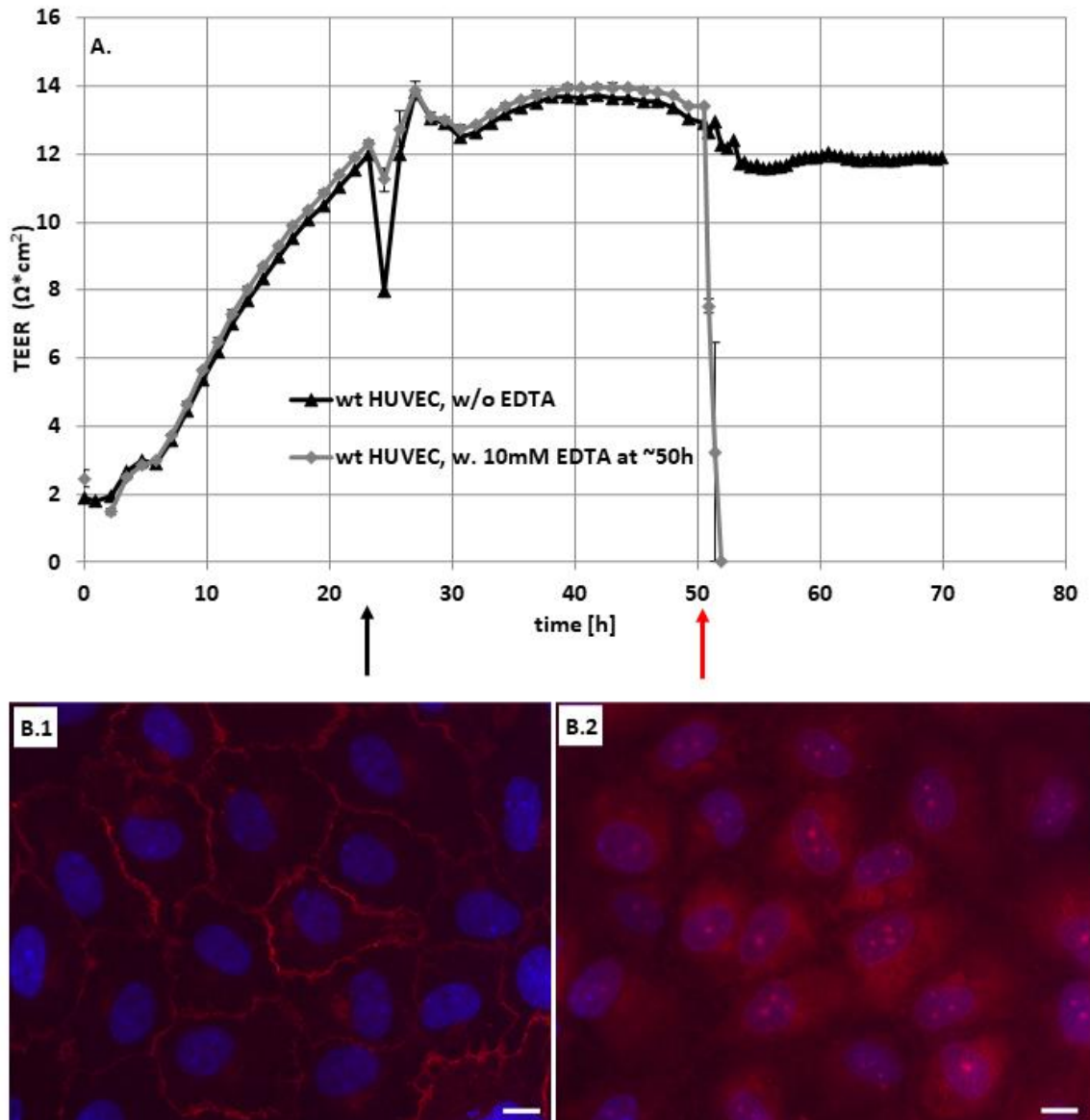


Figure 9: HUVECs provide electrical impedance caused by VE-Cadherin related adherence junctions that can be disrupted by EDTA treatment.

A. TEER values are normalized to blank filter (values >0 indicates increase in electrical resistance compared to blank filter). Culture media was exchanged after ~24h (black arrow). Exchange of media w/o EDTA vs. w. 10mM EDTA after ~50h (red arrow). Results show mean \pm SD of technical duplicates (individual seeded filters). **B.** IF of VE-Cadherin (red) of HUVECs from TEER experiment after ~72h. **B.1** untreated HUVECs **B.2.** HUVECs treated with 10mM EDTA

4. Results, Aim 1

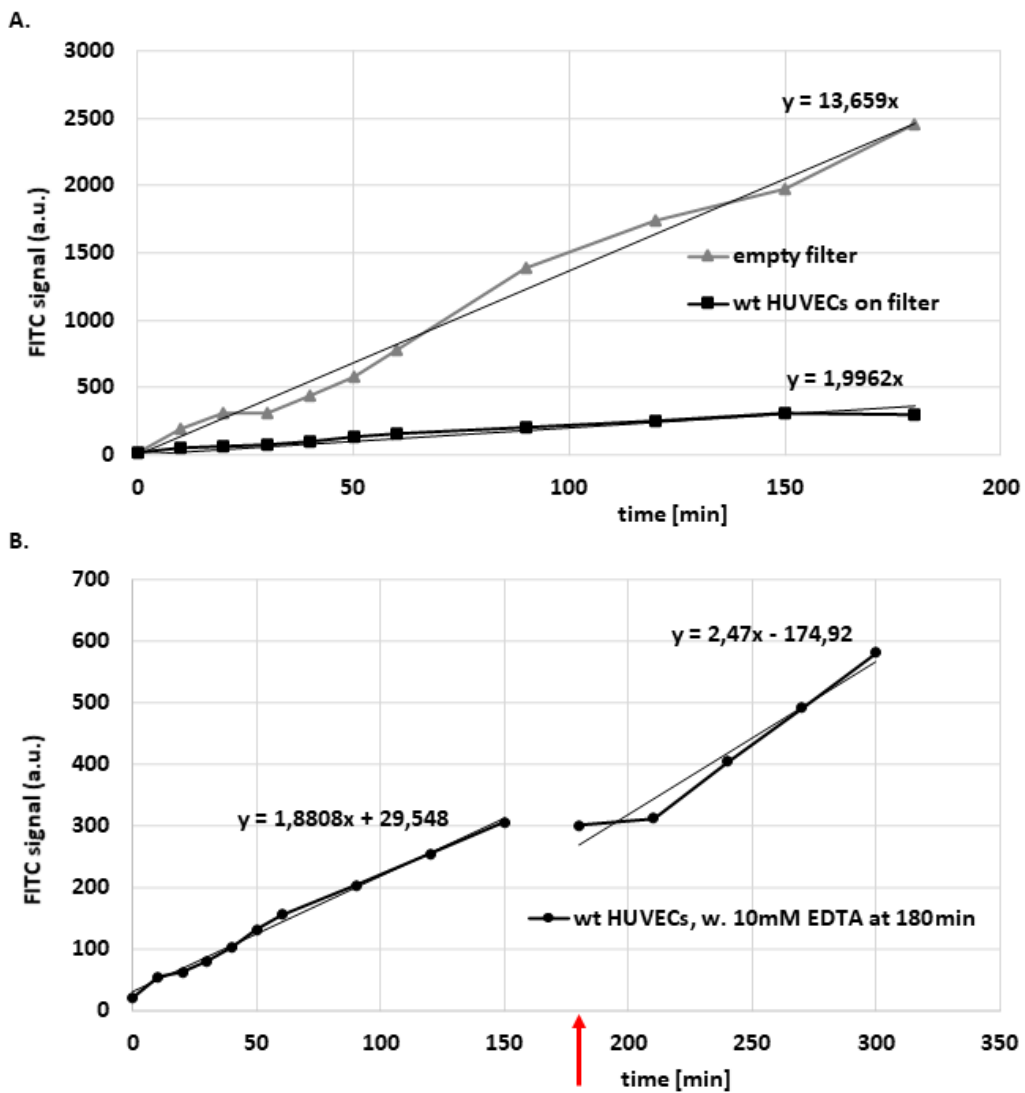


Figure 10: HUVECs diminish the transport of FITC-dextran across the filter membrane. Slope was applied as a mean of transport rates (signal / time). Results include one independent experiment. Difference between empty filter and confluent HUVEC monolayer was confirmed in two independent experiments. Here, focus on effect of EDTA treatment is shown **A**. Transfer of FITC-dextran (70kDa) across empty filter (grey line, triangle dots) vs. HUVECs grown on filter (black line, square dots). **B**. Transfer of FITC-dextran through trans-well filter covered with HUVECs. After 180 min, HUVECs were treated with 10mM EDTA (red arrow).

4.2 Aim 2: Evaluation of the effect of increased FATP4 activity on FA uptake in primary endothelial cells (adherent HUVECs)

The initial process for trans-endothelial FA transport is the apical uptake into endothelial cells. One prominent hypothesis assumes that the FA uptake correlates with upregulation of intracellular ACS enzymes, such as FATP4. In order to test this hypothesis, the impact of different extracellular FA concentrations was weight against the impact of upregulation of the FA transport protein FATP4 to drive FA uptake into endothelial cells.

The endogenous abundance of different ACS enzymes was assessed and their individual contribution to the total ACS activity was evaluated. Then, a retroviral expression system followed by antibiotic selection to receive a pool of HUVECs overexpressing FATP4 (FATP4.HUVEC / FATP4) was applied. In addition, HUVECs, were transduced with an empty vector as control (prvU6.HUVEC / prvU6). Then, different extracellular FA concentrations were tested against FATP4 overexpression for their impact on FA uptake. In addition, changing extracellular FA availability was simulated by switching the binding ratio of FA and albumin in the extracellular compartment. Lastly, intracellular lipids were analysed in FATP4.HUVECs vs. prvU6.HUVECs (control).

4.2.1 Expression of FATPs and other acyl-coA synthetases in HUVECs

FATPs and other ACS enzymes were analyzed for their endogenous abundance in HUVECs using Qualitative Real-Time PCR (qPCR). Then, qPCR using specific calibration plasmids and absolute quantification was applied to compare expression levels of abundant candidates. In order to evaluate their individual contribution to the total cellular ACS activity, individual ACS enzymes were upregulated, and total ACS activity was assessed in cell lysates of corresponding cell lines.

As shown in figure 11, among the Acsl family, Acsl 4 showed the highest relative expression followed by Acsl3. Acsl 1, Acsl 5 and Acsl 6 as well as FATP1, FATP2 and FATP3 displayed a marginal difference compared to water control and were therefore considered as not expressed in HUVECs. The other FATP members, i.e. FATP4, FATP5 and FATP6, were expressed. Taken together, the proteins Acsl3, Acsl4, FATP4, FATP5, FATP6 were endogenously abundant in HUVECs. PCR efficiency varies depending on template and primers. Hence, efficiency corrected qPCR using calibration plasmids and standard curves was applied.

4. Results, Aim 2

As shown in figure 12, the mRNA of FATP4 was the most abundant among endogenously expressed FATPs, followed by FATP5. The amount of mRNA of FATP6 was around 64% less abundant than FATP4. In comparison to Acsl3 and Acsl4, other Acsls were ~10 times higher expressed than FATPs. Here, Acsl3 displayed increased endogenous expression compared to Acsl4.

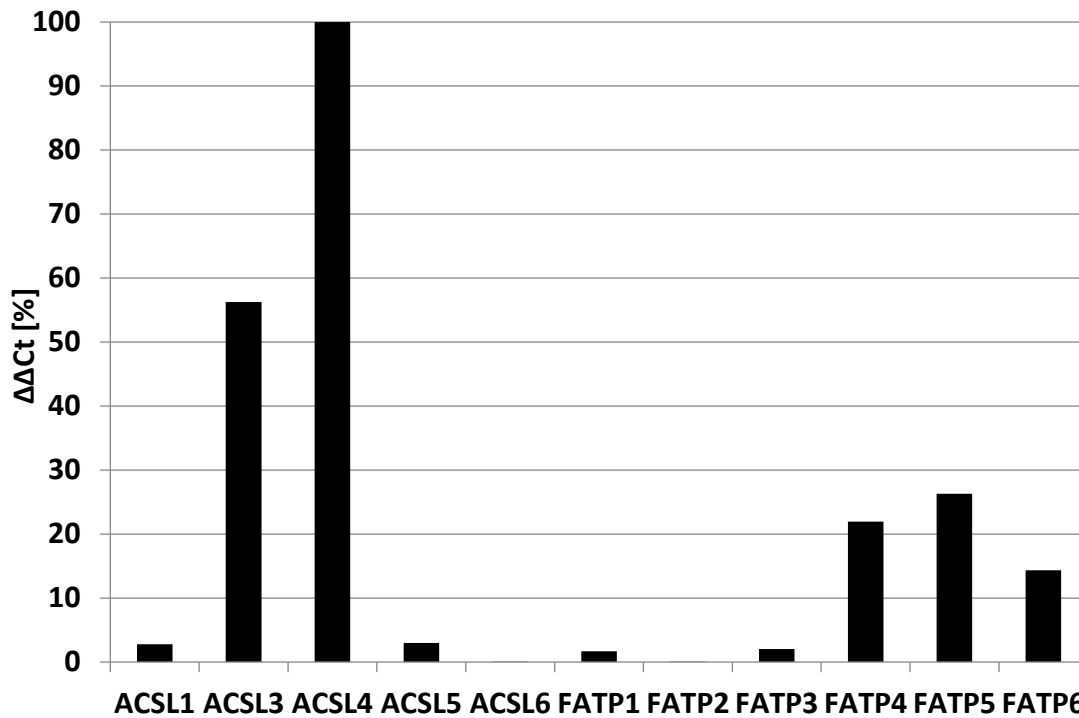


Figure 11: Relative comparison of expression levels between different target proteins of the Acsl and FATP families.

For data analysis Ct values for target proteins were first normalized to the Ct value of β -actin to acquire Δ Ct. Then, Δ Ct values were normalized to the Δ Ct value of Acsl4 (highest expression profile). Bar charts represent mean of technical triplicates of one experiment. SD was <5% of mean.

4. Results, Aim 2

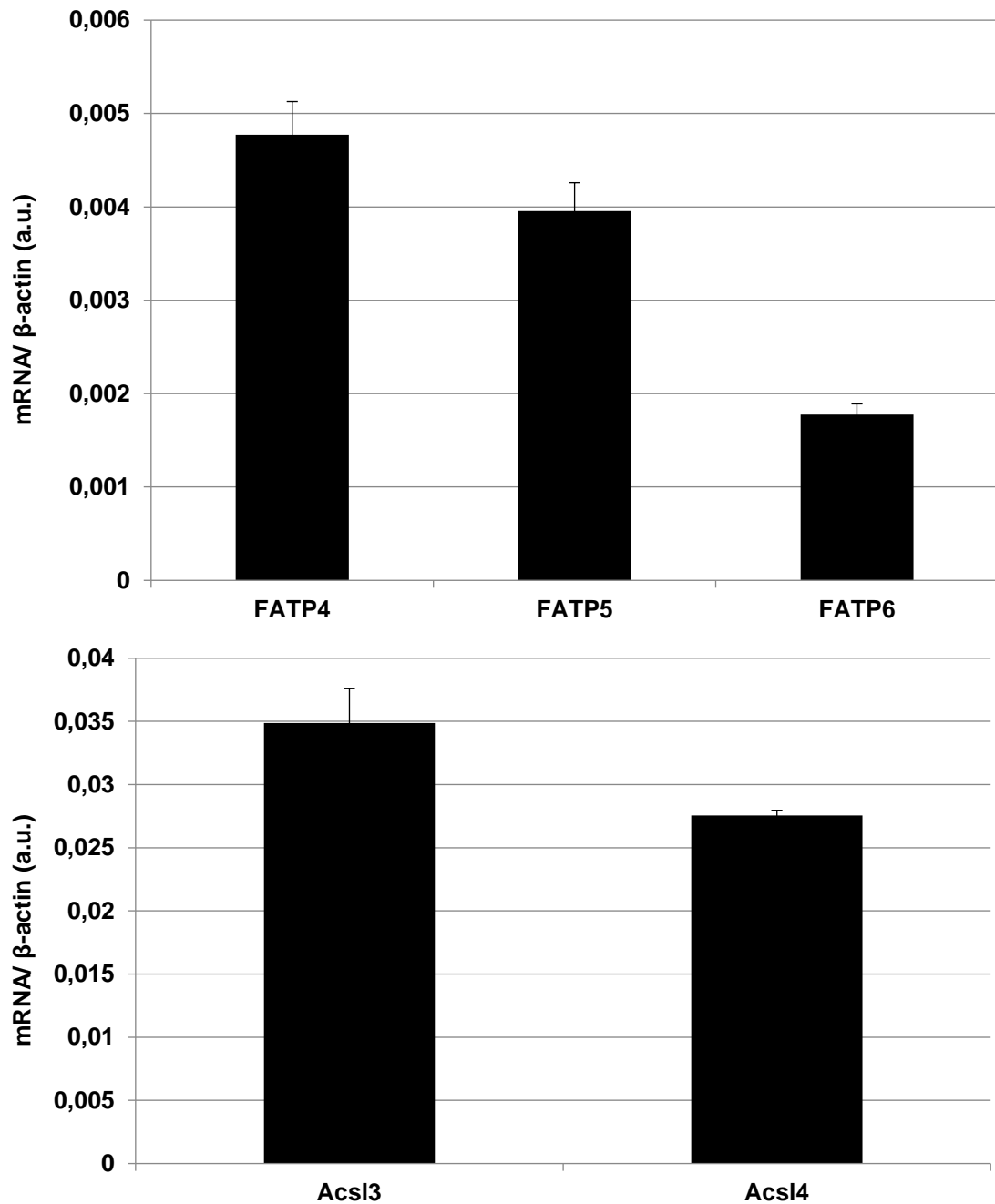


Figure 12: Absolute quantification of Acsl and FATP members with endogenous expression in HUVECs.

Quantities of mRNA were defined using serial dilution of corresponding plasmids and results were normalized to β -actin. Note the different scales for FATP vs. Acsl. Acsls were found to be ~ 10 fold higher expressed than FATPs. Bar charts represent mean \pm SD of technical replicates.

4. Results, Aim 2

4.2.2 Upregulation of FATP4 and Acsl3 increases total ACS activity in HUVECs using radiolabelled oleate

Here, stable overexpression of FATP4, FATP5, FATP6 and Acsl3, Acsl4 with retroviral constructs in HUVECs was mediated. The overexpression cell lines were applied for total cellular ACS activity assay. The ACS activity in supernatants from cell lysates is a direct measure of the functional overexpression. As the determination of the cell line specific ACS activity was analysed in cell lysates, the experimental approach is named as “in-vitro” ACS activity. In addition, overexpression of FATP4 was qualitatively validated by immunofluorescence and Western Blot (see appendix figure 1 and figure 2).

As shown in figure 13, overexpression of FATP4 yielded an ~8-fold increase in intracellular acyl-CoA synthetase activity. In contrast, overexpression of FATP5 and FATP6 did not increase intracellular ACS activity. As shown in figure 14, upregulation of Acsl3 increased the total ACS activity ~2 fold compared to control. Overexpression of Acsl4 did not affect esterification of oleate. Extracted cell lysate from control HUVECs catalysed the esterification of ~1.3 pmol oleate/ μ g protein/min.

Results in figure 13 and figure 14 showed that among all generated overexpression cell lines, FATP4 and Acsl3 increased the total ACS activity. In order to evaluate the individual contribution of Acsl3 and FATP4 to the total ACS activity a cell line was generated using a small hairpin RNA under control of a H1 promoter to induce RNA interference resulting in knockdown of Acsl3. However, the stable expression of the target shRNA under control of H1 promoter only led to a knockdown efficiency of 40-60% of total Acsl3 assessed by Western Blot (appendix figure 5). As the target shRNA resulted in >80% knockdown in other cell lines (laboratory data, not shown here), the H1 promoter was exchanged with a U6 promoter achieving a knockdown efficiency of 83% in HUVECs evaluated by Western Blot after stable expression using the retroviral construct (appendix figure 5).

Knockdown of Acsl3 significantly decreased the ACS activity by ~50%. Taking in account that ~80% reduction of Acsl3 resulted in a reduction of ~50% of total cellular ACS activity, the contribution of Acsl3 to the total cellular ACS activity is ~60%. In addition, the contribution of FATPs, especially FATP4, to the total cellular ACS activity is ~40%.

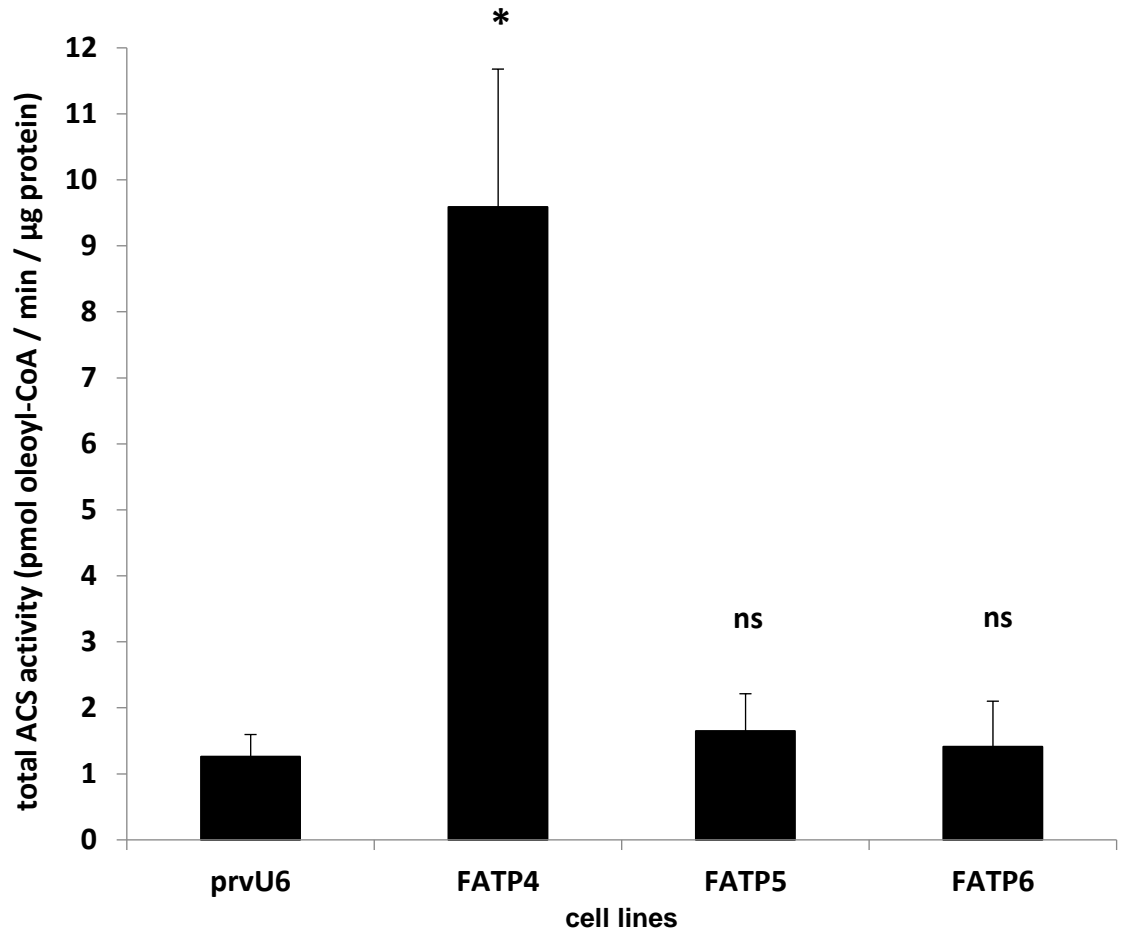


Figure 13: Acyl-CoA synthetase activity of FATP4, FATP5 or FATP6 upregulation in HUVECs.

Results show mean \pm SD of three independent experiments with technical triplicates. * denotes statistically significant difference to prvU6 (control) using student's t-test, p -value > 0.05 ; ns denotes no statistically significant difference. prvU6 (control) mean: 1.26 ± 0.34 ; FATP4 mean: 9.59 ± 2.09 ; FATP5 mean: 1.65 ± 0.57 ; FATP6 mean: 1.41 ± 0.69

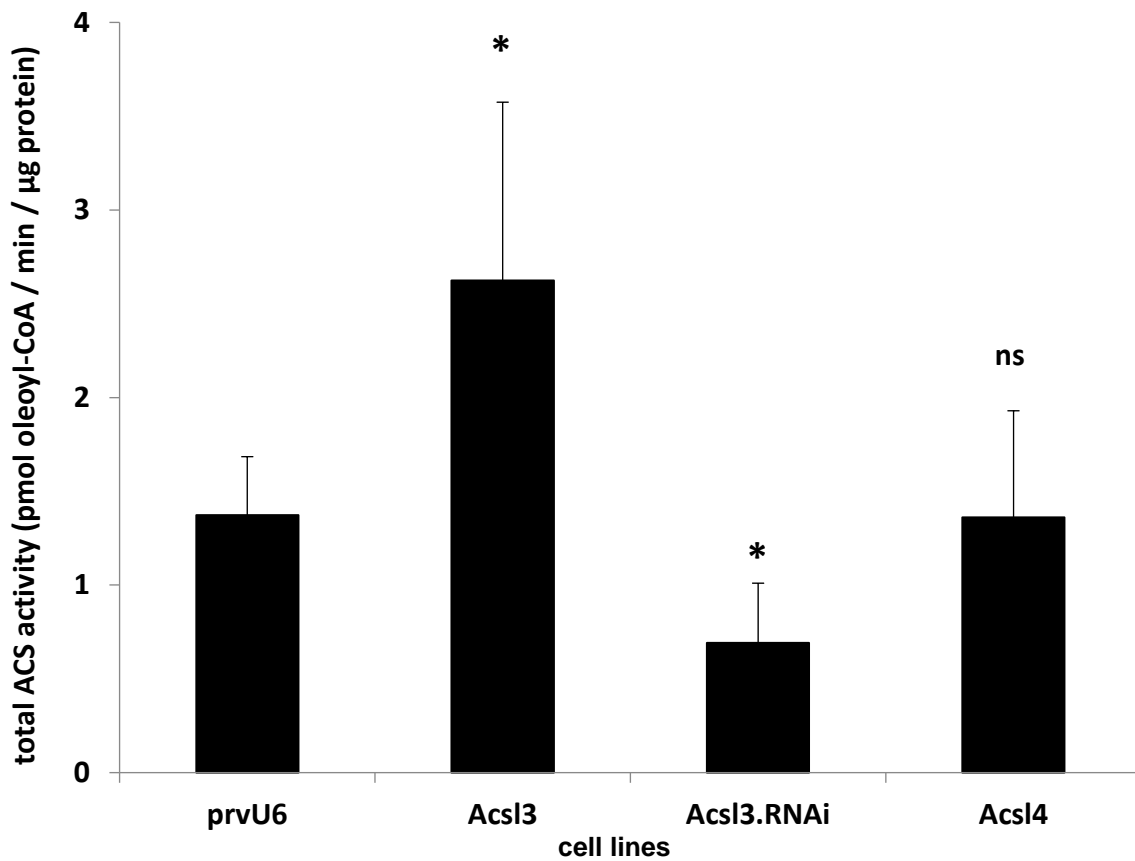


Figure 14: Acyl-CoA synthetase activity of either Acsl3 or Acsl4 upregulation or Acsl3 knockdown in HUVECs.

Results show mean \pm SD of at least three independent experiments with technical triplicates. * denotes statistically significant difference to prvU6 (control) using student's t-test, p -value > 0.05 ; ns denotes no statistically significant difference to prvU6. prvU6 (control) mean: 1.37 ± 0.31 ; Acsl3 mean: 2.62 ± 0.91 ; Acsl3.RNAi mean: 0.69 ± 0.32 ; Acsl4 mean: 1.36 ± 0.57

4. Results, Aim 2

4.2.3 Upregulation of FATP4 activity has a marginal effect on FA uptake compared to the effect of different extracellular OA levels

The initial process of trans-endothelial FA transport is the apical uptake into endothelial cells. To evaluate the driving force of fatty acid uptake the impact of extracellular FA concentration and the impact of the putative FA transport protein FATP4 were compared. In detail, three different extracellular FA concentrations (20, 200 and 900 μM) were applied and total OA uptake into HUVECs was assessed after 3 hours incubation. Differences in OA uptake were evaluated in control HUVECs (prvU6.HUVEC) versus FATP4 overexpressing HUVECs (FATP4.HUVEC).

As shown in figure 15, increasing the extracellular OA concentration resulted in an increased OA uptake in both, overexpressed FATP4 and control cell line. Thereby, the OA uptake rose (110-120%) upon a \sim 10-fold increase in extracellular OA concentrations (20 μM to 200 μM). Further increase in extracellular OA concentration from 200 μM to 900 μM resulted in a 30-40% increase of OA uptake but was not statistically significant indicating a saturation effect.

Upregulation of FATP4 activity in HUVECs displayed higher OA uptake (n.s.) at all three extracellular OA concentrations compared to control cells. While 20 μM extracellular OA was applied, HUVECs with increased FATP4 activity displayed a 19% higher OA uptake compared to control. At 200 μM extracellular OA concentration the difference in OA uptake declined to 16% while at 900 μM extracellular OA concentration, FATP4.HUVECs took up only 2% more OA compared to control. This observation shows that the difference between prvU6.HUVECs and FATP4.HUVECs decreased with increasing extracellular OA concentrations.

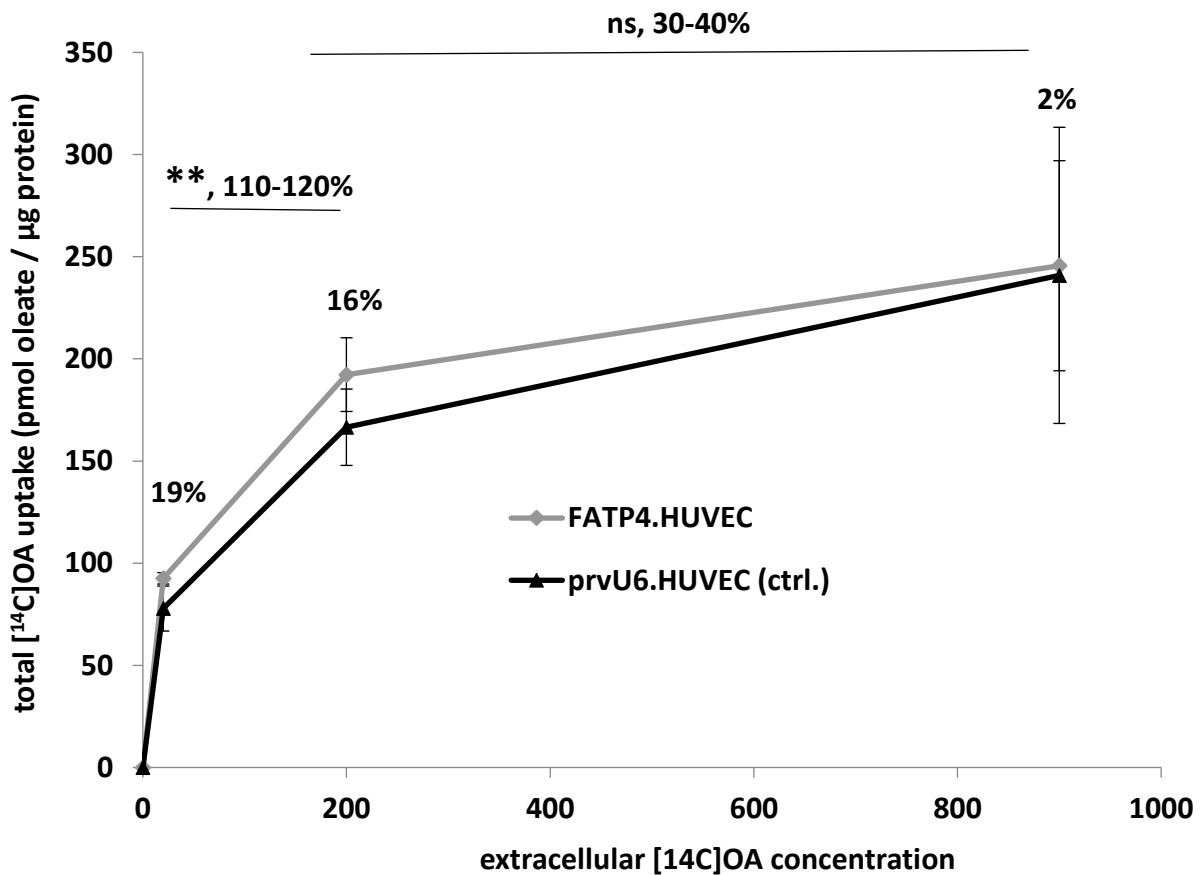


Figure 15: Uptake of FAs correlates with extracellular FA concentration while the putative FA transport protein FATP4 has a minor effect.

HUVEC cell lines were seeded in 12-well plate (surface area of 3,8 cm²) and labelled with either 20, 200 or 900 µM [14C]OA bound to FA-free albumin in a 6:1 ratio. After 180 min the cells were lysed and total incorporated [14C]OA was analysed by liquid scintillation counting. Results show mean ±SD from n=3 independent experiments with technical triplicates (individually seeded wells), student's ttest, ** p-value<0.01, ns is not significant. Maximum uptake capacity is reached with increasing extracellular FA concentrations. Total uptake of [14C]OA correlates with different extracellular [14C]OA concentrations. 10-fold increase of extracellular oleate concentration (20 µM to 200 µM) doubles (114%, **) the total oleate uptake. In comparison, 8-fold increase in ACS activity (FATP4 overexpression) increases uptake by 19% (20 µM, ns), 16% (200 µM, *), 2% (900 µM, ns)

4. Results, Aim 2

4.2.4 Already a slight increase in extracellular OA level outperforms the effect of increased FATP4 activity on FA uptake

In this experiment, the effect of FATP4 overexpression was compared against the effect of extracellular OA concentrations on OA uptake. Therefore, OA uptake of FATP4 overexpressed cells at 200 μM extracellular OA concentration level was compared to gradually elevated, i.e. by 25 μM steps, extracellular OA concentration levels in control cells.

As shown in Figure 16, elevation of extracellular OA concentration by 25 μM (from 200 μM to 225 μM) increased OA uptake in control cells by $\sim 18\%$ after 5 min incubation and $\sim 14\%$ after 30 min incubation time (compared to the starting point of 200 μM extracellular OA concentration). However, the OA uptake of control cells at 225 μM extracellular OA concentration level was $\sim 13\%$ smaller (not significant) than the OA uptake in HUVECs with increased FATP4 activity (after 5 min and 30 min incubation time). Further increase of extracellular OA concentration to 250 μM elevated the OA uptake in control cells by $\sim 32\%$ and $\sim 34\%$ after 5 min and 30 min incubation time, respectively. In addition, while 250 μM extracellular OA was applied, OA uptake in prvU6.HUVECs was significantly higher compared to the OA uptake in FATP4.HUVECs with 200 μM extracellular OA. These results shows that an increase of extracellular OA levels by 50 μM outperforms the effect of ~ 8 fold increased FATP4 activity in HUVECs regarding OA uptake.

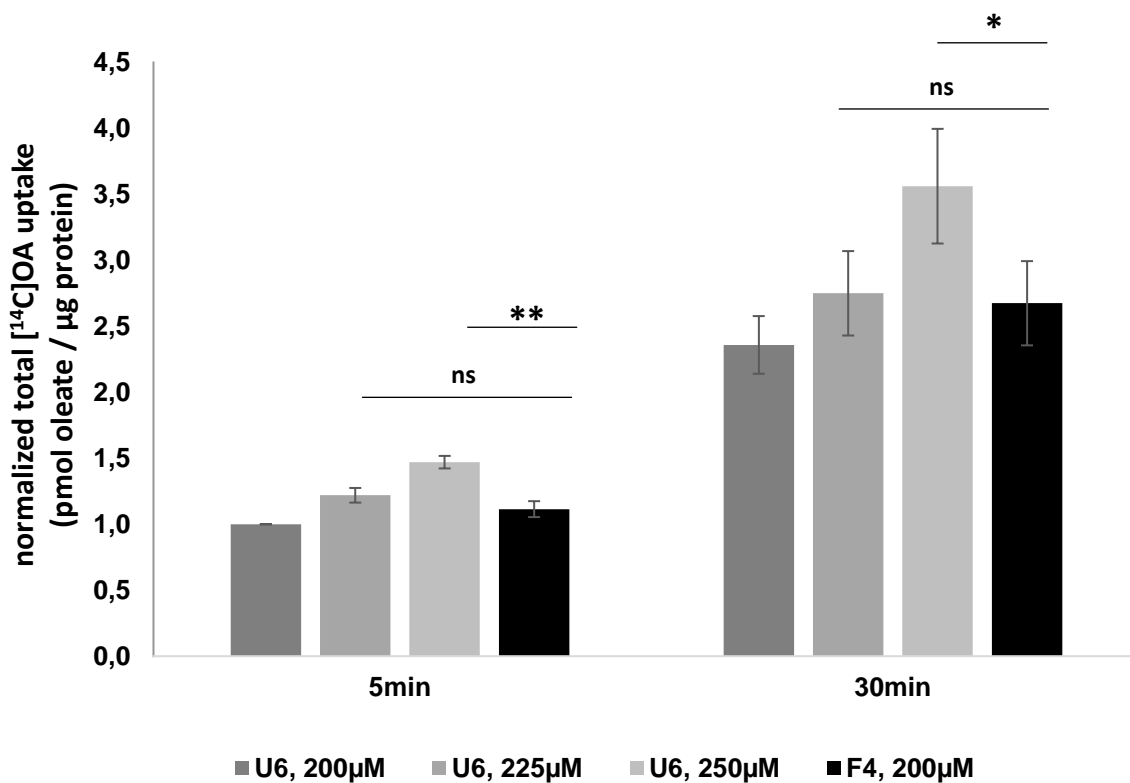


Figure 16: Increasing the extracellular OA concentration increases FA uptake to a larger extent than increased FATP4 activity.

HUVEC cell lines were seeded in 12-well plate (surface area of 3.8 cm²) and labeled with either 200, 225 or 250 µM [¹⁴C]OA bound to FA-free albumin in a 6:1 ratio. After 5 min and 30 min the cells were lysed and total incorporated radiolabeled [¹⁴C]OA was analyzed by liquid scintillation counting. Results show mean±SD from n=3 independent experiments with triplicates (individual seeded wells), student's ttest, ** p-value<0.01, * p-value<0.05, ns is not significant. Results were normalized to U6, 200 µM at 5 min. denotations: U6 is prvU6.HUVEC (control cell line), F4 is FATP4.HUVEC

4. Results, Aim 2

4.2.5 FA uptake increases with availability of free FAs

To mimic different availability of extracellular free FAs, two different binding ratios of OA to albumin were applied. This experiment is an orthogonal approach to previous experiments (5.2.3 and 5.2.4) where different availability of extracellular OA was simulated by applying different extracellular OA concentrations. Here in detail, a fixed extracellular [¹⁴C]OA concentration (200µM) was applied, but the binding ratio to (FA-free) albumin was switched from 6:1 to 4:1. Higher binding ratio (6:1), will lead to higher saturation of available binding pockets and shifts the binding equilibration towards dissociation of OA from albumin in close proximity to the target endothelial cells.

As shown in figure 17, elevating the binding ratio of OA to albumin from 4:1 to 6:1 resulted in significant increase of OA uptake by ~45% in prvU6.HUVECs and by ~42% in FATP4.HUVECs. No significant difference was observed between the two cell lines at both, 4:1 and 6:1 albumin binding ratio. In addition, FATP4.HUVECs displayed higher OA uptake ~19% with a OA to albumin binding ratio of 4:1 compared to the OA uptake ~16%, when OA was initially bound to albumin in a ratio of 6:1. These results indicate that an increase in albumin binding ratio increases OA uptake to a larger extent than increased intracellular FATP4 activity in endothelial cells.

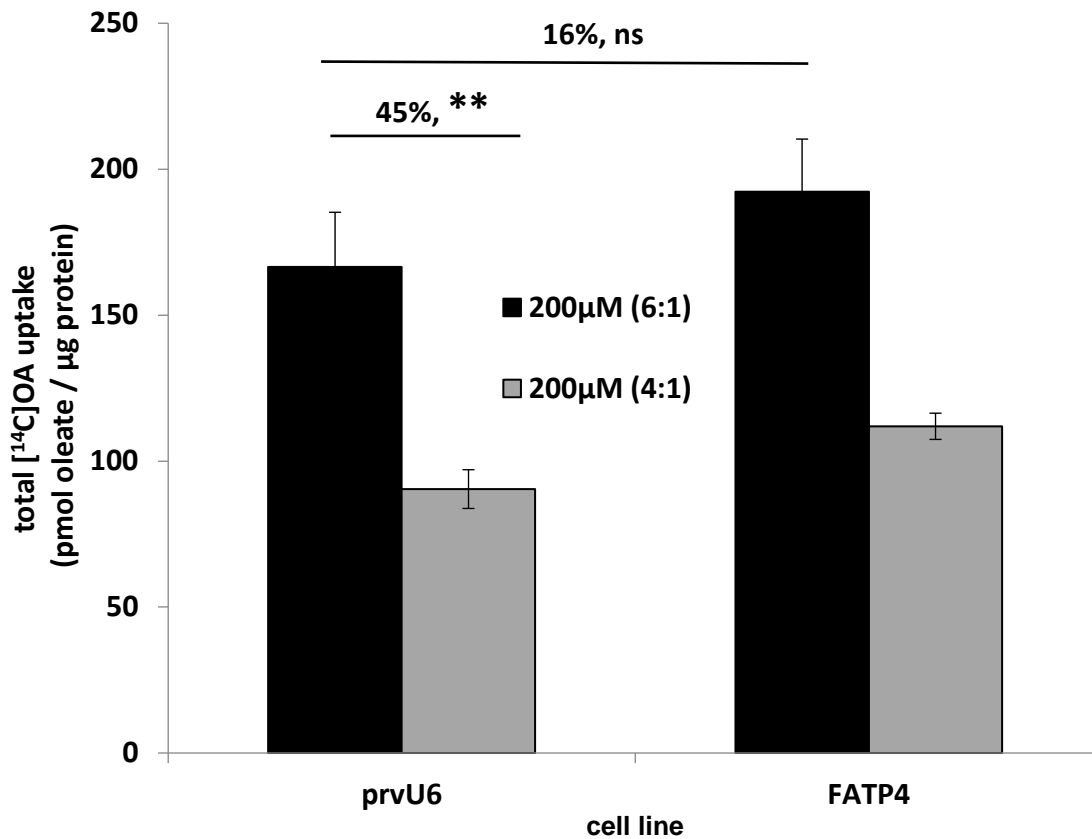


Figure 17: Increasing the FA to albumin binding ratio increases FA uptake.

HUVEC cell lines were seeded in 12-well plate (surface area of 3,8 cm²) and labeled with 200 µM [¹⁴C]OA bound to FA-free albumin either in a 6:1 or 4:1 ratio. After 180 min the cells were lysed and total incorporated radiolabeled [¹⁴C]OA was analysed by liquid scintillation counting. Uptake experiments using 200µM (6:1) were performed in three independent experiments (taken from experiment figure 15) and uptake of 200µM (4:1) were performed in two independent experiments, each with technical triplicates (individual seeded wells). student's ttest, ** p-value<0.01, ns is not significant.

4. Results, Aim 2

4.2.6 Uptake rate of oleate is initially fast and correlates with the rate of esterification during prolonged incubation.

In order to evaluate the coherency between OA uptake and intracellular in-vivo ACS activity, OA uptake was performed with HUVECs seeded in 12-well plate (surface area of 3,8 cm²) and incorporation of total [¹⁴C]OA was compared to intracellular esterified [¹⁴C]OA and intracellular non-esterified [¹⁴C]OA using evaluation by LSC and thin-layer chromatography. In detail, prvU6.HUVECs (control), FATP4.HUVECs and Acs13kd.HUVECs were incubated with 200µM [¹⁴C]OA for 1, 5 and 30 min and the speed of incorporation was determined by dividing the total OA uptake by time. The rate of metabolism was defined as the rate of esterification. Thereby, all lipid classes that require initial activation for their synthesis were taken together and total amount was divided by time. In addition, the uptake- and metabolism rate was normalized to the growth area to allow further comparison with HUVECs cultivated in trans-well system.

As shown in figure 18, there are different trends for the different lipid classes observable. The maximum storage capacity of intracellular non-esterified OA was reached after one minute and does not further increase during prolonged incubation. Further oleate was esterified and primarily metabolized into phospholipids and neutral lipids. Within the phospholipids the majority of esterified-OA was channeled into phosphatidylcholine and a comparable smaller proportion was transferred into phosphatidylinositol, phosphatidic acid, and phosphatidylethanolamine. Regarding the neutral lipids, triacylglycerol was increasing with time and diacylglycerol peaks around five minutes and decreases afterwards. FATP4.HUVECs incorporate ~185 pmol (~16%) more [¹⁴C]OA into TG than prvU6.HUVECs after 30 min incubation. The total amount of intracellular non-esterified [¹⁴C]OA was not affected by increased FATP4 activity. Regarding the esterification rates during different time frames revealed that the in-vivo ACS activity showed a trend to be increased by ~4% (first minute), ~7% (1 to 5 min and 5 to 30 min) with increased FATP4 activity.

As the incorporation of OA into phospholipids and neutral lipids initially require activation by esterification of the OA, hence for further evaluation the phospholipids and neutral lipids were combined as “esterified OA”. The rate of esterification (= rate of metabolism) was defined as the amount of esterified OA per time.

4. Results, Aim 2

As shown in figure 19, after normalization to the growth area (3.8 cm^2 , one well of 12-well plate), the metabolic rate of endothelial cells (prvU6) was $\sim 1.17 \text{ pmol} / \text{s} / \text{cm}^2$ during the initial first minute. After 1 minute the metabolic rate adjusted around ~ 0.33 or $\sim 0.29 \text{ pmol} / \text{s} / \text{cm}^2$ during prolonged incubation. As the intracellular pool of non-esterified OA reached the maximum level after 1 minute, the total OA uptake rate was equal to the rate of metabolism during prolonged incubation. During the first minute the incorporation rate consists of increase in non-esterified OA as well as the esterification rate indicating that the esterification was initiated as soon as intracellular non-esterified OA was available.

Taken together, these data support the notion that the initial high OA uptake rate correlates with the increase in intracellular non-esterified OA. The intracellular metabolism was slow but provided high storage capacity by channelling non-esterified OA into phospho- and neutral lipids. In addition, FA uptake was initially fast and rapidly attenuated into steady state.

4. Results, Aim 2

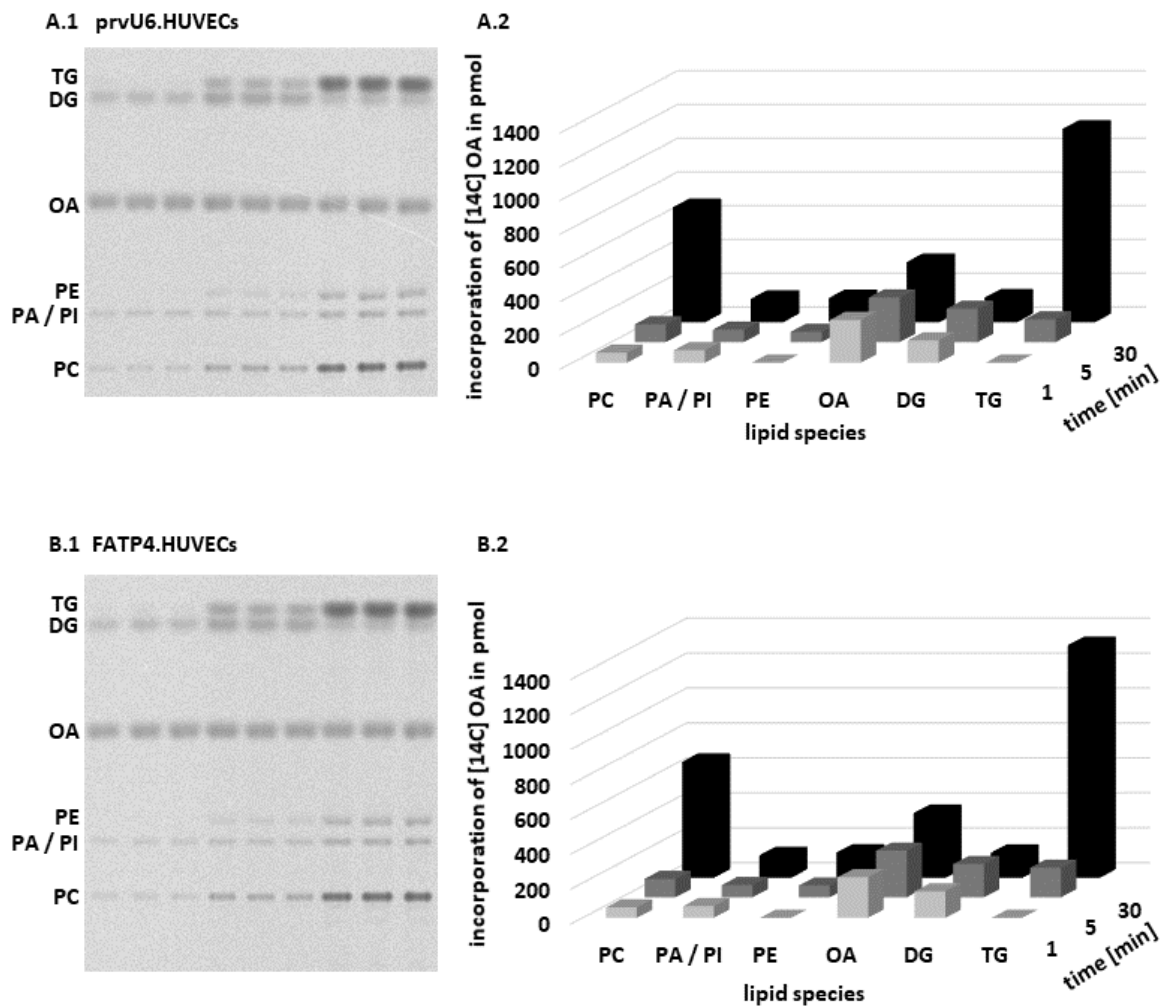


Figure 18: Separation of lipid classes after incubation with 200µM (6:1) radiolabeled oleate.

PC and TG increased over time, while the non-esterified OA reached the maximum capacity after one minute incubation. FATP4.HUVECs incorporate ~185 pmol (~16%) more [¹⁴C]OA into TG than prvU6.HUVECs after 30min. Results show mean of technical triplicates (individual seeded wells) denotations: TG triacylglycerol, DG diacylglycerol, OA oleic acid/ oleate, PE phosphatidylethanolamine, PI phosphatidylinositol, PA phosphatidic acid, PC phosphatidylcholine. **A.1** separation of lipid classes **A.2** molar quantities after incorporation of [¹⁴C]OA into prvU6.HUVECs **B.1** separation of lipid classes **B.2**. molar quantities after incorporation of [¹⁴C]OA into FATP4.HUVECs.

4. Results, Aim 2

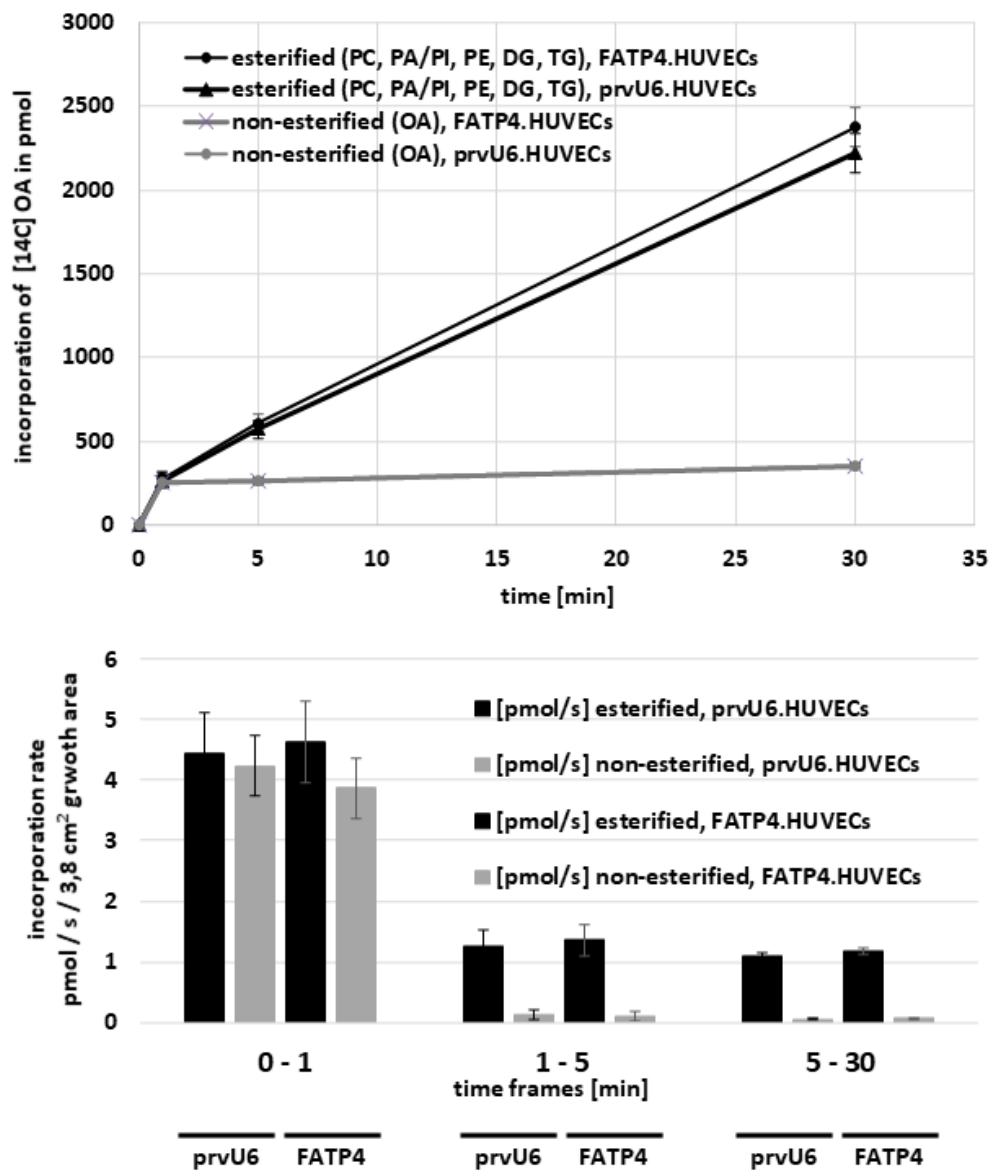


Figure 19: oleate metabolism of adherent endothelial cells after incubation with 200µM [14C]OA for 1, 5 and 30min.

Amount of esterified [14C]OA and retained non-esterified [14C]OA at different time points. Rate of esterification is rate of metabolism. Results show mean ±SD from triplicates (three individual seeded wells). Note the rate of esterification is shown without normalization to growth area.

4. Results, Aim 2

4.2.7 Upregulation of FATP4 activity increases Bodipy-C12 uptake into endothelial cells

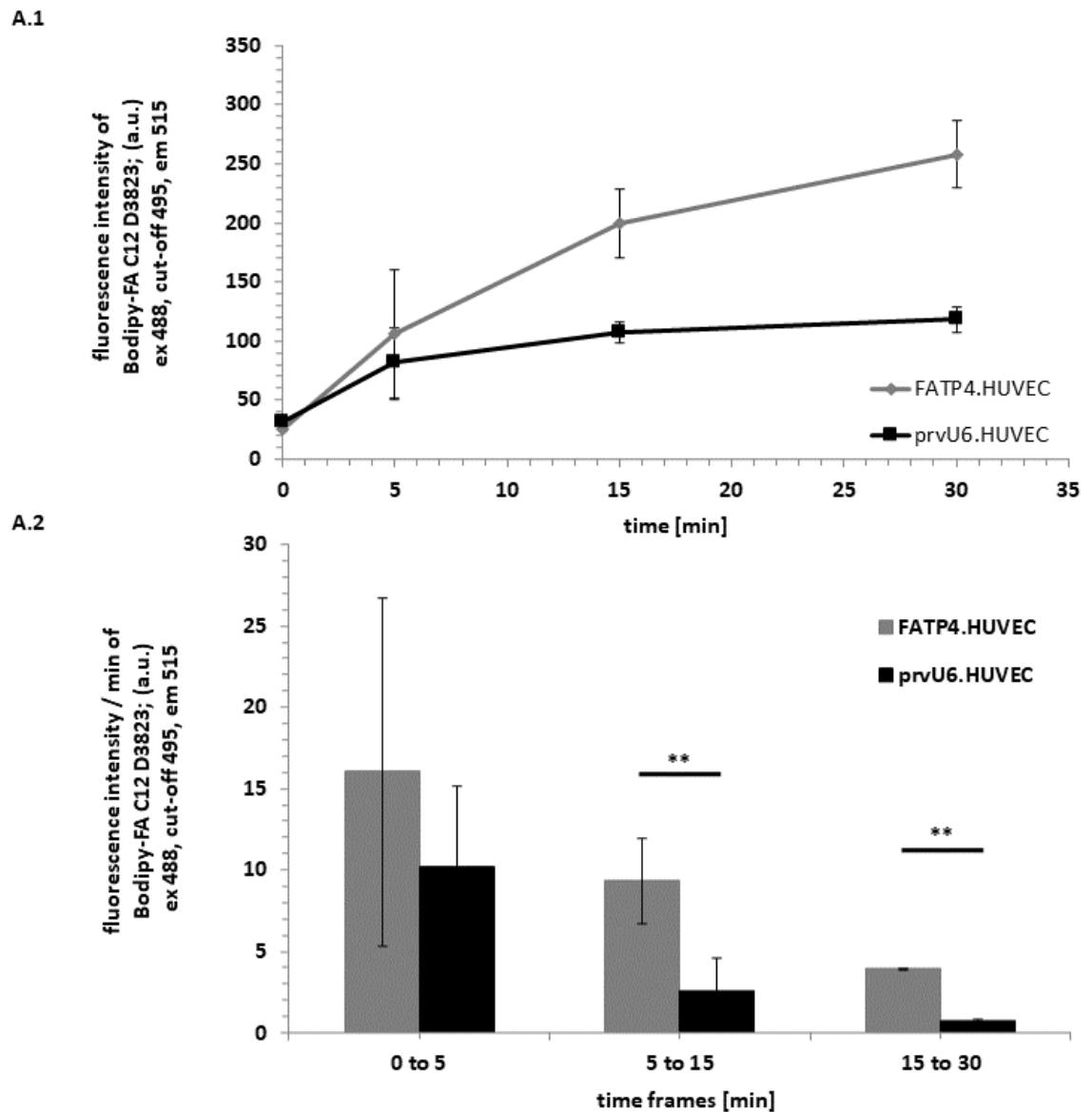


Figure 20: Upregulation of FATP4 increases Bodipy-C12 uptake into endothelial cells. 2 μ M Bodipy-FA, 1 μ M fatty acid-free albumin, EBM-2; graphs represent mean \pm SD from four independent experiments with technical unicum. student's ttest, ** p-value<0.01, ns is not significant. **A.1** Uptake of Bodipy-C12 (a.u.) into endothelial cells is doubled after 15 and 30 minutes of incubation. **A.2** Uptake rates of Bodipy-C12 in endothelial cells.

4.3 Aim 3: Assessment of parameters affecting trans-endothelial FA transport

In order to evaluate trans-endothelial fatty acid transport, endothelial cells (HUVECs) were grown on trans-well filter inserts and transport of [¹⁴C]OA from the apical to the basolateral compartment was tracked. Here, the intracellular lipid species after uptake of FAs was analysed. Then, pulse/chase experiments were applied to elucidate changes in intracellular lipids during FA transport. In the next step, the speed of FA transport was evaluated and compared to the speed of metabolism. Also, transported lipids were analysed for their chemical identity. At last, different parameters, such as intracellular ACS activity, extracellular FA supply and basolateral albumin concentrations were evaluated for their effect on trans-endothelial FA transport.

4.3.1 Besides intracellular non-esterified FAs, also lipolysis contributes to the efflux of fatty acids

For evaluation of transported lipid species, pulse / chase experiments were performed. The incorporation of [¹⁴C]OA directly after pulse was compared to the remaining incorporated [¹⁴C] lipid species after pulse/ chase using liquid scintillation counting and phosphorimaging of TLCs.

As shown in Figure 21, there were three major bands on the thin-layer chromatography of the pulse control visible. The three bands were corresponding to phosphatidylcholine, non-esterified OA and triacylglycerol of which TG and non-esterified OA were the most prominent. The % distribution of bands did not differ from the % distribution of bands observed in the thin layer chromatography from HUVECs cultivated in a 12-well plate. As a result, HUVECs incorporated around 1986.7 ± 167.4 pmol / filter of total lipids, of which 54.7 ± 3.3 % was incorporated into neutral lipids and 22.8 ± 2.3 % phospholipids, while 22.5 ± 5.5 % of total incorporated lipids remained non-esterified.

As shown in figure 21, after pulse/ chase 41.1 ± 2.3 % of total incorporated lipids was released resulting in a total transport of 820.0 ± 90.0 pmol OA / cm² (filter) in 2min. Considering that the duration of chase (duration of FA transport) was 2 min (120 sec), the transport rate was 6.8 ± 0.8 pmol OA / s / cm² (filter). Comparing the rate of metabolism normalised to growth area (shown in figure 19, >1min: ~ 0.3 pmol / s / cm²) to the rate of transport, revealed that the transport rate of OA is 22.8 times higher than the rate of metabolism during prolonged incubation (>1min, figure 19). In comparison

4. Results, Aim 3

to the rate of metabolism during the initial first minute of incorporation (figure 19, <1min: $\sim 1.17 \text{ pmol / s / cm}^2$) the rate of transport was 5.8 times higher.

Further shown in figure 21, it was remarkably that in addition to $406.0 \pm 121.7 \text{ pmol}$ non-esterified OA, also $376.7 \pm 33.0 \text{ pmol}$ [^{14}C]OA from the neutral lipids, primarily triacylglycerol was released after pulse / chase. Hence, lipolysis of triacylglycerol contributed $\sim 47\%$ and the release of transiently stored non-esterified OA contributed $\sim 50\%$ to the total amount of released fatty acids. The remaining 3% was made up from phospholipids but was not significant.

For investigation whether lipolysis of TG for FA transport is linked to the adipose triglyceride lipase (ATGL), an ATGL specific inhibitor (Atglistatin) was applied. During labelling HUVECs were treated with either $20 \mu\text{M}$ Atglistatin or 0.1% DMSO as control. Then, pulse / chase experiments were performed to evaluate the effect of ATGL inhibition on FA efflux from endothelial cells.

As shown in figure 22, fatty acid efflux reduces TG content by $\sim 36\%$. Pre-incubation of endothelial cells with $20 \mu\text{M}$ Atglistatin for 30 min decreases lipolysis of TG by $\sim 42\%$ compared to control during 2 min of fatty acid transport/efflux.

Taken together, endothelial cells retained high amounts of non-esterified FAs, while further FAs were metabolized into phospho- and neutral lipids. Endothelial cells favour FA transport over FA metabolism regarding the speed of the individual processes. The total FA transport of FAs consisted of transiently incorporated non-esterified FAs and FAs released by lipolysis from triacylglycerol.

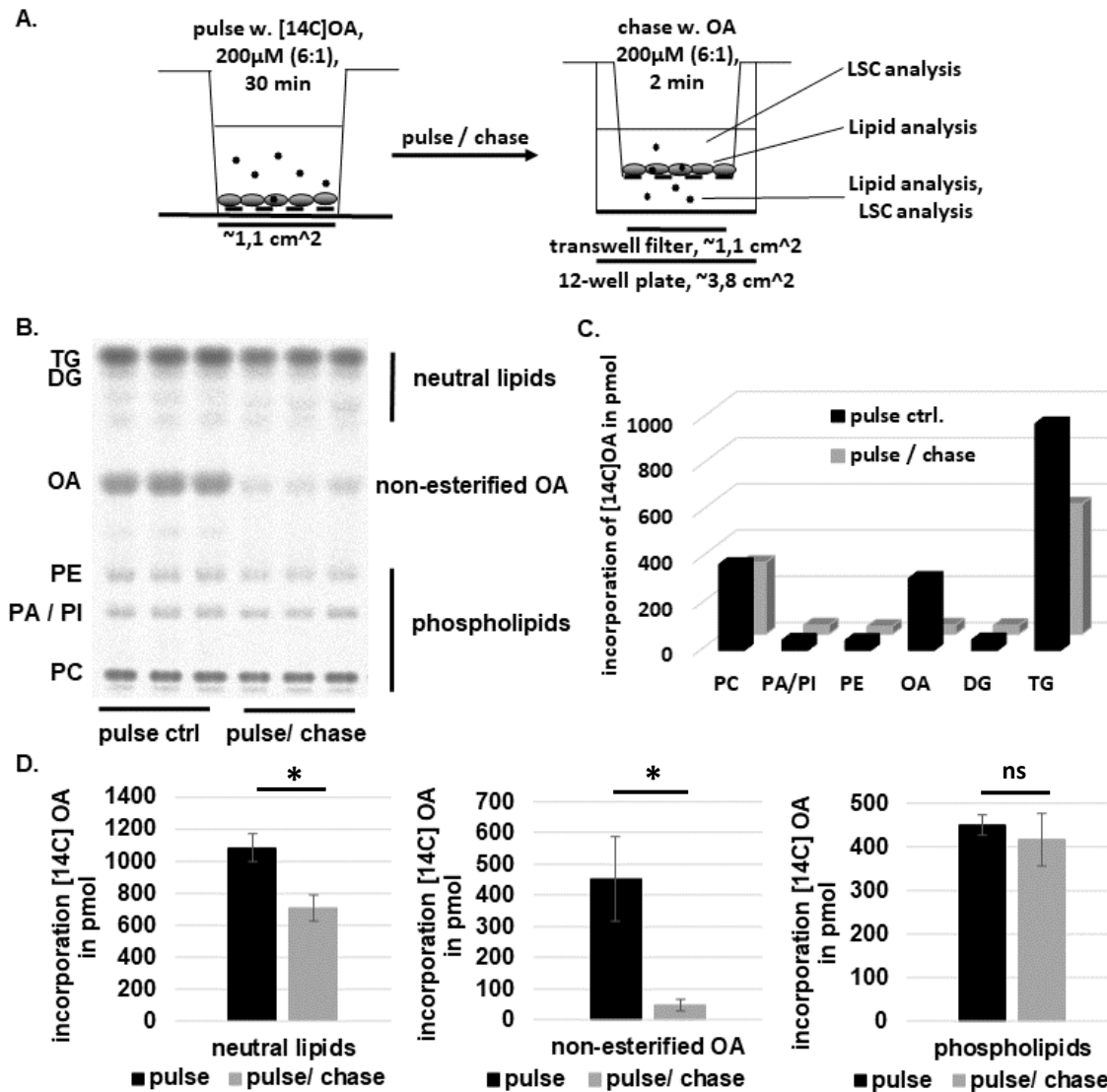


Figure 21: Lipolysis of TG contributes to the efflux of non-esterified FAs.

Intracellular neutral lipids, especially Triacylglycerol and non-esterified OA were reduced after FA transport. graphs represent mean \pm SD from three independent experiments with each technical triplicate (individual filters). student's t-test, * p-value < 0.05, ns is not significant. **A.** Schematic overview of experimental set-up. Here, data was evaluated by lipid analysis of incorporated $[^{14}\text{C}]\text{OA}$ in HUVECs **B.** Representative TLC. Separation of lipid classes after incubation with radiolabeled oleate. TG triacylglycerol, DG diacylglycerol, OA oleic acid/ oleate, PE phosphatidylethanolamine, PI phosphatidylinositol, PA phosphatidic acid, PC phosphatidylcholine **C.** molar quantities of different lipid classes for representative TLC. **D.** comparison of total incorporated neutral -, phospho- and non-esterified OA after pulse versus remaining incorporated radiolabeled lipid species after pulse / chase.

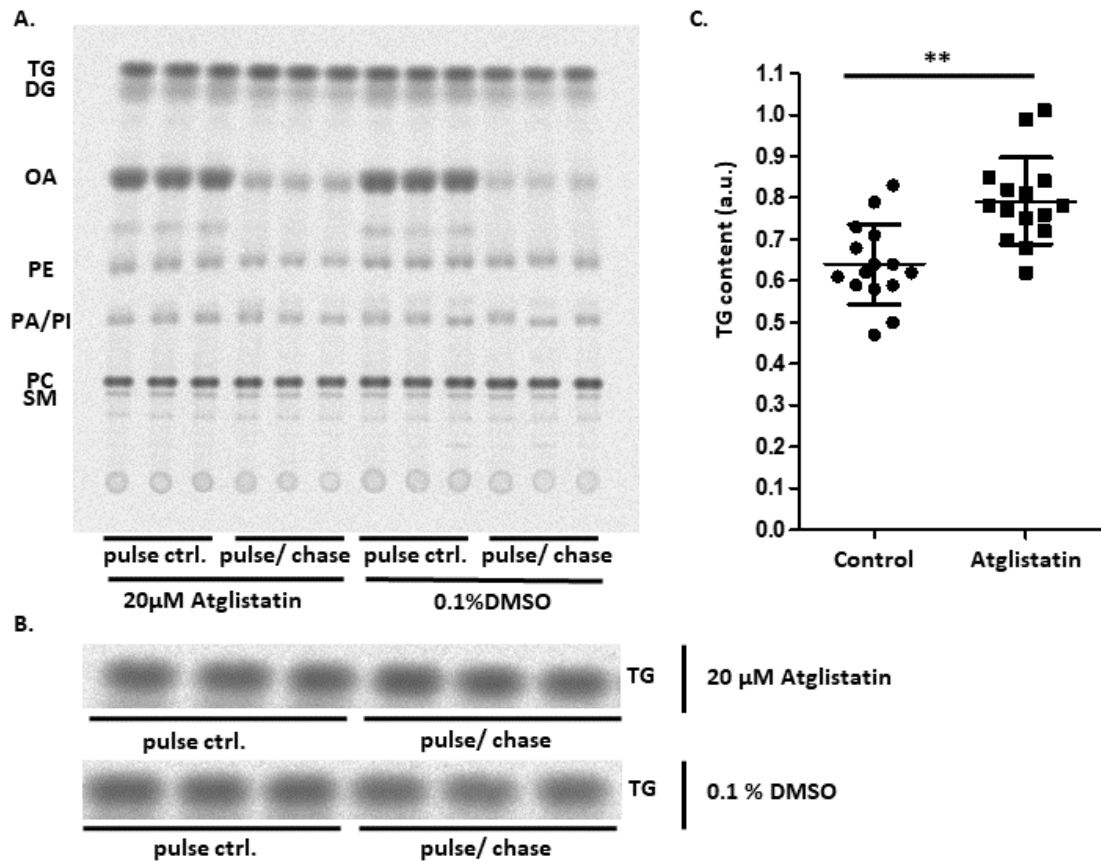


Figure 22: Atglistatin treatment reduced lipolysis of TG during FA transport.

Pre-incubation of endothelial cells with 20 μM Atglistatin prior to pulse/ chase experiment. **A.** Representative TLC. Separation of lipid classes after incubation with radiolabelled oleate. TG triacylglycerol, DG diacylglycerol, OA oleic acid/ oleate, PE phosphatidylethanolamine, PI phosphatidylinositol, PA phosphatidic acid, PC phosphatidylcholine, SM Sphingomyelin. **B.** spliced image of TG specific bands **C.** Atglistatin treatment reduces lipolysis of TG for FA transport. Relative TG content normalized to pulse control. Graph represents mean ±SD from five independent experiments with each technical triplicate (individual filters). student's t-test, ** p-value<0.01.

4. Results, Aim 3

4.3.2 Extracellular OA concentration affects the transport of non-esterified OA

In order to test how different extracellular OA concentrations, affect the trans-endothelial fatty acid transport, two different apical FA concentrations were applied during chase of pulse/chase experiments.

As shown in figure 23, increasing the extracellular “cold” OA concentration by ~10 fold (20 μ M to 200 μ M) during chase increases the efflux of non-esterified OA from endothelial cells by ~49%, but showed a trend to reduce lipolysis of TG for transport. In addition, with 20 μ M extracellular apical “cold” OA concentration already ~87% of total non-esterified OA was released from HUEVCs. In comparison, with 200 μ M extracellular apical “cold” OA concentration ~96% of total non-esterified OA was released from HUVECs after 2 min. The other lipid classes were not significantly affected.

4. Results, Aim 3

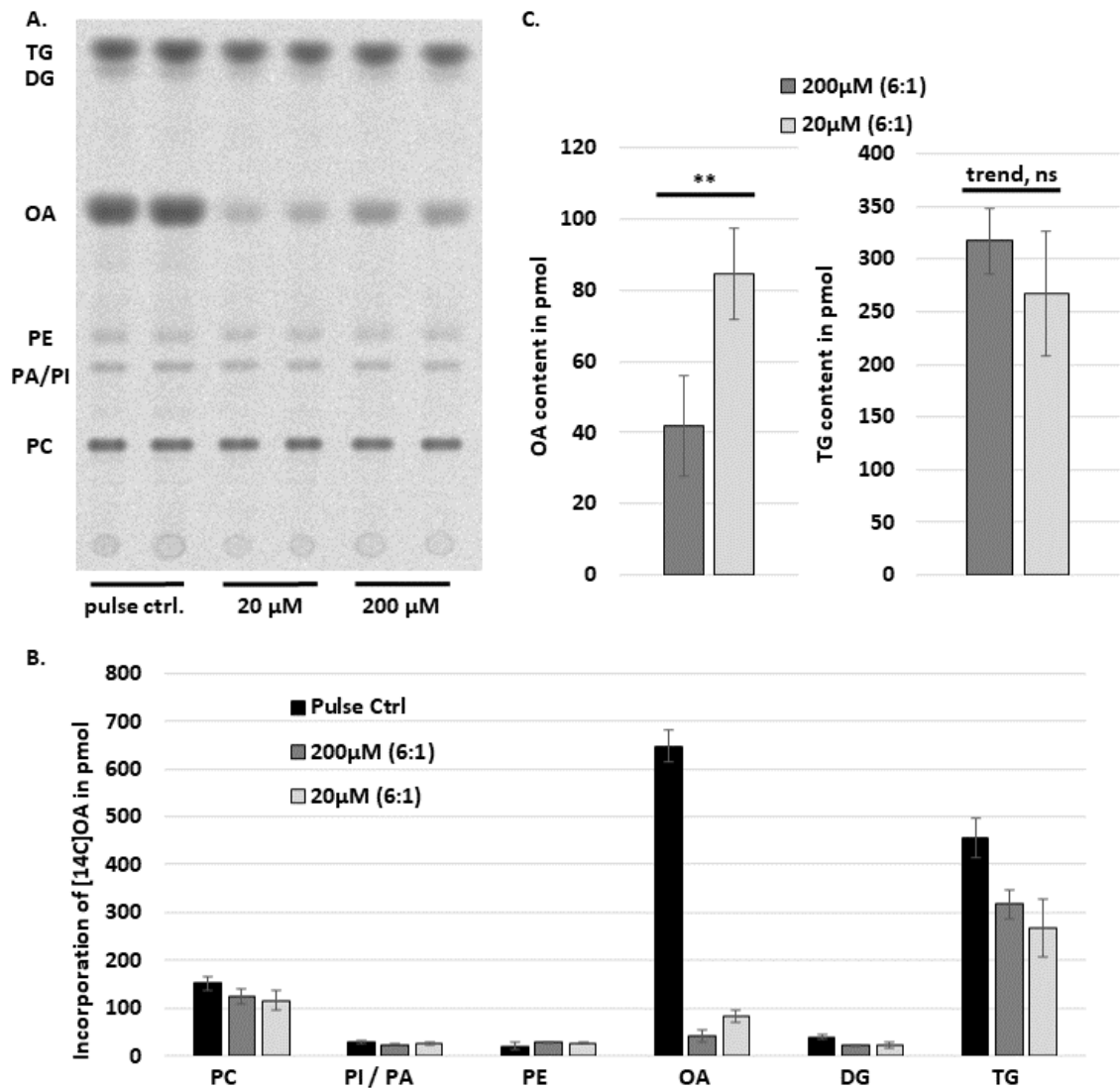


Figure 23: Increasing the extracellular OA concentration increases efflux of intracellular non-esterified OA. 20 μ M apical OA concentration was sufficient to facilitate FA transport.

200 μ M vs. 20 μ M apical “cold” OA concentration during chase. Graphs represent mean \pm SD from two independent experiments with each at least technical duplicate (individual filters). student’s t-test, ** p-value<0.01, ns is not significant. **A.** Representative TLC. Separation of lipid classes after incubation with radiolabelled oleate. TG triacylglycerol, DG diacylglycerol, OA oleic acid/ oleate, PE phosphatidylethanolamine, PI phosphatidylinositol, PA phosphatidic acid, PC phosphatidylcholine, SM Sphingomyelin. **B.** molar quantities of incorporated lipid species **C.** Efflux of non-esterified OA is increased with increasing apical OA concentrations. TG content showed a trend to be reduced with lower apical OA concentrations.

4. Results, Aim 3

4.3.3 Endothelial cells provide increased FA transport when intracellular FA metabolism is diminished.

In order to evaluate the impact of the intracellular FA metabolism on FA transport, the FATP4 overexpression cell line was compared against the Acs13 knockdown cell line in pulse/chase experiments. Samples were taken from the basolateral compartment during the time frame <2min and transport of radiolabelled OA from the intracellular lumen to the basolateral compartment was evaluated by liquid scintillation counter.

As shown in figure 24 A.1 and A.2, after 120 seconds endothelial cells with reduced intracellular metabolism due to knockdown of Acs13 released ~100 pmol more [¹⁴C]OA to the basolateral compartment than the control. FATP4 overexpressing HUVECs did not significantly differ from the control regarding the efflux of OA. However, with FATP4 overexpression there was a trend of diminished OA efflux observable. The increased OA transport with Acs13 knockdown was accomplished during the initial 15 seconds, while the transport rate of the Acs13 knockdown cell line was nearly doubled compared to control.

After 2 min, cells were lysed, and incorporated lipids were compared to pulse control (start condition of transport). Intracellular lipids of pulse control (start condition) and after 120 seconds of OA transport were analysed and intracellular amount of labelled neutral lipids, phospholipids and non-esterified OA was compared between the cell lines.

As shown in figure 24 B, the ACS13 knockdown cell line retained more non-esterified OA in pulse control than the prvU6 control cell line. In addition, the pool of non-esterified OA showed a tendency to be increased with FATP4 overexpression. Common for all cell lines was the observation that the majority of transported OA originates from the pools of triacylglycerol (diff to pulse ctrl.: ~35%) and non-esterified OA (~90%).

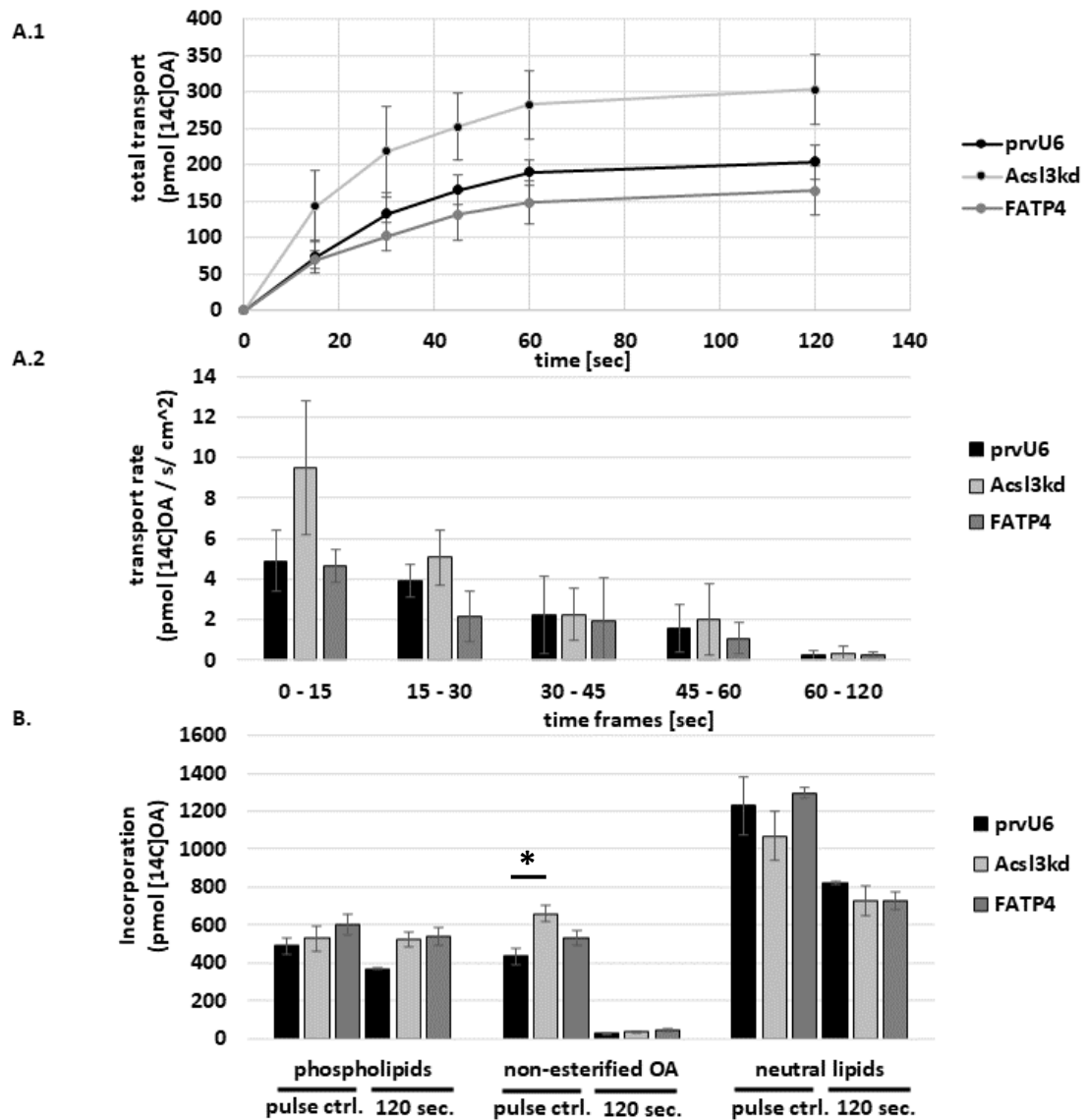


Figure 24: Oleate transport is increased with reduced intracellular ACS activity.

A.1 Transport of radiolabelled OA from the intracellular lumen to the basolateral compartment was evaluated by liquid scintillation counter. **A.2** Transport rates of radiolabelled [14C]OA from figure A1. were calculated by dividing with respective time of transport. graphs represent mean \pm SD from n=2 independent experiments with technical triplicates (individual filters). **B.** Endothelial cells with reduced intracellular ACS activity display an increased pool of non-esterified FAs. Incorporated lipids from different HUVEC cell lines were extracted and analysed by thin-layer chromatography and phosphor imaging. graphs represent mean \pm SD from one individual experiment of figures A using technical triplicates (individual filters). student's t-test, * p-value<0.05.

4. Results, Aim 3

4.3.4 Efflux of FAs from endothelial cells correlates with increasing concentrations of FA-free albumin in the basolateral compartment

Different concentrations of FA acceptors in the basolateral compartment simulated by varying FA-free albumin concentrations were tested for their efficiency to affect FA transport. Consequently, the pulse / chase experiment using either 10, 33.3 or 100 μM FA-free BSA in the basolateral compartment was applied.

As shown in figure 25, with increasing basolateral FA-free albumin concentrations, the amount of released FA from endothelial cells was increased. The total transport and transport rates correlate with extracellular “demand” for FAs simulated by FA-free albumin as FA acceptor. While $\sim 25\%$ of total released [^{14}C]OA was found in the basolateral compartment after 15 s, the speed of transport was $\sim 5,6 \pm 2,6 \text{ pmol/ s/ cm}^2$ during the initial time period with 100 μM FA-free albumin in the basolateral compartment. During the initial 30 seconds, the transport follows a linear trend. After ~ 60 sec. the total transported lipids were replaced by non-labelled OA giving the appearance of transport saturation.

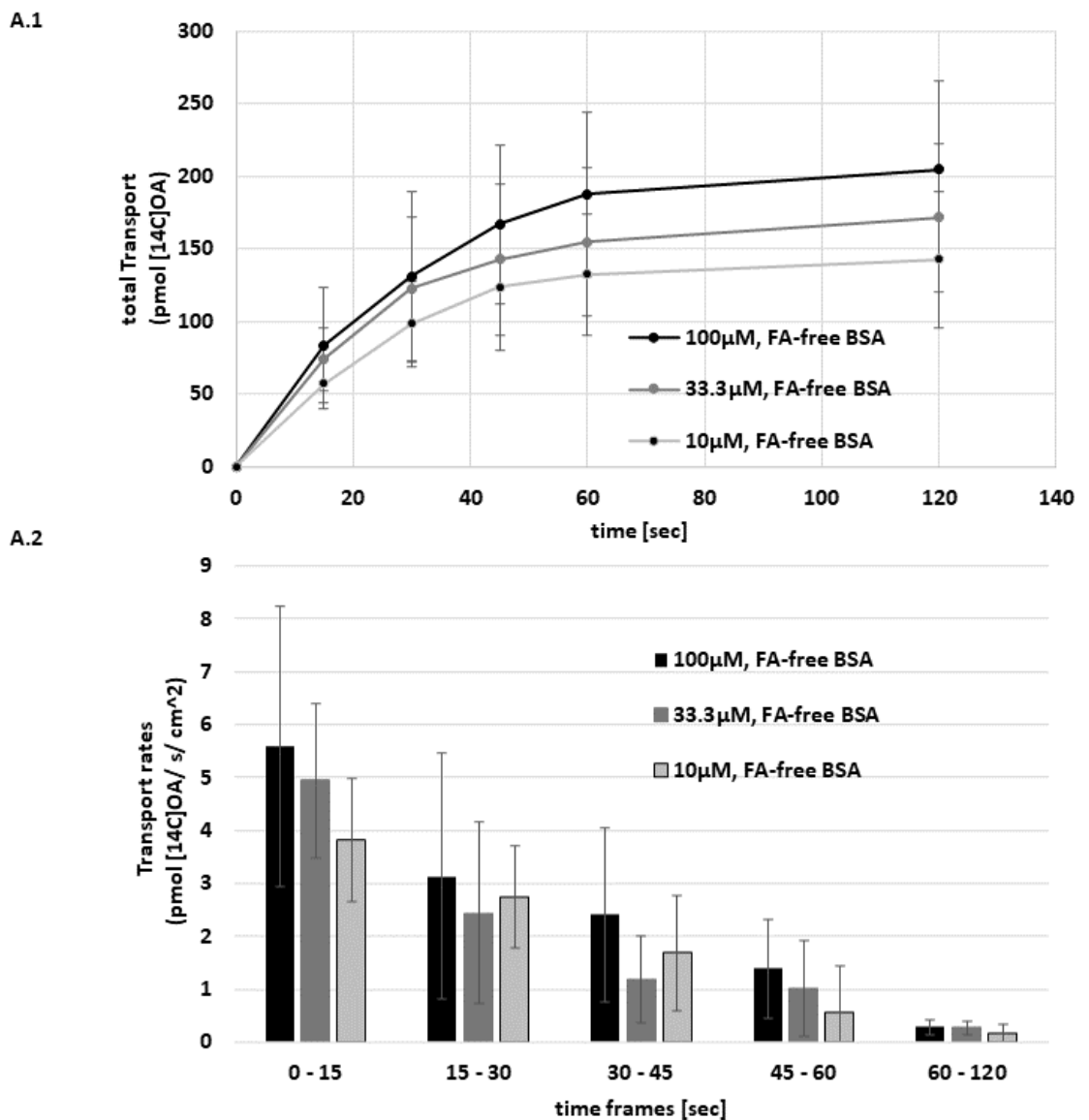


Figure 25: Oleate transport correlates with different extracellular FA-free albumin concentrations in the basolateral compartment.

Either 10, 33.3 or 100 μM FA-free albumin was applied to the basolateral compartment. Transport of radiolabelled OA from the intracellular lumen to the basolateral compartment was evaluated by liquid scintillation counter. graphs represent mean ±SD from three independent experiments with technical triplicates (individual filters).

4. Results, Aim 3

4.3.5 FAs are transported as they are, i.e. non-esterified FA

For evaluating in which form FAs were released from endothelial cells, medium from the basolateral compartment was collected. The lipids from the samples were extracted and analysed by thin-layer chromatography and phosphorimaging.

As shown in figure 26, >90% of lipids found in the basolateral compartment after transport were non-esterified OA. There was another band near the band representing non-esterified OA visible. By comparison of both bands to the [¹⁴C]OA standard showed that the additional band was affiliated to non-esterified [¹⁴C]OA.

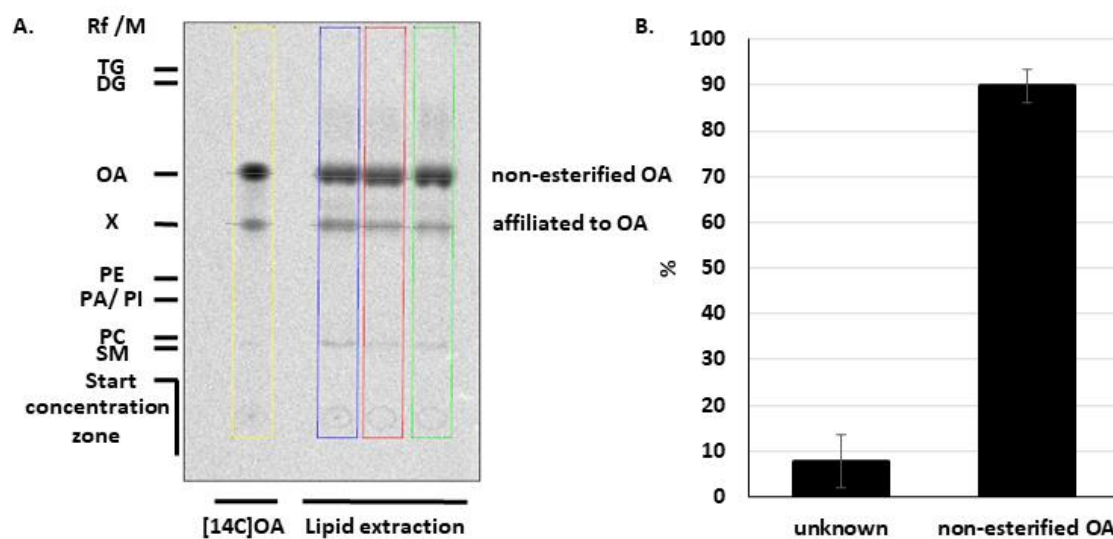


Figure 26: Figure: FAs are transported as they are, i.e. non-esterified.

Transported lipids from the basolateral compartment were extracted and analysed by thin-layer chromatography and phosphorimaging. **A.** Representative raw data image. Marker according to R_f described in methods. As control, [¹⁴C]OA was run in parallel as standard. **B.** % amount of transported lipids. ~90% of transported lipids was non-esterified OA. The unknown band was identified as affiliated to [¹⁴C]OA standard. Other lipid species were not observable (>1%). Graph represents mean \pm SD from n=2 independent experiments with technical triplicates (individual lipid extraction from three transwell filters).

5. Discussion

Regarding the distance and obstacles, that FAs need to overcome on their journey from the blood stream towards the FA metabolizing tissue, the trans-endothelial fatty acid transport is a complex process. Initially, the FAs need to dissociate from protein carriers and go into proximity towards the endothelial cells. Then the FAs need to overcome at least two phospholipid bilayers and travel through the hydrophilic intracellular lumen of the endothelial cells. Hereby, fatty acids need to bypass the endothelial metabolism. Lastly, fatty acids are released towards the basolateral side of the endothelial cells. Regarding the diversity of the obstacles, it seems to be clear that the trans-endothelial FA transport is complex. Hence, the exact mechanisms remain largely unknown. Multiple research questions – some of which addressed in this thesis – may contribute to a better understanding.

In this study, primary endothelial cells (HUVECs) were assessed for their spatial dimensions, growth parameters and barrier function. Then, the hypothesis that upregulation of fatty acid transport protein 4 drives FA uptake and transport was tested. Lastly, pulse / chase experiments were performed to evaluate different effectors of trans-endothelial fatty acid transport.

5.1 Aim 1: Characterization of primary endothelial cells (HUVECs), evaluation of growth parameters and assessment of barrier function

After 8-16 hours post-isolation, HUVECs attached to the collagen-coated cell culture dish and formed cell islands spread over the plate. HUVECs displayed an elongated rod-shaped form while less cell-cell contacts were established. In this state the cells obtained higher proliferation rates and can be passaged for a maximum of 10-12 passages. After HUVECs reached confluency, the cells developed their typical hexagonal/ cuboidal form termed cobblestone morphology (see. figure 5, A.) [77]. Furthermore, typical for HUVECs is an ellipsoid nucleus with 2-3 nucleoli. As shown in figure 5, in most of the cells observed in image A. there were oval, rod-shaped bodies observable, which showed typical morphological characteristics and were located within the nucleolus. In addition, isolated endothelial cells differed strongly in their morphology compared to spindle-like fibroblasts or large rectangular smooth muscle cells, which grow in multilayers and were described as primary source of contaminating cell lines originating from surrounding tissue [78].

5. Discussion

The endothelium provides selective transport of molecules required in the parenchyma [79]. Failure in barrier- or transport functions lead to severe pathological conditions. Hence, endothelial cells provide repair mechanisms, such as release of factors required for blood coagulation [80]. One important component of the coagulation cascade is the glycoprotein named Von Willebrand factor (vWF). vWF is a multimeric glycoprotein, expressed in endothelial cells and megakaryocytes and secreted from endothelial cells after cell layer damage happened [81]. In the blood stream the glycoprotein functions as carrier of factor VIII and protects it from degradation [82]. In endothelial cells of the vein, vWF is translated at the endoplasmic reticulum and transferred by vesicle associated transport inside the golgi apparatus. After encapsulation from the golgi, the so called “Weibel Palade” bodies travel towards the cell periphery and undergo a maturation process [82, 83]. As shown in figure 5 B., vWF was detected in the cell periphery in one direction of the nucleolus. The fluorescence pattern displayed an “intact golgi”-like structure [84]. This observation leads to the assumption that Weibel Palade bodies including vWF were found in a pre-mature form, as encapsulation of the Weibel Palade bodies from the Golgi apparatus had not yet happened. Further analysis of the vWF protein requires more time efforts and techniques with higher resolution. For the purpose of this study, morphological analysis and detection of HUVEC specific biomarker (vWF) in the isolated cells provided strong evidence that the method of HUVEC isolation achieved a monoculture of HUVECs.

HUVECs build up monolayers with tight cell-cell contacts, characterized by expression of cell-cell adhesion proteins. Providing a protective barrier between parenchyma and the blood stream by its specific location is the primary task of endothelial cells. A prominent adherence junction protein expressed in HUVECs is vascular endothelial cadherin [85]. As shown in figure 5, VE-Cadherin is found at cell-cell contacts and is ubiquitously expressed throughout the endothelial monolayer. VE-Cadherin is associated with adherence Junctions and cell layer integrity assessed by e.g., TEER measurements, as performed in this study. Traditionally, the assessment of TEER values was applied for epithelial cell layers showing values ranging between 500 to 1500 $\Omega \cdot \text{cm}^2$ [86]. Epithelial cells achieve larger values due to morphological and functional differences, such as expression of tight-junction proteins (occludins) [87]. In contrast, HUVECs provide adherence junctions by expression of cadherins, such as VE-Cadherin [87]. For HUVECs

5. Discussion

grown on transwell filter, the regular TEER values are ranging between 10-12 $\Omega \cdot \text{cm}^2$ [88]. However, the value varies with differences of filter coating, cultivation conditions and methodological differences. As shown in figure 9, HUVECs grown on transwell filter provided impedance for electric currents in a range between 12-14 $\Omega \cdot \text{cm}^2$ after cultivation of ~30h on pre-coated transwell filter membranes. After the second media exchange (~50h) the TEER values were adjusting on a constant level of ~12 $\Omega \cdot \text{cm}^2$ for untreated HUVECs. The application of EDTA to chelate bivalent cation ions led to a dramatic decrease in TEER values ~30 min after application and barrier function was diminished during prolonged cultivation. Ca^{2+} is relevant for Cadherin-5 (VE-Cadherin) to build up cell-cell interactions and diminishing Ca^{2+} by EDTA treatment leads to weakening of cell layer integrity [85, 89]. Application of IF showed that the signal of VE-Cadherin was lost after application of EDTA showing that the cell layer integrity correlates with VE-cadherin specific adherence junctions. Furthermore, addition of EDTA doubled the transport of FITC-dextran (size like albumin ~70kDa) after ~30min of cultivation showing that disruption of VE-cadherin specific adherence junction leads to leakage in HUVEC barriers.

In conclusion, I showed that the identity of HUVECs was proven by morphological assessment and identification of HUVEC specific biomarkers. HUVECs grown on transwell filter as performed in my study provided physiological barrier formation assessed by TEER measurement and prevention of transport of FITC-dextran (70kDa) across the HUVEC barrier. In addition, my results provide evidence that barrier formation in HUVECs is associated with VE-Cadherin specific adherence junctions.

5.2 Aim 2: Evaluation of the effect of increased FATP4 activity on FA uptake in primary endothelial cells (adherent HUVECs)

According to the previously described model of “vectorial acylation” (Introduction 1.3), FA uptake is primarily dependent on the expression and activity of intracellular acyl-CoA synthetases [66]. This theory requires the endothelial cells to actively adjust their proteome for FA metabolism with changing extracellular FA “supply” and “demand”. As described recently, the parenchyma secretes molecules, such as vascular endothelial growth factor B (VEGF b), that promote upregulation of FATP3/ FATP4 in endothelial cells that leads to increased FA uptake and transport in / across the endothelium [85]. If one follows this thought, the straightforward approach is to directly increase FATP4

5. Discussion

specific activity in endothelial cells and test the efficiency on FA uptake with application of different extracellular FA concentrations. In this study, this approach was tackled.

Upregulation of FATP4 in primary endothelial cells was achieved by retroviral expression. As shown in figure 13, the upregulation of FATP4 led to ~8-fold increase in total oleoyl-CoA activity in HUVECs. Upregulation of other members of the endogenous abundant FATPs did not increase total oleoyl-CoA activity, though Western Blot (appendix figure 2) showed that in all generated cell lines the respective FATP-FLAG construct was findable. One reason might be that respective endogenous FATP was downregulated to balance the increase in the artificial FATP overexpression and expression analysis on transcriptional level of genetically manipulated cell lines wasn't performed here. However, as the FATP4 overexpression cell line displayed increased ACS activity, for this cell line downregulation to balance the overexpression did not happen. In addition, Western Blot and IF (appendix figure 1 and 2) provided evidence for significant upregulation of FATP4. Another reason might be the substrate specificity varies between different FATP members. FATP5 was described to be expressed primarily in liver tissue metabolizing bile acids [90]. FATP6 was found to be exclusively located in heart tissue and metabolizing LCFAs and VLCFAs, including oleic acid, but to a smaller extent than FATP4 [91]. Although FATP6 overexpression slightly increased total oleoyl-CoA activity, but not to a statistically significant extent. FATP3 was not abundant in HUVECS according to the expression analysis, therefore FATP3 was excluded from upregulation experiments. Although, it has been shown that FATP3 is commonly expressed in different types of ECs [30, 68]. Among other members of the Acsl family, acsl3 and acsl4 were endogenously abundant in HUVECs (fig. 11, fig.12). As shown in figure 14, upregulation of Acsl3 increased the total oleoyl-CoA activity by ~2-fold and ~80% reduction of Acsl3 using shRNA induced knockdown reduced the total oleoyl-CoA activity by ~50%. The Acsl4 wasn't expected to increase oleoyl-CoA specific activity, as Acsl4 primarily utilizes arachidonic acid as substrate [92].

Taken together, upregulation of FATP4 extended the total intracellular oleoyl-CoA activity by ~8-fold. Also, the contribution of endogenously expressed FATP4 to the total oleoyl-CoA activity was ~40%, making Acsl3 the dominant protein of the FATP/ Acsl family to esterify oleic acid into metabolically active oleoyl-CoA in endothelial cells.

5. Discussion

In the next step, the FATP4 overexpression phenotype was applied to test the hypothesis whether increased FATP4 activity drives FA uptake in endothelial cells. As shown in figure 15, increased FATP4 activity increased OA uptake at different extracellular OA concentrations by around 2% to 19%, although the efficiency to increase OA uptake was a minor event compared to 10-fold increase in extracellular OA concentrations that increased the uptake by ~110 to 120%. In addition, upregulation of FATP4 activity had more impact when extracellular FA concentrations were low. This observation stands in contrast to transcriptional regulation of FA uptake as the total FA uptake correlates with extracellular FA concentration rather than upregulation of FATP4 activity. In addition, the effect of increased FATP4 activity on OA uptake compared to the control cell line (prvU6.HUVECs) was outperformed by small increases in extracellular FA concentrations (fig. 16). Taking in account that due to prolonged fasting or exercise, the free fatty acids in the blood stream can increase to levels more than $\sim 1500\mu\text{M}$ [29], upregulation of FATP4 is not capable of facilitating the uptake of such numbers. Another argument is delivered by the observation that expressional adjustments are way too slow to quickly upregulate and downregulate required proteins in time. In addition, half-life of mRNA (~ 10 hours) and protein (~ 1 day) are too long for quick adjustments [93]. Furthermore, the experiments in this study showed that trans-endothelial fatty acid transport is fast and therefore expressional regulation of FATP4 to drive FA transport is unlikely.

Although the “in-vitro” ACS activity (figure 13) was increased by ~ 8 fold, the “in-vivo” rate of esterification (figure 19) was only slightly increased by upregulation of FATP4 activity (figure 19). The reason for the minor effect might be due to insufficient intracellular supply of co-factors or energy (ATP) for the nucleophile reaction. The ATP required for the enzymatic reaction was shown to be directly obtained from mitochondria and the spatial localization of FATP4 in node points between ER and mitochondria is necessary for its function [70]. Hence, with high FATP4 overexpression, the available ATP might not be sufficient to serve each enzyme available. Furthermore, this observation shows that though transcriptional upregulation of specific acyl-CoA synthetases happens, the endothelial ATP configuration does not allow further increase of “in-vivo” enzymatic activity. Another explanation is that accessibility of intracellular non-esterified OA is limited due to protection from endothelial metabolism by FABPs, especially FABP4 [94] or intracellular non-esterified FAs are associated within

5. Discussion

membranes. In both scenarios, the initial uptake of FAs is independent of the intracellular rate of esterification, therefore independent of upregulation of FATPs. The only scenario where the “in-vivo” esterification rate correlates with the rate of uptake was during prolonged incubation when cells were grown in adherence, without any possibility for trans-endothelial FA transport. Here, upregulation of FATP4 led to an increase in incorporation of [¹⁴C]OA into triacylglycerol by ~16% when 200 μM [¹⁴C]OA was applied in the extracellular compartment after 30 min (figure 18). The uptake rate slowed down and adjusted according to the rate of esterification when the maximum intracellular amount of non-esterified OA content was reached during the initial minute. Moreover, the total uptake of FAs reached saturation with high extracellular FA concentrations (figure 15) on the reasoning that the endothelium protects underlying tissue as well as themselves from lipotoxicity from overload of free FAs [95] [96].

In conclusion, my results shift the focus towards a hypothesis, where the apical FA “supply” is dictating the efficiency of FA uptake and upregulation of the putative fatty acid transport protein FATP4 has only a minor effect. Moreover, vectorial acylation and extracellular FA concentrations as driving force are not mutually exclusive. However, their impact varies tremendously.

5.3 Aim 3: Assessment of parameters affecting trans-endothelial FA transport

FA transport across endothelial cells, as applied in this study, was based on pulse/chase experiments using HUVECs cultured on transwell filter inserts. The idea of this experimental approach was to track the fate of [¹⁴C]OA once they were incorporated into the cells. This experimental approach has the advantage to identify the intracellular origin of transported FAs. Furthermore, analysis of lipid species in the basolateral compartment allows identification in which form FAs were transported.

After pulse, HUVECs incorporated ~1986.7 ± 167.4 pmol / filter of total lipids, of which 54.7 ± 3.3 % was incorporated into neutral lipids and 22.8 ± 2.3 % phospholipids, while 22.5 ± 5.5 % of total incorporated lipids remained non-esterified (figure 21).

It was unexpected as HUVECs retained high amounts of non-esterified FAs. In different cell lines, the total amount of non-esterified OA was around 3-5% (laboratory data, not shown here), which is 4 times less than observed in HUVECs. In the blood stream, levels of free fatty acids bound to albumin as well as levels of TGs inside chylomicrons can vary

5. Discussion

to a large extent [28, 29, 97]. Most fatty acids are in general insoluble in water, hence every time fatty acids switch from one hydrophilic milieu to another, they require molecular changes or a binding partner to be soluble. Otherwise, FAs accumulate and clog cells or tissues, which leads to breakdown of cellular or systemic functions. Hence, by the pure nature of the intracellular hydrophilic milieu [98], FAs require platforms to facilitate storage and transport. So, how are non-esterified FAs stored in endothelial cells? According to literature, there is high abundance of FABPs in the cytosol of endothelial cells [94, 99, 100]. It is possible that FABPs transiently retain non-esterified FAs from intracellular metabolism and likewise provide a storage capacity. To test this hypothesis, protein separation can be conducted and analysis of FABPs in parallel to analysis of radiolabelled OA can be performed. Another hypothesis is that non-esterified FAs are stored within membranes of the endothelial cells. The quick accessibility, fast uptake rates and even faster transport rates could be explained by this assumption. Cellular membranes are omnipresent in cells and non-esterified FAs can reside within the hydrophobic domains. In addition, lateral diffusion of FAs within lipid bilayer is fast ($1\mu\text{m/s}$) allowing the fatty acids to quickly reach their targeted destination within the cell [101]. At the target location, membrane junctions may facilitate intracellular transport of FAs from one membrane to another [65]. To test this hypothesis, cellular membranes can be isolated by ultracentrifugation, after cells were incubated with radiolabelled fatty acids, then cpm can be investigated in cytosolic and membrane fractions from the endothelial cells. Analysis would allow tracking of [14]OA inside defined membranes and transport routes within different membranes from apical to the basolateral side of the endothelial cell could be tracked. Furthermore, high resolution microscopy may identify membrane junctions connecting two different membranes.

In this study, the results showed that the uptake of fatty acids is fast and already after one-minute radiolabelled oleic acid is incorporated into neutral and phospholipids. Results showed that after one minute this process follows a linear trend and the rate is constant ($\sim 0,3 \text{ pmol} / \text{s} / \text{cm}^2$, results figure 19). As the total uptake of FAs saturated with increasing extracellular OA concentration, the FA metabolism is the limiting factor for further FA uptake. The results showed that excess of FAs was metabolized in primarily triacylglycerol and phosphatidylcholine. Triacylglycerol is the main energy storage molecule and found primarily in lipid droplets of the cells. Phosphatidylcholine

5. Discussion

build up most molecules in cell membranes [102]. Both PC and TG are synthesized in the Kennedy pathway [103] and final enzymes compete for the common pre-cursor diacylglycerol. Incorporation of FAs into PC and TG is generally regarded as intracellular fat storage, especially in the adipose tissue [104, 105].

From this point of view, it was remarkably, that lipolysis contributed to the efflux of fatty acids. This observation leads to the assumption that beside FA storage, the TG pool also plays an important role in FA transport. Furthermore, the results showed that transported lipids originated from equal parts from intracellular stored non-esterified FAs and lipolysis of triacylglycerol (figure 21). This observation provides evidence that there are at least two pathways for trans-endothelial FA transport existing. Both mechanisms must happen in parallel. Because, if there would be only one pathway existing, the remaining labelled non-esterified FAs would have been esterified and channelled in the TG pool for following lipolysis and efflux. But the incorporated labelled non-esterified OA pool was released in parallel to the reduction of TG for FA transport. It is important to note that intracellular labelled lipids are probably replaced by extracellular non-labelled OA present in the apical extracellular space. In further experiments, two different labelling of OA could be applied to test whether, newly incorporated lipids are esterified and replace transported fatty acids from lipolysis or if the newly incorporated lipids are directly transported without activation. The process of TG lipolysis primarily consists of two steps. Firstly, triacylglycerol is hydrolysed by adipose triglyceride lipase (ATGL), also called desnutrin or patatin-like phospholipase domain containing protein 2 (PNPLA2), into diacylglycerol and one FA [106, 107]. Secondly, the diacylglycerol is hydrolysed by hormone sensitive lipase (HSL) into monoacylglycerol and one FA [108]. In order to confirm the finding that lipolysis of TG contributes to the efflux of FAs, Atglistatin, an ATGL specific inhibitor was applied. The results showed that upon inhibition of the primary step of lipolysis the reduction of TG due to FA transport was reduced. This observation confirms the finding that lipolysis contributes to the efflux of FAs from endothelial cells. Recently, it was shown that among other functions, the hydrolysis of TG by ATGL, generates “branched fatty acid esters of hydroxy FAs (FAHFAs)” [109]. These FAHFAs contribute to positive physiological conditions, such as improved glucose homeostasis [110] and increased systemic insulin sensitivity [111]. If FAHFAs are also generated in endothelial cells due to lipolysis of TG

5. Discussion

during trans-endothelial fatty acid transport, it is to speculate whether the positive systemic effects are derived from the specific endothelial metabolism during trans-endothelial fatty acid transport.

In the next step, transported [¹⁴C] lipids in the basolateral compartment were extracted and analysed to evaluate in which form FAs were transported. The lipid fraction of the medium in the basolateral compartment underneath the HUVECs contained only fatty acids, as analysed by thin-layer chromatography (TLC). This suggests that FAs are transported as they are, i.e. non-esterified. This observation contributes to the fundamental understanding that fatty acids always require liberation prior to bypassing a cellular membrane. It must be taken into consideration that due to the limitations of TLC, molecular changes such as generation of FAHFAs are not able to identify without additional standards.

Further experiments showed that the pool of non-esterified OA showed a tendency to be increased with FATP4 upregulation, which was unexpected as higher intracellular ACS activity would shift the incorporated FAs towards esterified lipids. However, the increased pool of non-esterified OA inside *Acs13* knockdown endothelial cells was probably responsible for the initial high FA transport rates when FA transport was increased due to diminished endothelial FA metabolism. Common for all cell lines was the observation that the majority of transported OA originates from the pools of triacylglycerol (~35%) and non-esterified OA (~90%). It is important to note that due to the limitations of transwell filter (details in 5.4.) the total amount of released OA differed from the total amount of [¹⁴C]OA found in the basolateral compartment as the cells also released FAs towards the apical compartment. Those FAs were also included into the FA release/ efflux.

5.4 Limitations of the study

This study is limited to transport experiments across HUVECs grown on transwell filters. The microenvironment of the endothelium is very diverse, and the influence of blood flow, the variety of blood FAs, activity of the parenchyma, and other physiological parameters are not considered here. In addition, due to collagen pre-coating and the small transport area, the normalization to μg protein assessed by BCA assay was not feasible using transwell inserts. Also, transwell filters are plastic membranes, that have limitations in transport capacity regarding pore area ($\sim 11.4\%$ of total filter membrane), travel distance of molecules through one pore ($11.5\mu\text{m}$) and unphysiological material compositions. However, transwell filters, as applied in this study and many others, is a very elegant tool for studying transport across a confluent cell layer.

In this study incorporation and efflux of FAs was assessed by thin-layer chromatography and phosphorimaging. This methodological approach allows insights into changes in major lipid classes (phosphor-, neutral- and non-esterified FAs), but does not provide further insights, such as modern state-of-the-art lipidomic analysis. Also, this technique does not allow direct localization of incorporated FAs or minor molecular or structural changes. To balance the limitations, pulse/chase experiments were designed as an elegant methodological approach to detect changes in lipid incorporation due to FA transport.

Another important point to mention is that the uptake and corresponding uptake rate of Bodipy-C12 (figure 20) was tremendously increased compared to control with upregulation of FATP4 activity. The results strongly differed from the uptake of more physiological relevant FAs, such as [^{14}C]OA and therefore were not considered for final conclusion. The Bodipy-FA (4,4-difluoro-5,7-diphenyl-4-bora-3a,4a-diaza-s-indacene-3-dodecanoic acid, D3823, life technologies, California, USA) applied consists of a fluorescent label at the first carbon atom of a C12 fatty acid (lauric acid). The total carbon atom chain (including the fluorescent label) consists of 22 consecutive carbon atoms and is therefore regarded as long-chain fatty acid. The reason for the artificial increase in Bodipy-C12 uptake by FATP4 upregulation is not clear and therefore require further research and development prior to the application.

Lastly, other putative fatty acid transporters, such as CD36 and the role of vesicle-mediated transport through caveolae were not included in this study.

6. General conclusion

In conclusion, my results show that lipolysis contributes to the efflux of fatty acids and inhibition of ATGL reduces this effect. Transport of fatty acids is fast and ~22 times higher than the rate of metabolism in endothelial cells. In addition, I conclude that due to low FA metabolic capacity, endothelial cells are able to provide a large pool of non-esterified FAs required for transport, while further FAs are metabolized into phospho- and neutral lipids. Transport of FAs correlates with the extracellular FA concentration and is increased when intracellular FA metabolism is diminished. Furthermore, FA transport correlates with different extracellular FA-free albumin concentrations in the basolateral compartment. The putative FA transporter FATP4 changed intracellular FA metabolic capacity, but not FA transport.

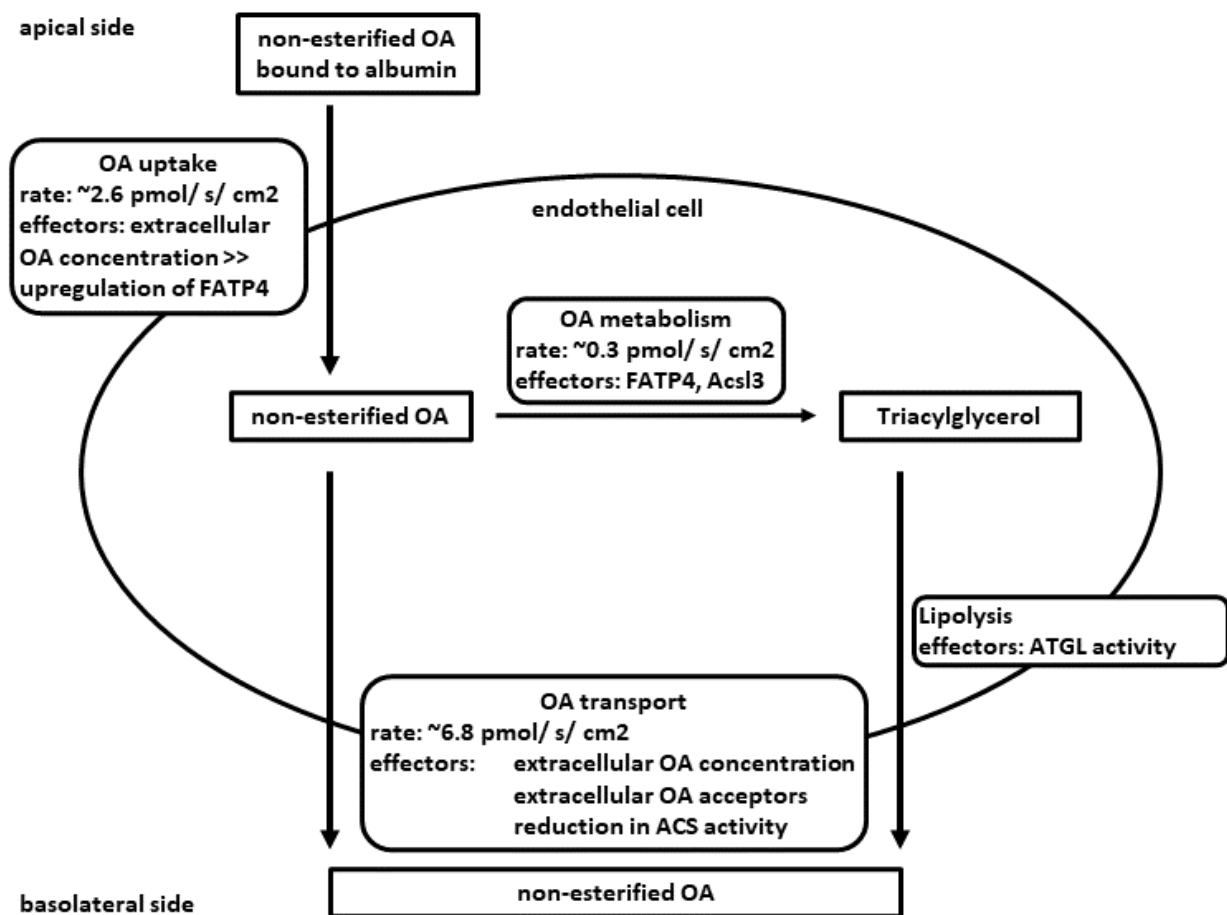


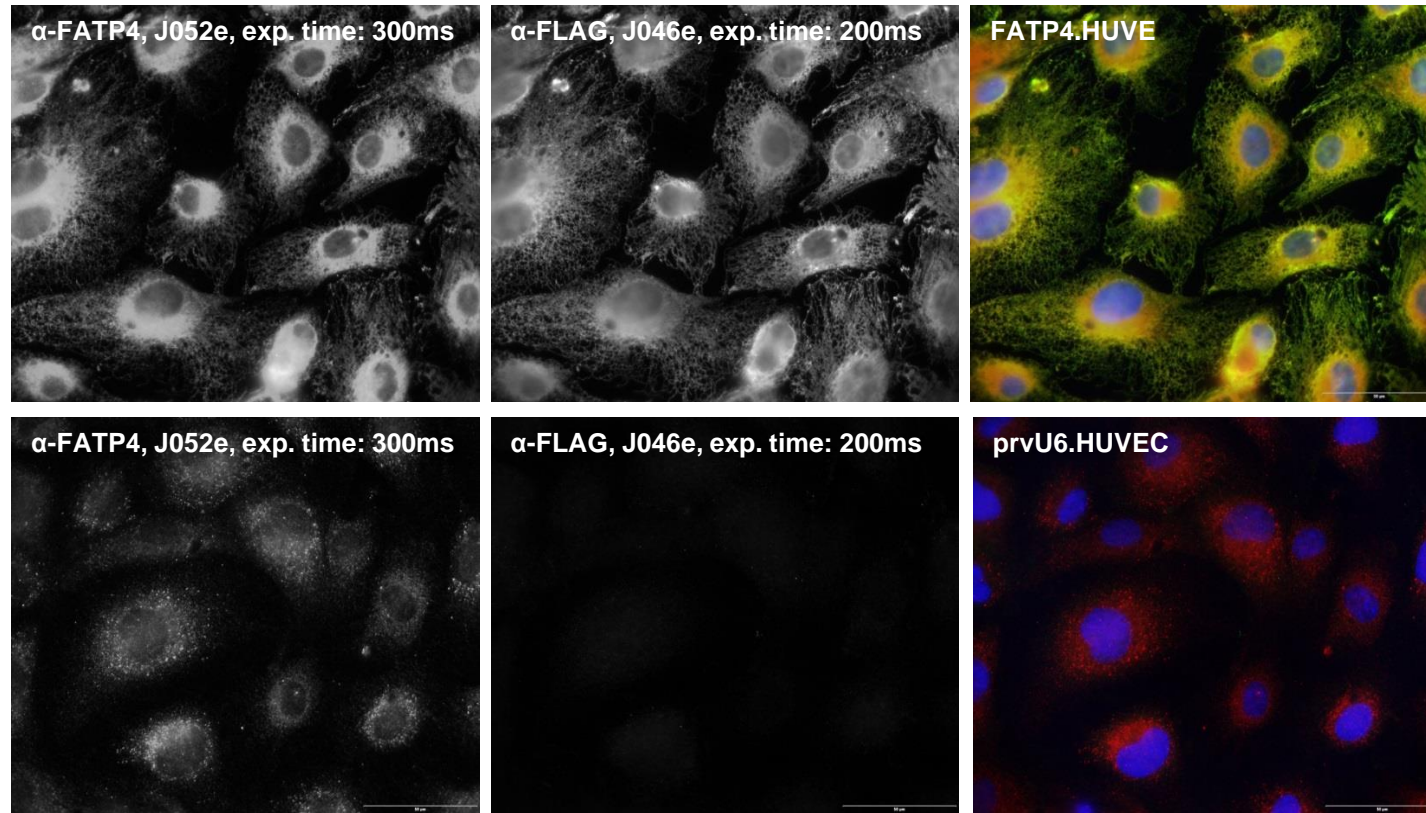
Figure 27: Contribution of this study to the concept of trans-endothelial fatty acid transport. OA uptake is fast until intracellular pool of non-esterified OA reaches maximum, then OA uptake correlates with OA metabolism. Extracellular OA concentration drives OA uptake and transport, FATP4 has a minor effect. Lipolysis of TG contributes to FA transport and can be diminished by ATGL inhibition.

7. Appendix

7.1 Qualitative analysis of upregulation of FATP4 in HUVECs by immunofluorescence and Western Blot

After transduction, selection, and expansion of genetically manipulated HUVECs, upregulation of FATP4 was qualitatively validated by immunofluorescence and Western Blot. As the overexpressed construct included a FLAG-tag at the C-terminus, two different antibodies were applied for immunofluorescence. In one approach, the primary antibody was targeting an epitope in the FATP4 amino acid structure and in the other approach, the primary antibody was targeting the FLAG tag.

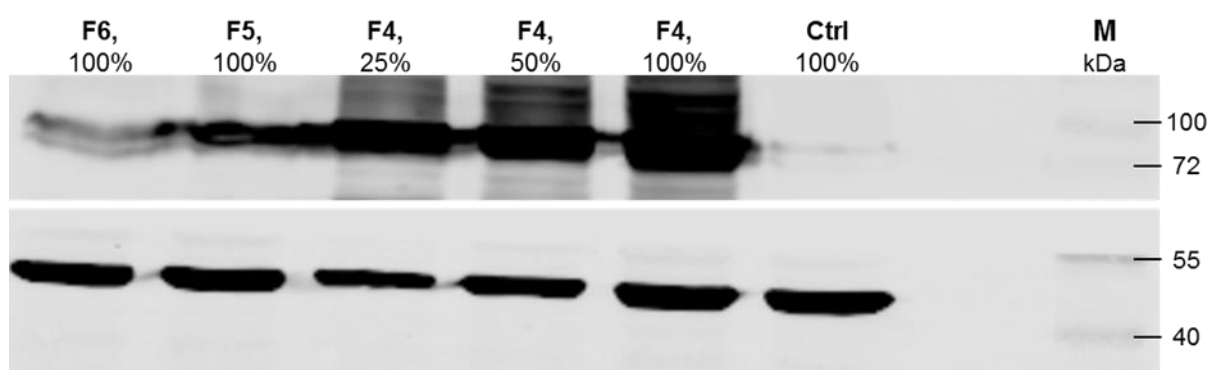
7. Appendix



Appendix Figure 1: immunofluorescence of hFATP4-FLAG expression in HUVECs. The primary antibodies applied are α -FATP4 (rabbit, J052e, affinity purified α -FATP4 C4 C3/5, 1/1000) and α -FLAG (mouse, J046e, Sigma F1804, 1/2000). The secondary antibodies applied are α -ms Al488 1/250 and α -rb Cy3 1/1000.

7. Appendix

As shown in appendix fig. 1, the primary antibody against FATP4 (J52e) recognizes both, endogenous as well as overexpressed FATP4. As expected, the primary antibody targeting the FLAG tag only displays a signal in the overexpression, not in the control cell line. Merge shows that both antibodies confirm the transduction and expression of hFATP4-FLAG in HUVECs. In the following approach the antibody targeting the FLAG-tag was applied for Western Blot analysis. Furthermore, the overexpression of FATP4 was compared to the overexpression of other FATPs in HUVECs. All FATP constructs were expressed with a C-terminal FLAG tag to allow target specific detection by immunolabeling. Here, Western Blot was applied to semi-quantitatively determine the amount of FATP4, 5 and 6 expressed in their respective HUVEC cell lines:



Appendix Figure 2: Western Blot, protein expression levels for FATP overexpressing cell lines. α -FLAG antibody; α - β Actin antibody; Lane 1: FATP6 100% loaded (~70kDa); Lane 2: FATP5 100% loaded (~75kDa); Lane 3 – 5: FATP4 25, 50, 100% loaded (~72kDa); Lane 6: Ctrl HUVECs (no FLAG tag) 100%; β Actin (~42kDa). Primary antibodies applied are α -FLAG (mouse, J046e, Sigma F1804, 1/2000). Secondary antibodies applied are α -ms 800CW 1/10000 (J093, LICOR 926-32210).

Here, FATP4-FLAG shows the strongest signal in the Western Blot followed by FATP5-FLAG and FATP6-FLAG in order. Comparing 50% and 25% of the FATP4 sample with the FATP5 or FATP6 sample qualitatively indicates that the expression of FATP4 is at least four times stronger than the FATP5 or FATP6 expression in their respective cell lines. To quantitatively evaluate the Western Blot a densitometrical analysis was performed. FLAG tag specific signal was normalized to β -Actin for each lane, ratios were normalized to the sample with the lowest expression (FATP6):

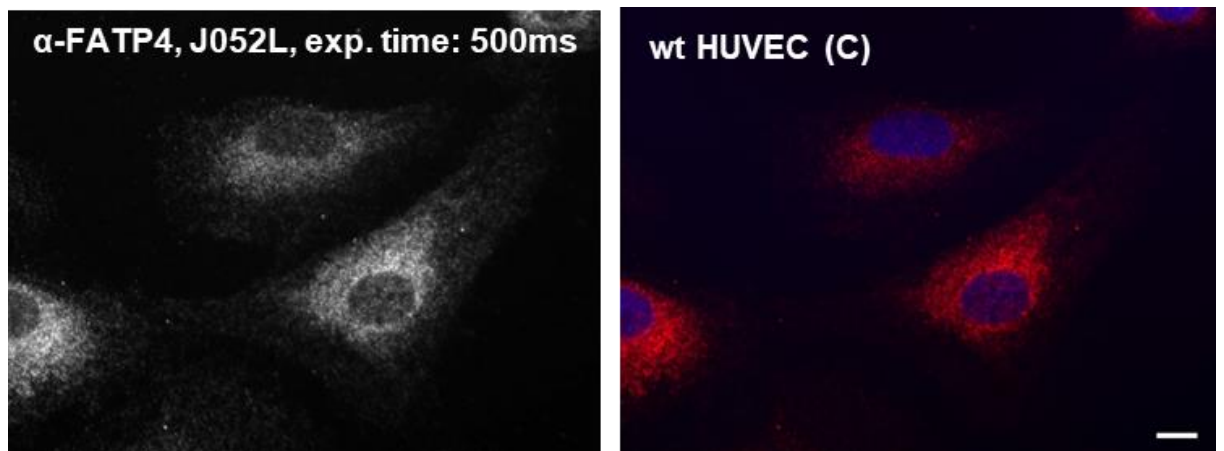
7. Appendix

Appendix Table 1: Western Blot, estimation of protein expression levels for FATP overexpressing cell lines. (Column1) ratio of signals FLAG-tag divided by β -Actin for each lane. (Column2) ratio of signals normalized to control sample. (Column3) ratio of signals normalized to FATP6 sample.

| Signal (sample/actin) | | normalized to Control | | normalized to lowest expression (FATP6) |
|-----------------------|-----|-----------------------|-------|---|
| Control | 0,0 | Control | 1,0 | |
| FATP6 | 0,8 | FATP6 | 18,9 | 1,0 |
| FATP5 | 1,6 | FATP5 | 37,2 | 2,0 |
| FATP4_25% | 5,7 | FATP4_25% | 132,9 | |
| FATP4_50% | 4,8 | FATP4_50% | 110,4 | 6,3 |
| FATP4 | 4,9 | FATP4 | 113,2 | |

As shown in appendix tab. 1, FATP4 is around 6.3 times higher expressed than FATP6. In addition, FATP5 is around two times higher expressed than FATP6. As the Western Blot was prepared with α -FLAG antibody the abundance of endogenous FATPs is not considered here. The Western Blot confirms additional abundance of each FATP construct in their respective cell line.

7.2 Assessment of endogenous FATP4 in HUVECs by IF



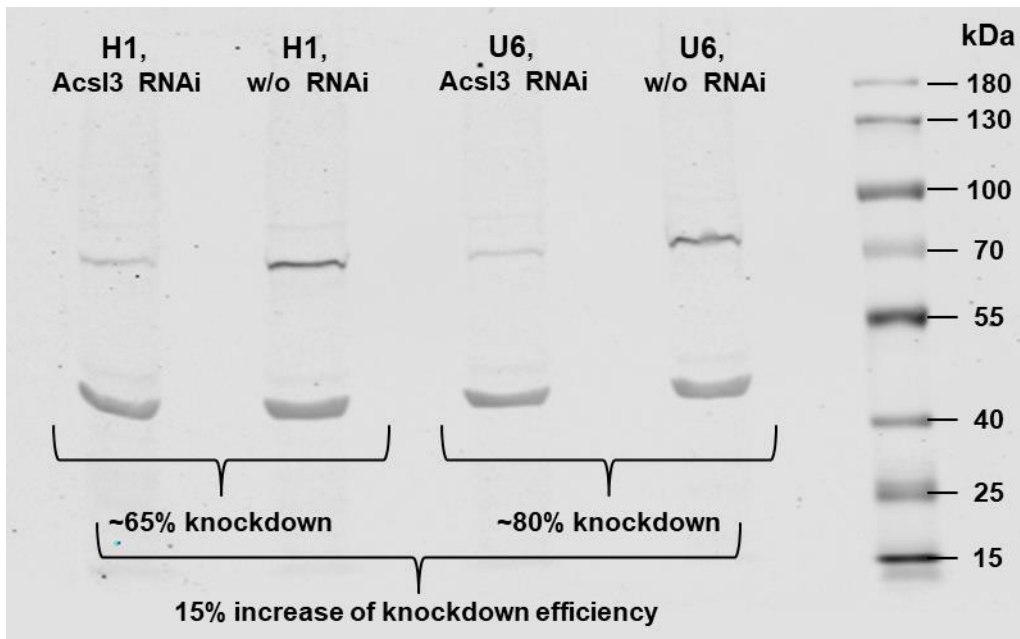
Appendix Figure 4: endogenous expression of hFATP4 shows pattern of endoplasmic reticulum. The primary antibody applied is α -FATP4 (rabbit, J052L, abcam200353, 1/100). The secondary antibody applied is α -rb Cy3 1/1000.

7.3 U6 promoter was more efficient for shRNA transmitted Acs13 knockdown in HUVECs than H1 promoter

Western Blot analysis of endogenous Acs13 knockdown by stable retroviral expression of shRNA under control of the H1 promoter revealed a knockdown efficiency of 40-65% (data not shown). Hence, the H1 promoter was exchanged

7. Appendix

with the U6 promoter. Next, knockdown efficiencies using H1 promoter was compared to U6 promoter by assessment using Western Blot:



Appendix figure 5: shRNA associated knockdown of Acs13 is increased by replacing H1 with U6 promoter.

Acknowledgements

Immeasurable appreciation and deepest gratitude for help and support are extended to the following persons who in one way or another have contributed to making this study possible.

Foremost among, to Mr. **apl. Prof. Dr. rer. nat. Joachim Füllekrug**, for granting me the opportunity to work in his research group, for his untiring support and valuable advice in doing this research. Moreover, for his readiness to discuss data and results. And last for sharing ideas and visions in the completion and success of this study.

To Mr. **Prof. Dr. rer. nat. Walter Nickel** and Mr. **Prof. Dr. rer. nat. Gert Fricker** of my Thesis Advisory Committee, for sharing time and efforts in discussing my project and giving guidance in doing this research.

To Mr. **Dr. rer. nat. Wilhelm Palm** for sharing time and efforts in discussing my project during participation in the viva voce of my thesis.

To all **Laboratory Colleagues** of the **AG Füllekrug**, for cooperation and for sharing time and efforts in terms of providing materials and needed information. And for the pleasant atmosphere in the laboratory.

To **Franziska Mohr** and Colleagues (**AG Wagner, Institut für Physiologie und Pathophysiologie**) for sharing protocols, materials and teaching me the principles of HUVEC isolation. And for her time and effort during consultations in the completion and success of this study.

To **Dr. rer. nat. Viktor Balzer (AG Fricker, IPMB Heidelberg)** for sharing protocols, methods and teaching me the application of TEER measurements. And for his time and effort during consultations in the completion and success of this study.

To my **family and friends**.

8. References

1. Mehrotra, D., et al., *Endothelium as a gatekeeper of fatty acid transport*. Trends Endocrinol Metab, 2014. **25**(2): p. 99-106.
2. Krüger-Genge, A., et al., *Vascular Endothelial Cell Biology: An Update*. Int J Mol Sci, 2019. **20**(18).
3. Godo, S. and H. Shimokawa, *Endothelial Functions*. Arterioscler Thromb Vasc Biol, 2017. **37**(9): p. e108-e114.
4. Pearson, J.D., *Normal endothelial cell function*. Lupus, 2000. **9**(3): p. 183-8.
5. Michiels, C., *Endothelial cell functions*. J Cell Physiol, 2003. **196**(3): p. 430-43.
6. Joó, F., *Endothelial cells of the brain and other organ systems: some similarities and differences*. Prog Neurobiol, 1996. **48**(3): p. 255-73.
7. Kniesel, U. and H. Wolburg, *Tight junctions of the blood-brain barrier*. Cell Mol Neurobiol, 2000. **20**(1): p. 57-76.
8. Braet, F. and E. Wisse, *Structural and functional aspects of liver sinusoidal endothelial cell fenestrae: a review*. Comp Hepatol, 2002. **1**(1): p. 1.
9. Shetty, S., P.F. Lalor, and D.H. Adams, *Liver sinusoidal endothelial cells - gatekeepers of hepatic immunity*. Nat Rev Gastroenterol Hepatol, 2018. **15**(9): p. 555-567.
10. Aird, W.C., *Phenotypic heterogeneity of the endothelium: I. Structure, function, and mechanisms*. Circ Res, 2007. **100**(2): p. 158-73.
11. Dejana, E. and F. Orsenigo, *Endothelial adherens junctions at a glance*. J Cell Sci, 2013. **126**(Pt 12): p. 2545-9.
12. Minshall, R.D. and A.B. Malik, *Transport across the endothelium: regulation of endothelial permeability*. Handb Exp Pharmacol, 2006(176 Pt 1): p. 107-44.
13. Hu, Y.J., et al., *Regulation of paracellular permeability: factors and mechanisms*. Mol Biol Rep, 2013. **40**(11): p. 6123-42.
14. Félétou, M., *The Endothelium: Part 1: Multiple Functions of the Endothelial Cells—Focus on Endothelium-Derived Vasoactive Mediators*, in *San Rafael (CA): Morgan & Claypool Life Sciences*. 2011.
15. Field, C.J. and L. Robinson, *Dietary Fats*. Adv Nutr, 2019. **10**(4): p. 722-724.
16. Mu, H. and C.E. Høy, *The digestion of dietary triacylglycerols*. Prog Lipid Res, 2004. **43**(2): p. 105-33.
17. Mansbach, C.M., 2nd and F. Gorelick, *Development and physiological regulation of intestinal lipid absorption. II. Dietary lipid absorption, complex lipid synthesis, and the intracellular packaging and secretion of chylomicrons*. Am J Physiol Gastrointest Liver Physiol, 2007. **293**(4): p. G645-50.
18. Grundy, S.M., *Does Dietary Cholesterol Matter?* Curr Atheroscler Rep, 2016. **18**(11): p. 68.
19. Küllenberg, D., et al., *Health effects of dietary phospholipids*. Lipids Health Dis, 2012. **11**: p. 3.
20. Tso, P., A. Nauli, and C.M. Lo, *Enterocyte fatty acid uptake and intestinal fatty acid-binding protein*. Biochem Soc Trans, 2004. **32**(Pt 1): p. 75-8.
21. Khatun, I., et al., *Characterization of a Novel Intestinal Glycerol-3-phosphate Acyltransferase Pathway and Its Role in Lipid Homeostasis*. J Biol Chem, 2016. **291**(6): p. 2602-15.
22. Ho, S.Y. and J. Storch, *Common mechanisms of monoacylglycerol and fatty acid uptake by human intestinal Caco-2 cells*. Am J Physiol Cell Physiol, 2001. **281**(4): p. C1106-17.
23. Tso, P. and J.A. Balint, *Formation and transport of chylomicrons by enterocytes to the lymphatics*. Am J Physiol, 1986. **250**(6 Pt 1): p. G715-26.
24. Dash, S., et al., *New Insights into the Regulation of Chylomicron Production*. Annu Rev Nutr, 2015. **35**: p. 265-94.
25. Hazzard, W.R., D. Porte, Jr., and E.L. Bierman, *Abnormal lipid composition of chylomicrons in broad-beta disease (type 3 hyperlipoproteinemia)*. J Clin Invest, 1970. **49**(10): p. 1853-8.

References

26. Fielding, C.J. and P.E. Fielding, *Chylomicron protein content and the rate of lipoprotein lipase activity*. J Lipid Res, 1976. **17**(4): p. 419-23.
27. Cifarelli, V. and A. Eichmann, *The Intestinal Lymphatic System: Functions and Metabolic Implications*. Cell Mol Gastroenterol Hepatol, 2019. **7**(3): p. 503-513.
28. Klein, S. and R.R. Wolfe, *Carbohydrate restriction regulates the adaptive response to fasting*. Am J Physiol, 1992. **262**(5 Pt 1): p. E631-6.
29. Fraser, D.A., et al., *Changes in plasma free fatty acid concentrations in rheumatoid arthritis patients during fasting and their effects upon T-lymphocyte proliferation*. Rheumatology (Oxford), 1999. **38**(10): p. 948-52.
30. Hagberg, C.E., et al., *Vascular endothelial growth factor B controls endothelial fatty acid uptake*. Nature, 2010. **464**(7290): p. 917-921.
31. Jang, C., et al., *A branched-chain amino acid metabolite drives vascular fatty acid transport and causes insulin resistance*. Nat Med, 2016. **22**(4): p. 421-6.
32. Birrane, G., et al., *Structure of the lipoprotein lipase-GPIHBP1 complex that mediates plasma triglyceride hydrolysis*. Proc Natl Acad Sci U S A, 2019. **116**(5): p. 1723-1732.
33. Bonen, A., et al., *Is membrane transport of FFA mediated by lipid, protein, or both? Mechanisms and regulation of protein-mediated cellular fatty acid uptake: molecular, biochemical, and physiological evidence*. Physiology (Bethesda), 2007. **22**: p. 15-29.
34. Rupert, J.E. and M.G. Kolonin, *Fatty acid translocase: a culprit of lipid metabolism dysfunction in disease*. Immunometabolism (Cobham), 2022. **4**(3): p. e00001.
35. Jay, A.G. and J.A. Hamilton, *The enigmatic membrane fatty acid transporter CD36: New insights into fatty acid binding and their effects on uptake of oxidized LDL*. Prostaglandins Leukot Essent Fatty Acids, 2018. **138**: p. 64-70.
36. Goldberg, I.J. and K.E. Bornfeldt, *Lipids and the endothelium: bidirectional interactions*. Curr Atheroscler Rep, 2013. **15**(11): p. 365.
37. Stremmel, W., et al., *A new concept of cellular uptake and intracellular trafficking of long-chain fatty acids*. Lipids, 2001. **36**(9): p. 981-9.
38. Son, N.H., et al., *Endothelial cell CD36 optimizes tissue fatty acid uptake*. J Clin Invest, 2018. **128**(10): p. 4329-4342.
39. Bonen, A., et al., *Regulation of fatty acid transport by fatty acid translocase/CD36*. Proc Nutr Soc, 2004. **63**(2): p. 245-9.
40. Goto, K., et al., *Peroxisome proliferator-activated receptor- γ in capillary endothelia promotes fatty acid uptake by heart during long-term fasting*. J Am Heart Assoc, 2013. **2**(1): p. e004861.
41. Kanda, T., et al., *PPAR γ in the endothelium regulates metabolic responses to high-fat diet in mice*. J Clin Invest, 2009. **119**(1): p. 110-24.
42. Gogg, S., et al., *Human adipose tissue microvascular endothelial cells secrete PPAR γ ligands and regulate adipose tissue lipid uptake*. JCI Insight, 2019. **4**(5).
43. Iso, T., et al., *Capillary endothelial fatty acid binding proteins 4 and 5 play a critical role in fatty acid uptake in heart and skeletal muscle*. Arterioscler Thromb Vasc Biol, 2013. **33**(11): p. 2549-57.
44. Elmasri, H., et al., *Fatty acid binding protein 4 is a target of VEGF and a regulator of cell proliferation in endothelial cells*. Faseb j, 2009. **23**(11): p. 3865-73.
45. van der Vusse, G.J., *Albumin as fatty acid transporter*. Drug Metab Pharmacokinet, 2009. **24**(4): p. 300-7.
46. Vogel, S.M., et al., *Albumin uptake and transcytosis in endothelial cells in vivo induced by albumin-binding protein*. Am J Physiol Lung Cell Mol Physiol, 2001. **281**(6): p. L1512-22.
47. Garcia-Cardena, G., et al., *Endothelial nitric oxide synthase is regulated by tyrosine phosphorylation and interacts with caveolin-1*. J Biol Chem, 1996. **271**(44): p. 27237-40.
48. Matveev, S., et al., *The role of caveolae and caveolin in vesicle-dependent and vesicle-independent trafficking*. Adv Drug Deliv Rev, 2001. **49**(3): p. 237-50.

References

49. Mattern, H.M., L.S. Raikar, and C.D. Hardin, *The effect of caveolin-1 (Cav-1) on fatty acid uptake and CD36 localization and lipotoxicity in vascular smooth muscle (VSM) cells*. *Int J Physiol Pathophysiol Pharmacol*, 2009. **1**(1): p. 1-14.
50. Schubert, W., et al., *Caveolae-deficient endothelial cells show defects in the uptake and transport of albumin in vivo*. *J Biol Chem*, 2001. **276**(52): p. 48619-22.
51. Schaffer, J.E. and H.F. Lodish, *Expression cloning and characterization of a novel adipocyte long chain fatty acid transport protein*. *Cell*, 1994. **79**(3): p. 427-36.
52. Anderson, C.M. and A. Stahl, *SLC27 fatty acid transport proteins*. *Mol Aspects Med*, 2013. **34**(2-3): p. 516-28.
53. Kazantzis, M. and A. Stahl, *Fatty acid transport proteins, implications in physiology and disease*. *Biochim Biophys Acta*, 2012. **1821**(5): p. 852-7.
54. Hall, A.M., et al., *Enzymatic properties of purified murine fatty acid transport protein 4 and analysis of acyl-CoA synthetase activities in tissues from FATP4 null mice*. *J Biol Chem*, 2005. **280**(12): p. 11948-54.
55. Mihalik, S.J., et al., *Participation of two members of the very long-chain acyl-CoA synthetase family in bile acid synthesis and recycling*. *J Biol Chem*, 2002. **277**(27): p. 24771-9.
56. Jia, Z., et al., *Fatty acid transport protein 4 is the principal very long chain fatty acyl-CoA synthetase in skin fibroblasts*. *J Biol Chem*, 2007. **282**(28): p. 20573-83.
57. Falcon, A., et al., *FATP2 is a hepatic fatty acid transporter and peroxisomal very long-chain acyl-CoA synthetase*. *Am J Physiol Endocrinol Metab*, 2010. **299**(3): p. E384-93.
58. Hamilton, J.A., *Transport of fatty acids across membranes by the diffusion mechanism*. *Prostaglandins Leukot Essent Fatty Acids*, 1999. **60**(5-6): p. 291-7.
59. Khan, A., W.A. Ducker, and M. Mao, *Flip-flop in adsorbed bilayers*. *J Phys Chem B*, 2006. **110**(46): p. 23365-72.
60. Hamilton, J.A., W. Guo, and F. Kamp, *Mechanism of cellular uptake of long-chain fatty acids: Do we need cellular proteins?* *Mol Cell Biochem*, 2002. **239**(1-2): p. 17-23.
61. Pashkovskaya, A.A., et al., *Mechanism of Long-Chain Free Fatty Acid Protonation at the Membrane-Water Interface*. *Biophys J*, 2018. **114**(9): p. 2142-2151.
62. Kamp, F. and J.A. Hamilton, *pH gradients across phospholipid membranes caused by fast flip-flop of un-ionized fatty acids*. *Proc Natl Acad Sci U S A*, 1992. **89**(23): p. 11367-70.
63. Black, P.N., et al., *Targeting the fatty acid transport proteins (FATP) to understand the mechanisms linking fatty acid transport to metabolism*. *Immunol Endocr Metab Agents Med Chem*, 2009. **9**(1): p. 11-17.
64. Black, P.N. and C.C. DiRusso, *Vectorial acylation: linking fatty acid transport and activation to metabolic trafficking*. *Novartis Found Symp*, 2007. **286**: p. 127-38; discussion 138-41, 162-3, 196-203.
65. Füllekrug, J., R. Ehehalt, and M. Poppelreuther, *Outlook: membrane junctions enable the metabolic trapping of fatty acids by intracellular acyl-CoA synthetases*. *Front Physiol*, 2012. **3**: p. 401.
66. Mitchell, P. and J. Moyle, *Group-translocation: a consequence of enzyme-catalysed group-transfer*. *Nature*, 1958. **182**(4632): p. 372-3.
67. Black, P.N., et al., *Fatty Acid Transport Proteins: Targeting FATP2 as a Gatekeeper Involved in the Transport of Exogenous Fatty Acids*. *Medchemcomm*, 2016. **7**(4): p. 612-622.
68. Hagberg, C., et al., *Endothelial fatty acid transport: role of vascular endothelial growth factor B*. *Physiology (Bethesda)*, 2013. **28**(2): p. 125-34.
69. Milger, K., et al., *Cellular uptake of fatty acids driven by the ER-localized acyl-CoA synthetase FATP4*. *J Cell Sci*, 2006. **119**(Pt 22): p. 4678-88.
70. Ibrahim, A., et al., *Local Mitochondrial ATP Production Regulates Endothelial Fatty Acid Uptake and Transport*. *Cell Metab*, 2020. **32**(2): p. 309-319.e7.
71. Culic, O., M.L. Gruwel, and J. Schrader, *Energy turnover of vascular endothelial cells*. *Am J Physiol*, 1997. **273**(1 Pt 1): p. C205-13.

References

72. De Bock, K., et al., *Role of PFKFB3-driven glycolysis in vessel sprouting*. Cell, 2013. **154**(3): p. 651-63.
73. Hunt, M.A., et al., *Optimizing transfection of primary human umbilical vein endothelial cells using commercially available chemical transfection reagents*. J Biomol Tech, 2010. **21**(2): p. 66-72.
74. Schuck, S., et al., *Generation of single and double knockdowns in polarized epithelial cells by retrovirus-mediated RNA interference*. Proc Natl Acad Sci U S A, 2004. **101**(14): p. 4912-7.
75. Kuerschner, L., et al., *Polyene-lipids: a new tool to image lipids*. Nat Methods, 2005. **2**(1): p. 39-45.
76. Füllekrug, J. and M. Poppelreuther, *Measurement of Long-Chain Fatty Acyl-CoA Synthetase Activity*. Methods Mol Biol, 2016. **1376**: p. 43-53.
77. Baudin, B., et al., *A protocol for isolation and culture of human umbilical vein endothelial cells*. Nat Protoc, 2007. **2**(3): p. 481-5.
78. Jaffe, E.A., *Cell biology of endothelial cells*. Hum Pathol, 1987. **18**(3): p. 234-9.
79. Pries, A.R. and W.M. Kuebler, *Normal endothelium*. Handb Exp Pharmacol, 2006(176 Pt 1): p. 1-40.
80. Rajendran, P., et al., *The vascular endothelium and human diseases*. Int J Biol Sci, 2013. **9**(10): p. 1057-69.
81. Gralnick, H.R., et al., *Platelet von Willebrand factor*. Mayo Clin Proc, 1991. **66**(6): p. 634-40.
82. Nightingale, T. and D. Cutler, *The secretion of von Willebrand factor from endothelial cells; an increasingly complicated story*. J Thromb Haemost, 2013. **11 Suppl 1**(Suppl 1): p. 192-201.
83. Weibel, E.R. and G.E. Palade, *NEW CYTOPLASMIC COMPONENTS IN ARTERIAL ENDOTHELIA*. J Cell Biol, 1964. **23**(1): p. 101-12.
84. Wortzel, I., et al., *Applying imaging flow cytometry and immunofluorescence in studying the dynamic Golgi structure in cultured cells*. STAR Protoc, 2022. **3**(2): p. 101278.
85. Vestweber, D., *VE-cadherin: the major endothelial adhesion molecule controlling cellular junctions and blood vessel formation*. Arterioscler Thromb Vasc Biol, 2008. **28**(2): p. 223-32.
86. Chen, S., R. Einspanier, and J. Schoen, *Transepithelial electrical resistance (TEER): a functional parameter to monitor the quality of oviduct epithelial cells cultured on filter supports*. Histochem Cell Biol, 2015. **144**(5): p. 509-15.
87. Frost, T.S., et al., *Permeability of Epithelial/Endothelial Barriers in Transwells and Microfluidic Bilayer Devices*. Micromachines (Basel), 2019. **10**(8).
88. Dewi, B.E., T. Takasaki, and I. Kurane, *In vitro assessment of human endothelial cell permeability: effects of inflammatory cytokines and dengue virus infection*. J Virol Methods, 2004. **121**(2): p. 171-80.
89. Pauty, J., et al., *A Vascular Permeability Assay Using an In Vitro Human Microvessel Model Mimicking the Inflammatory Condition*. Nanotheranostics, 2017. **1**(1): p. 103-113.
90. Nie, B., et al., *Specific bile acids inhibit hepatic fatty acid uptake in mice*. Hepatology, 2012. **56**(4): p. 1300-10.
91. Gimeno, R.E., et al., *Characterization of a heart-specific fatty acid transport protein*. J Biol Chem, 2003. **278**(18): p. 16039-44.
92. Kuwata, H. and S. Hara, *Role of acyl-CoA synthetase ACSL4 in arachidonic acid metabolism*. Prostaglandins Other Lipid Mediat, 2019. **144**: p. 106363.
93. Shamir, M., et al., *SnapShot: Timescales in Cell Biology*. Cell, 2016. **164**(6): p. 1302-1302.e1.
94. Furuhashi, M. and G.S. Hotamisligil, *Fatty acid-binding proteins: role in metabolic diseases and potential as drug targets*. Nat Rev Drug Discov, 2008. **7**(6): p. 489-503.
95. Kuo, A., M.Y. Lee, and W.C. Sessa, *Lipid Droplet Biogenesis and Function in the Endothelium*. Circ Res, 2017. **120**(8): p. 1289-1297.

References

96. Ibrahim, A. and Z. Arany, *Does Endothelium Buffer Fat?* *Circ Res*, 2017. **120**(8): p. 1219-1221.
97. Schaefer, E.J., et al., *Comparison of fasting and postprandial plasma lipoproteins in subjects with and without coronary heart disease.* *Am J Cardiol*, 2001. **88**(10): p. 1129-33.
98. Popkin, B.M., K.E. D'Anci, and I.H. Rosenberg, *Water, hydration, and health.* *Nutr Rev*, 2010. **68**(8): p. 439-58.
99. Storch, J. and B. Corsico, *The emerging functions and mechanisms of mammalian fatty acid-binding proteins.* *Annu Rev Nutr*, 2008. **28**: p. 73-95.
100. Haunerland, N.H. and F. Spener, *Fatty acid-binding proteins--insights from genetic manipulations.* *Prog Lipid Res*, 2004. **43**(4): p. 328-49.
101. Lindblom, G. and G. Orädd, *Lipid lateral diffusion and membrane heterogeneity.* *Biochim Biophys Acta*, 2009. **1788**(1): p. 234-44.
102. Kanno, K., et al., *Structure and function of phosphatidylcholine transfer protein (PC-TP)/StarD2.* *Biochim Biophys Acta*, 2007. **1771**(6): p. 654-62.
103. Kennedy, E.P. and S.B. Weiss, *The function of cytidine coenzymes in the biosynthesis of phospholipides.* *J Biol Chem*, 1956. **222**(1): p. 193-214.
104. Ahmadian, M., et al., *Triacylglycerol metabolism in adipose tissue.* *Future Lipidol*, 2007. **2**(2): p. 229-237.
105. Denning, G.M., et al., *Role of triglycerides in endothelial cell arachidonic acid metabolism.* *J Lipid Res*, 1983. **24**(8): p. 993-1001.
106. Zimmermann, R., et al., *Fat mobilization in adipose tissue is promoted by adipose triglyceride lipase.* *Science*, 2004. **306**(5700): p. 1383-6.
107. Kulminkaya, N., et al., *Optimized expression and purification of adipose triglyceride lipase improved hydrolytic and transacylation activities in vitro.* *J Biol Chem*, 2021. **297**(4): p. 101206.
108. Vaughan, M., J.E. Berger, and D. Steinberg, *HORMONE-SENSITIVE LIPASE AND MONOGLYCERIDE LIPASE ACTIVITIES IN ADIPOSE TISSUE.* *J Biol Chem*, 1964. **239**: p. 401-9.
109. Patel, R., et al., *ATGL is a biosynthetic enzyme for fatty acid esters of hydroxy fatty acids.* *Nature*, 2022. **606**(7916): p. 968-975.
110. Syed, I., et al., *Palmitic Acid Hydroxystearic Acids Activate GPR40, Which Is Involved in Their Beneficial Effects on Glucose Homeostasis.* *Cell Metab*, 2018. **27**(2): p. 419-427.e4.
111. Zhou, P., et al., *PAHSAs enhance hepatic and systemic insulin sensitivity through direct and indirect mechanisms.* *J Clin Invest*, 2019. **129**(10): p. 4138-4150.